Ph. D. Thesis

# Numerical Study of Multi-Component Hydrodynamic Escape: Application to the Early Venusian Atmosphere

Takanori Sasaki

Department of Earth and Planetary Science,
The University of Tokyo

2008

**Abstract**

Venus is free of molecular oxygen but it is thought to have contained a primordial water ocean. Present lack of water is considered to be due to photodissociation of $H_2O$ followed by thermal escape of H at early stage. Then, the lack of oxygen on present Venus is puzzling. Meanwhile, Venus may have lost some Ne, since it is enriched about 10% in $^{22}Ne/^{20}Ne$ with respect to solar abundances. On the other hand, Venus appears to have lost no Ar, as indicated by near solar $^{36}Ar/^{84}Kr$ and $^{38}Ar/^{36}Ar$ ratios. Then, the fractionation of Ne and Ar is puzzling. A key to solve these problems would be a hydrodynamic escape of oxygen or noble gases from the early Venusian atmosphere.

Hydrodynamic escape is one of a few mechanisms that can change the composition of a planetary atmosphere irreversibly. So far, several numerical models have been developed to solve the hydrodynamic escape problem. Previous models, however, are unsatisfactory to apply actual atmospheric evolutions quantitatively because they cannot solve transonic solutions or multi component solutions. Their quantitative uncertainties cause their conclusions of the Venusian problems to be all different each other. These problems should be solved by use of the numerical method to derive the precise quantitative solutions. Here I present the first study on the multi-component time-dependent hydrodynamic equations for transonic neutral gas escape from the early Venusian atmosphere.

The numerical model consists of the one-dimensional time-dependent non-viscous Euler equations with thermal conduction in spherical geometry. The effects of collisions with other species are included in the momentum equation to solve the multi-component hydrodynamic escape. I develop the numerical code of hydrodynamic escape using CIP method, which is well suited to solve the transonic flow. A two-dimensional energy deposition calculation method is adapted to provide an accurate approximation of the complicated radiative transfer processes in an extended spherical atmosphere. I also use the power-law fits of solar fluxes against solar age to estimate the energy deposition by solar EUV heating in numerical calculations; the emission of the younger Sun in EUV wavelength intervals is orders of magnitude larger than the current solar flux. The solution technique is validated in an isothermal atmosphere, polytropic atmosphere, and adiabatic atmosphere. I apply the developed numerical

model to the escape of hypothetical early Venusian atmosphere to consider (1) water loss from early Venus and (2) fractionation of noble gases on Venus.

(1) Water loss from early Venus: According to the results, water loss from early Venus can be achieved if the homopause number densities of $H_2$ and O are maintained around $9.0 \times 10^{15}$ [molecules/$m^3$] for a long time; in such a case, timescale of water loss as amount of terrestrial ocean is about $1.5 \times 10^8$ years. Except in that case (i.e., when the homopause number densities vary with time), the hydrogen molecules escape more than oxygen molecules from the water-rich Venusian atmosphere, and then the relative abundance of oxygen to hydrogen inevitably increases with time. Moreover, the larger the relative abundance of oxygen to hydrogen is, the harder the oxygen escapes from the Venusian atmosphere, so that the oxygen relative abundance would increase at an accelerating pace.

Eventually, the results indicate that the complete water loss from early Venus by hydrodynamic escape of oxygen as well as hydrogen would be very difficult but not be impossible. Under special circumstances, hydrodynamic escape of $H_2$ and O by itself can solve the water loss problem for Venus. This is an important consequence of this study. However, in the most cases, the oxygen would be left behind while the hydrogen would escape from the Venus, so that the oxygen consequently concentrates in the Venusian atmosphere. How the oxygen concentrate and how the concentrated oxygen was consumed and/or escaped are also discussed.

(2) Fractionation of noble gases on Venus: I show the fractionation of Ne and Ar would not be explained simply by mass-dependent hydrodynamic escape of primordial Venusian atmosphere. So, I consider the CO rotational cooling to realize the fine-tuning of hydrogen escape flux, which makes Ne escape and Ar unescape. When carbon monoxide is the same amount as hydrogen at the homopause in the early Venusian atmosphere, the Ne/Ar fractionation by hydrodynamic escape with CO cooling efficiently occurs. However, even in this case, quantitatively appropriate Ne/Ar fractionation cannot be achieved by hydrogen hydrodynamic escape. The results indicate that the present Venus' Ne/Ar abundance ratio cannot be explained by hydrodynamic escape of early Venusian atmosphere with solar-composition.

Present Venusian Ne/Ar abundance ratio could not be achieved by hydrodynamic escape even if an atmospheric temperature controlled by CO cooling is taken into consideration. However, other cooling mechanism such as $H_2O$ cooling and other noble gases' sources such as solar implanted materials and/or comets might make it

possible to achieve the proper Ne/Ar fractionation. Other possibilities of achieving noble gas patterns of present Venusian atmosphere are also discussed.

The results imply that simple explanations for these problems in previous studies are actually not enough to account for the present Venusian atmosphere. Thus, the results also imply that more detailed studies are required to understand the Venusian atmospheric evolution history.

# Contents

# List of Figures

# List of Tables

# Chapter 1

# General Introduction

Understanding how primordial atmospheres evolved to their present compositions is closely connected to the challenge of understanding the evolution of the planets themselves, in particular their geophysical histories of differentiation and outgassing, and emergences of coupled atmosphere-interior systems. Standard theories for the planetary formation predict that the following four processes should mainly determine the planetary atmospheres (Zahnle, 1998): capture of high-reduced gas from the primordial solar nebula, degassing from protoplanets and planetesimals, atmospheric loss by giant impacts, and atmospheric escape by hydrodynamic escape. When a planet grows up to be a lunar-size in the nebula gas, the planet starts to gravitationally capture the nebula gas. According to the modern planetary formation theory (e.g., Kokubo & Ida, 2000), terrestrial planets may capture the primordial solar nebula in the middle of planetary formation because the timescale of planetary formation would be smaller than that of dissipation of nebula gas (Strom et al., 1993). On the other hand, high velocity impacts of planetesimals into the growing planets have been considered to occur during accretion, which results in degassing of volatile materials contained in the planet forming planetesimals (Abe & Matsui, 1986). Therefore, the primordial planetary atmosphere should be mixture of atmospheres originated from nebula gas and degassing volatile materials (Abe et al., 2000). And a primordial planetary atmosphere should be reducing chemical composition initially, irrespective the source of atmosphere (Hashimoto et al., 2007). After the stage of planetary formation and mixed atmosphere formation, the atmosphere may have evolved to the present atmosphere following extensive loss and escape of the primordial atmosphere. Particularly, it has been implicated that the process of atmospheric escape could mainly bring the atmospheric and surficial differences of terrestrial planets (Earth, Venus, and Mars). Atmospheric loss mechanism by giant impacts have been studied in detail

by Genda & Abe (2003, 2005), and they have estimated the effect of atmospheric loss process following giant impacts. So far, however, we have no quantitatively reliable study for hydrodynamic escape of primordial terrestrial atmospheres yet, although there exists many qualitative studies of that (e.g., Zahnle & Kasting, 1986).

Hydrodynamic escape of the primordial atmospheres on terrestrial planets is key to account for the characteristics of planetary noble gas abundances as follows: With Venus, it is the lack of water and the related, extremely high D/H ratio - the latter an obvious remnant of large scale hydrogen escape. For Earth, it is the presence of strange isotopic anomalies in noble gases, especially neon and xenon. For Mars, it is all of the above, plus other isotopic anomalies (argon, nitrogen), and most telling of all, a general 100-fold depletion of nonradiogenic atmophiles when compared to Earth.

In this paper, I develop a numerical code of multi-component hydrodynamic escape to study the atmospheric escape process quantitatively, and also apply the numerical code to early Venusian atmosphere to give some constraint in the Venusian atmospheric evolution. The significance of this study is not exclusive to solve some remaining issues of Venusian atmospheres. It is noteworthy to develop a general numerical code of hydrodynamic escape because many atmospheric evolution problems can be solved using the code. The numerical code could be applicable to wide variety of planetary atmospheres including extrasolar planets, since early atmospheric evolution following hydrodynamic escape would be an inevitable evolutionary process for general planets in the universe. Advances of planetary formation and continued discovery of extrasolar planets have revealed large variety of planets and planetary atmospheres (Ida & Lin, 2004). It will be possible to illustrate the variety of evolutional history for each planet by use of the developed numerical code of hydrodynamic escape in this study. Therefore, I believe that this study has large possibility and expansibility to lead to more general study of planetary science including extrasolar planets, and of course astrobiology in the future; this huge potential is the greatest feature of this study.

# Part I

# Development of Numerical Model

# Chapter 2

# Introduction to Hydrodynamic Escape

## 2.1 Hydrodynamic Escape

The solar and polar winds are generally considered to be fluid-like or hydrodynamic and can be described by considering the equations of hydrodynamics rather than the particle picture of the collisionless exosphere. The theory of hydrodynamic escape of an atmosphere, as it applies to the solar wind, is described in standard references (e.g., Parker, 1964). Similar hydrodynamic models have been used to describe the loss of a planetary atmosphere for which the hydrodynamic escape parameter (HEP; see section 5.1) is small and the flow speed is large (e.g., Watson et al., 1981). Such large flow speeds may have existed during early planetary atmospheric formation. Hydrodynamic escape occurs when hydrogen-rich primordial atmospheres are strongly heated at high altitudes by intense extreme-ultraviolet (EUV) radiation from the young sun (e.g., Pepin, 1991). The likeliest energy source driving escape would have been solar EUV radiation ($\lambda < 100$ nm), i.e., radiation of short enough wavelength that it can be directly absorbed by hydrogen (Sekiya et al., 1980; Watson et al., 1981). Outflows from a hydrogen-rich atmosphere, consistent with hydrodynamic escape driven by atmospheric heating, have been directly observed during transits of an extrasolar giant planet in close orbit around a solar-type star (Vidal-Madjar et al., 2003).

The heated hydrogen escapes to space, and in the process its outward flow exerts upward drag forces on heavier atmospheric constituents. With powerful energy input, escape fluxes can be large enough to lift species as massive as noble gases out of terrestrial planets atmospheres (Hunten et al., 1987). Lighter species are more readily entrained and lost with the escaping hydrogen, leading to mass fractionation

of the residual atmosphere. Hydrogen escape fluxes high enough to sweep out and fractionate species as heavy as noble gases from terrestrial planets require energy inputs 2 to 3 orders of magnitude greater than presently supplied by solar EUV radiation (Pepin, 1991). The early Sun likely maintained a high EUV luminosity for only several hundred million years (Ribas et al., 2005). Thus, conditions favoring hydrodynamic escape were restricted to early epochs in planetary history. Therefore, the hydrodynamic escape of primordial atmospheres exposed to early strong EUV radiation should be an important process for terrestrial planets' atmosphere as large fractionations of atmospheric components, especially noble gases.

Hydrodynamic escape is one of a few mechanisms that can change the composition of a planetary atmosphere irreversibly (Hunten, 1990). The isotopic fractionation argues for hydrodynamic escape, which is fractionating, while the general deficiencies argue for erosion by impacts as a relatively violent process that does not produce much fractionation (Genda & Abe, 2005). So far, several numerical models have been developed to solve the hydrodynamic escape problem (Watson et al., 1981; Kasting & Pollack, 1983; Tian et al., 2005). Actually, hydrodynamic escape of hydrogen-rich primary atmospheres and outgassed volatile elements from the terrestrial planets, operating in an astrophysical environment for the early solar system inferred from observation of young star-forming regions in the galaxy, can qualitatively account for most of the known details of noble gas distributions in their present day atmospheres (Pepin 1991).

Previous models, however, is unsatisfactory to apply actual atmospheric evolution quantitatively because they cannot solve transonic solutions or multi component solutions. Here I present the first study on the multi component time-dependent hydrodynamic equations for transonic neutral gas escape from planetary atmospheres.

## 2.2 Applicability of Hydrodynamic Escape

In this study, I apply the developed numerical model to the escape of hypothetical early Venusian atmosphere. This numerical code of course can be applied to other terrestrial planets' atmospheres as well as the Venusian atmosphere. Mass fractionation in hydrodynamic escape may have contributed to explain the fractionation pattern of the isotopes of xenon on Earth (Hunten et al., 1987; Sasaki & Nakazawa, 1988; Pepin, 2006) and Mars (Pepin, 1991), the high Martian $^{38}Ar/^{36}Ar$ ratio (Pepin, 2006), and isotopic differences between atmospheric and mantle neon (Sasaki & Nakazawa, 1988; Pepin, 2006). Mass fractionation by hydrodynamic escape could also account for the

observed modest elemental fractionation of the Martian noble gases with respect to Earth (Hunten et al., 1987). However, it cannot easily explain both the elemental and the isotopic fractionations, because the relatively strong isotopic fractionations are incompatible with the relatively weak elemental fractionation, and vice versa. A more precise quantitative study by use of the developed numerical code would give some clear explanations for these elemental and isotopic fractionations.

# Chapter 3

# Previous Numerical Studies of Hydrodynamic Escape

Several analytical and numerical models have been developed previously to solve the hydrodynamic escape problem (e.g., Sekiya et al., 1980; Watson et al., 1981; Kasting & Pollack, 1983; Zahnle & Kasting, 1986; Sasaki & Nakazawa, 1988; Chassefiére, 1996; Tian et al., 2005). However, because a singularity point (where the gas flow velocity equals the sound speed) exists in the transonic time-independent hydrodynamic equations, a self-consistent transonic solution of the time-independent equations cannot be obtained easily.

## 3.1 Analytical Studies

Several models have been developed before to study the hydrodynamic escape from hydrogen-rich planetary atmospheres by solving the time-independent hydrodynamic equations directly. Here, some typical previous studies of hydrodynamic escape by analytical methods are introduced.

Watson et al. (1981) used a trial-and-error method to solve the problem. For a certain value of escape flux, this method calculates the required density and velocity distribution in the steady state. A 10% variation of the mass flux at the critical point can cause a change of density and velocity at the lower boundary by a factor of 10 or more (sometimes more than 4 orders of magnitude). Therefore, it is difficult to find solutions for a pure hydrogen atmosphere using this method as pointed by Kasting & Pollack (1983). Watson et al. (1981) assumed that heating by solar EUV radiation occurred in a single layer. However, because the optical depth depends on the absorption cross-section, the altitude of unity optical depth is not the same for

solar radiation at different wavelengths. In fact, the heating rate distribution has a broad structure (Fox & Dalgarno, 1979; Chassefiére, 1996). Their model and method are too simple to discuss hydrodynamic escape precisely.

Kasting & Pollack (1983) included photochemistry as well as infrared cooling by $H_2O$ and $CO_2$ in a study of the hydrodynamic escape from the atmosphere of early Venus. They developed a numerical method to solve the momentum and the energy equations iteratively. Their model included a self-consistent temperature profile. However, note that their method was limited to subsonic solutions. For most cases of interest, however, the actual outflow would have been transonic. The procedure used by their model is not valid under such circumstances because they neglected nonlinear terms in the momentum equation of the heavier constituent and because the boundary conditions imposed at large distances from the planet are inappropriate for transonic flow.

Chassefiére (1996a) matched the hydrodynamic escape flux to a modified Jeans escape flux at the exobase level and considered the interaction between the solar wind and the early Venusian atmosphere. This model forbids transonic solutions, because the exobase level is set to be below the transonic level. The single-layer heating assumption and the subsonic approximation limit the possibility of a self-consistent study of the hydrodynamic escape of neutral gases from planetary atmospheres.

In either case, developed models are unsatisfactory to apply actual atmospheric evolution of terrestrial planets because they cannot solve transonic solutions exactly. This is the fatal flaw of analytical studies.

## 3.2 Numerical Studies

Tian et al. (2005) developed a numerical model to study the hydrodynamic escape of neutral gas from planetary atmospheres by solving the time-dependent hydrodynamic equations. A robust numerical scheme capable of solving the transonic hydrodynamic escape problem with a distributed energy source is also developed. They presented the first study on the time-dependent hydrodynamic equations for single-component transonic neutral gas escape from planetary atmospheres. However, the hydrodynamic escape model in Tian et al. (2005) contains only one component - hydrogen molecules. As a result, the effects of the existence of other heavier components on the hydrogen hydrodynamic escape process (drag force on the hydrogen escape flow by heavier components, extra heating/cooling by the heavier components, etc.) are

not clear in their studies. Including other heavier gases into the model because of the downward drag force exerted on hydrogen by other gases can further decrease the expected escape rate. One should also include minor species, some of which may be radiatively active, because photochemical simulations to date suggest radiatively active species would be present in the primordial atmospheres of terrestrial planets. Therefore, the model in Tian et al. (2005) cannot solve multi-component hydrodynamic escape precisely. The multi-component numerical model of hydrodynamic escape is absolutely essential for considering the fractionation of noble gases on terrestrial planets as well as the hydrogen escape itself.

From the following chapter, first, I describe the development of numerical code for single-constituent hydrodynamic escape. Then next, I show some validation of the numerical code. Finally, I extend the code to multi-constituent case as a quantitative, self-consistent hydrodynamic escape model that includes the effects of mutual collisions and atmospheric heating/cooling by some constituents.

# Chapter 4

# Single-Component Numerical Model

## 4.1 Basic Equations for Single-Constituent Atmosphere

The singular behavior in the time-independent hydrodynamic equations no longer exists in the time-dependent model, thus allowing the transonic solution to be obtained through time marching to a steady state. My hydrodynamic model is one-dimensional, since a spherically symmetric atmosphere is assumed. The model solves the one-dimensional time-dependent non-viscous Euler equations for a single-constituent atmosphere with thermal conduction in spherical geometry:

$$\frac{\partial}{\partial t}(\rho r^2) + \frac{\partial}{\partial r}(\rho u r^2) = 0 \tag{4.1}$$

$$\frac{\partial}{\partial t}(\rho u r^2) + \frac{\partial}{\partial r}(\rho u^2 r^2) = -\rho G M - r^2 \frac{\partial p}{\partial r} \tag{4.2}$$

$$\frac{\partial}{\partial t}(p r^2) + \frac{\partial}{\partial r}(p u r^2) = (\gamma - 1)\left[-p r^2 \frac{\partial u}{\partial r} - 2 p u r + q r^2 + \frac{\partial}{\partial r}\left(\kappa r^2 \frac{\partial T}{\partial r}\right)\right] \tag{4.3}$$

Here, $\rho$ is the gas density, $r$ is the distance from the planet center, $u$ is the gas flow velocity, $p$ is the pressure, $G$ is the universal gravitational constant, $M$ is the mass of the planet, $\gamma$ is the adiabatic constant, $q$ is the volume heating rate (more details of heating rate are given in section 4.3), $\kappa$ is the thermal conductivity, and $T$ is the temperature, where $T = p/\rho R$ and $R$ is the molar gas constant. $\rho u r^2$ is a measure of the globally integrated escape rate and must be a constant in space in the steady state. $\kappa$ is given by a function of temperature (Watson et al., 1981)

$$\kappa = \kappa_0 \left(\frac{T}{T_0}\right)^s \tag{4.4}$$

where $\kappa_0$ is $4.45 \times 10^4$ [ergs/cm·s·K] (Hanley et al., 1970), $T_0$ is temperature at the bottom of atmosphere, and $s$ is about 0.7 for a primordial atmosphere (Banks & Kockarts, 1973). In practice, these equations are reduced to the following set of equations to be solved by numerical method:

$$\frac{\partial n}{\partial t} + u\frac{\partial n}{\partial r} = -n\frac{\partial u}{\partial r} - \frac{2nu}{r} \tag{4.5}$$

$$\frac{\partial u}{\partial t} + u\frac{\partial u}{\partial r} = -\frac{1}{nm}\frac{\partial p}{\partial r} - \frac{GM}{r^2} \tag{4.6}$$

$$\frac{\partial p}{\partial t} + u\frac{\partial p}{\partial r} = -\gamma p\frac{\partial u}{\partial r} - \frac{2\gamma pu}{r} + (\gamma - 1)q + \frac{\gamma - 1}{r^2}\frac{\partial}{\partial r}\left(\kappa r^2 \frac{\partial T}{\partial r}\right) \tag{4.7}$$

where, $n$ is the number density, $m$ is the mass of the molecule.

If the gas flow velocity is greater than the sound speed, the flow is supersonic. In the case of hydrodynamic escape, the flow is slow at the lower boundary (subsonic) and fast at the upper boundary (usually supersonic). Tian et al. (2005) used Lax-Friedrichs scheme (Toro, 1999; De Sterck et al., 2001) to solve the system. The first order Lax-Friedrichs scheme was used to solve the hydrodynamic equations. To solve the transonic flow, however, the Lax-Friedrichs scheme is not the optimum scheme. I use CIP method (Yabe and Aoki, 1991; Yabe et al., 2001) alternatively which is well suited to solve the transonic flow. Details of the CIP method are given in Appendix A.

When using an explicit time-marching method, the maximum time step is constrained by the CFL condition, which is dependent on the size of the grid cells. The distribution of grid cells in the model is not uniform. The grid size decreases exponentially with decreasing $r$ to compensate for the nearly exponential increase of density near the lower boundary (Keppens & Goedbloed, 1999). A global time step is then determined as the minimum of the local time steps, which can be defined by applying the CFL condition to each grid cell separately. In the numerical model, two ghost cells each are located below the lower and above the upper boundaries. Boundary conditions are imposed in the ghost cells, or the variables are extrapolated linearly to the ghost cells if there is no boundary condition to be imposed. The initial conditions in the numerical model are set so that density is proportional to $r^2$, and velocity is set to be a constant for all grid cells. It is note that the steady state results are insensitive to the initial conditions. Convergence to a steady state is measured

by the normalized difference of all variables between time steps,

$$\Delta = \sqrt{\frac{1}{N_{var}} \sum_{i=1}^{N_{var}} \left[ \frac{1}{N_{grid}} \sum_{grid=1}^{N_{grid}} \frac{\left(\delta_i^{n+1} - \delta_i^n\right)^2}{\left(\delta_i^n\right)^2} \right]} \tag{4.8}$$

Here $n$ represents the time level, $N_{var}$ is the number of variables in the system, and $N_{grid}$ is the number of grid cells in the system. Sensitivity tests show that if the steady state tolerance is set to a value that is not small enough, the steady state solution may not be approached sufficiently (Tian et al., 2005). In the model the steady state tolerance is set at $\Delta = 10^{-5}$.

## 4.2 Energy Deposition of Solar EUV Radiation

Assumption that heating due to solar EUV radiation occurs only in a single layer is not necessarily a good approximation, because the absorption cross-section depends on wavelength. The unity optical depth level occurs at a different altitude for each wavelength. As a result, the energy absorption altitude distribution may have a complicated structure. In the case of Earth's atmosphere, most of the energy is absorbed at altitudes above 1000 km, and the double-peaked feature between $10^3$ and $10^4$ km is caused by the wavelength dependence of the energy deposition (Chassefiére, 1996). The energy deposition levels off and then starts to increase at around $10^5$ km because of the geometric effect (Chassefiére, 1996) of the increasing size of the extended planetary atmosphere. The hydrogen molecule escape rates corresponding to different heating layer positions and energy deposition rates are calculated for the atmosphere of a Earth-like planets, with the lower boundary hydrogen density is set to be $10^{20}$ molecules/m$^3$ (Fig. 4.1). These nonlinear relations between escape rates and the position of the heating layer under the single-layer heating are also shown by Tian et al. (2005). Thus, the escape rates depend on the position of the heating layer as well as on the absolute amount of energy input. It is difficult for a model with a single heating layer to represent this dependence accurately.

For the application to the primordial atmospheres, I assume that the dominant gas in the upper atmosphere is hydrogen and the only energy source to drive the hydrodynamic escape is the solar EUV radiation below 105 nm. The solar EUV spectrum is taken from Woods & Rottman (2002). The spectrum of solar EUV radiation entering the top of the atmosphere is based on a 1994 rocket measurement from 0 to 105 nm (Woods & Rottman, 2002). The absorption cross-section data for

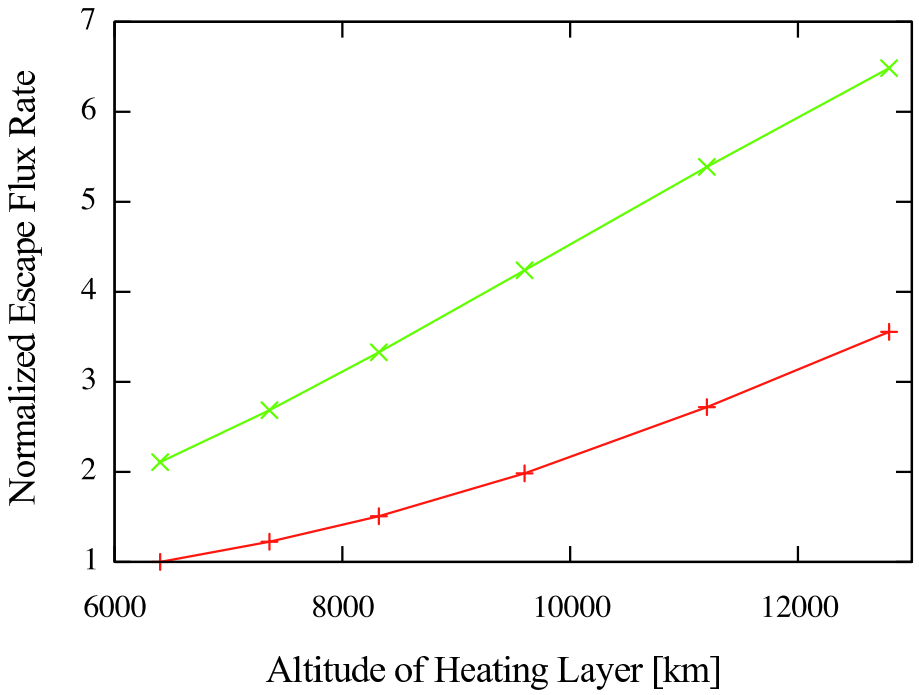


Figure 4.1: Nonlinear relations between escape flux rates and the position of the heating layer under the single-layer heating assumption such as Watson et al. (1981). The escape flux rates are normalized to the value at the bottom of atmosphere (100km). Input EUV energy is double for the upper green line. The nonlinear relation also depends on the amount of input EUV energy.

$H_2$ gas are from Avakyan et al. (1998). In Appendix B.1 and B.2, the data are presented on the spectrum of solar EUV radiation (Woods & Rottman, 2002) and cross-sections of photoabsorption for molecular hydrogen (Avakyan et al., 1998) at 0.1 to 105 nm. The interval numbers are given according to the practice accepted in the aeronomic calculations (Richards et al., 1994). Insignificant Rayleigh scattering is neglected. The same solar spectra and absorption cross-section data are used for all simulations in this paper.

All energy deposition calculations in the literature assume that solar radiation enters the top of the atmosphere isotropically. To account for the angular distribution of solar radiation, the mass path is usually calculated for an average solar zenith angle of about 60° (Kasting & Pollack 1983; Chassefiére, 1996). Although this approach is a good approximation for a thin, plane-parallel atmosphere, it is not appropriate for a dense, extended atmosphere, in which radiative transfer in spherical geometry is needed. Because of the lack of spherical symmetry, the problem of radiative transfer in an extended spherical atmosphere is complicated, and easy analytical expressions are not available (Sobolev, 1975). Then, a two-dimensional energy deposition calculation method (Tian et al., 2005) is adapted to provide a more accurate approximation of the complicated radiative transfer processes in an extended spherical atmosphere. Details of the geometrical consideration are described in Appendix B.3.

Not all energy absorbed by hydrogen molecules will be used to drive hydrodynamic escape flow. Some will be lost to space through thermal emission. Although the thermal emission process is not included in this paper, a heating efficiency ($\eta$) is defined as the percentage of energy absorbed by molecules that is effectively converted into the kinetic energy of the molecules. The heating efficiency was fixed at 15% in Watson et al. (1981) and Tian et al. (2005). I use the same value in this study as the first approximation, where I discuss transonic hydrodynamic escape from the atmosphere of the terrestrial planet. We should discuss in more detail the importance of different heating efficiency values for the simulation results in future work.

The hydrodynamic escape model used in this paper is a simple model, so the temperature is fixed to a constant at the lower boundary. A variation of solar EUV input will probably have an influence on the lower boundary temperature, and thus will have a more complicated impact on the hydrogen escape rate than we have considered. Intuitively a higher temperature will result in a stronger escape flux. Because the temperature, as well as the density at the lower boundary, is influenced by lower atmosphere dynamics and radiative transfer processes, other models working in the

lower part of the atmosphere are required to accurately determine these parameters for the primordial atmospheres. It will be an important future study to include a detailed photochemical model solving the energy absorption, radiation, and net deposition.

## 4.3 Evolution of the Solar Activity

Because of ever accelerating nuclear reactions in its core, the Sun is a slowly evolving variable star that has undergone about 40% increase in luminosity over the last 4.5 Gyr, as predicted by the standard solar evolution model (e.g., Girardi et al., 2000). The fundamental question of whether the Sun has always been a relatively inactive star or, in contrast, has experienced some periods of stronger magnetic activity has a strong impact on the evolution of the solar system. Compelling observational evidence (Güdel et al., 1997) shows that zero-age main-sequence solar-type stars rotate over 10 times faster than today's Sun. As a consequence of this, young solar-type stars, including the young Sun, have vigorous magnetic dynamos and correspondingly strong high-energy emissions. Simon et al. (1985), and others showed that the Sun loses angular momentum with time via magnetized winds (magnetic braking), thus leading to a secular increase of its rotation period (Durney, 1972). In response to slower rotation, the solar dynamo strength diminishes with time, causing the Sun's high-energy emissions also to undergo significant decreases.

"The Sun in Time" program (Dorren & Guinan, 1994) was established some 20 years ago to study a sample of accurately selected solar proxies (G0-G5 V stars) with different ages across the electromagnetic spectrum. The Sun in Time sample contains nearby single (or widely separated binary) G0-G5 stars that have known rotation periods and well-determined temperatures, luminosities, and metallicities. In addition, we have been able to estimate the stellar ages using their memberships in clusters and moving groups, rotation period-age relationships, and, for the older stars, fits to stellar evolution models. Data from the following space missions have been used in the present study: the Advanced Satellite for Cosmology and Astrophysics (*ASCA*), the Rontgen Satellite (*ROSAT*), the Extreme Ultraviolet Explorer (*EUVE*), the Far Ultraviolet Spectroscopic Explorer (*FUSE*), the Hubble Space Telescope (*HST*), and the International Ultraviolet Explorer (*IUE*). Ribas et al. (2005) present the results of the investigation of the long-term magnetic history of the Sun focusing on the high-energy emissions using the data obtained with the *ASCA*, *ROSAT*, *EUVE*, *FUSE* and *IUE* satellites from a homogeneous sample of single nearby G0 V main-sequence stars

Table 4.1: Integrated Fluxes

| $\lambda$ Interval (Å) | 0.10Gyr | 0.30Gyr | 0.65Gy | 1.6Gyr | 4.56Gyr | 6.7Gyr |
|---|---|---|---|---|---|---|
| 1-20 | 180.2 | 21.5 | 7.76 | 0.976 | 0.15 | 0.048 |
| 20-100 | 82.4 | 14.8 | 10.7 | 2.80 | 0.70 | 0.321 |
| 100-360 | 187.2 | 69.4 | 22.7 | 7.7 | 2.05 | 1.37 |
| 360-920 | 45.6 | 15.2 | 7.0 | 2.85 | 1.00 | 0.68 |
| 920-1180 | 18.1 | 8.38 | 2.90 | 1.70 | 0.74 | 0.50 |

*Note.* Units of fluxes are [erg/cm$^2$s]. The data are normalized to a distance of 1AU and to the radius of a 1 $M_\odot$ star, and scaled (using a simple radius-squared relationship) to the expected radius of the Sun at the star's age (Ribas et al., 2005). The intervals considered are 1-20 Å(*ASCA*), 20-100 Å(*ROSAT*), 100-360 Å(*EUVE*), and 920-1180 Å(*FUSE*). The fluxes in 360-920 Åare calculated from the observed solar flux.

which have known rotation periods and well-determined physical properties, including temperatures, luminosities, metal abundances and ages. The resulting stellar fluxes are presented in Table 4.1.

From the data from these space missions, we can plot the total integrated fluxes and a power-law fit that yields an excellent fit to the data (Ribas et al., 2005). In the complete wavelength interval, which is frequently used in aeronomy calculations, the flux ($F$ [ergs/cm$^2$s]) as a function of stellar age ($\tau$) is accurately reproduced by the expression

$$F = \alpha\tau^{\beta} \tag{4.9}$$

where the stellar age $\tau$ is in gigayears. Parameters of the power-law, $\alpha$ and $\beta$, are presented in Table 4.2. Also illustrative is the plot in Figure 4.2, which represents the stellar fluxes transformed into the values at Venus orbit normalized to the current solar values as a function of age. The steeper decrease of the higher energy emissions is evident in this plot. Also note that the emissions of the youngest stars in all wavelength intervals are orders of magnitude larger than the current solar flux. I use the power-law fits of solar fluxes to estimate the energy deposition by solar EUV heating in numerical calculations.

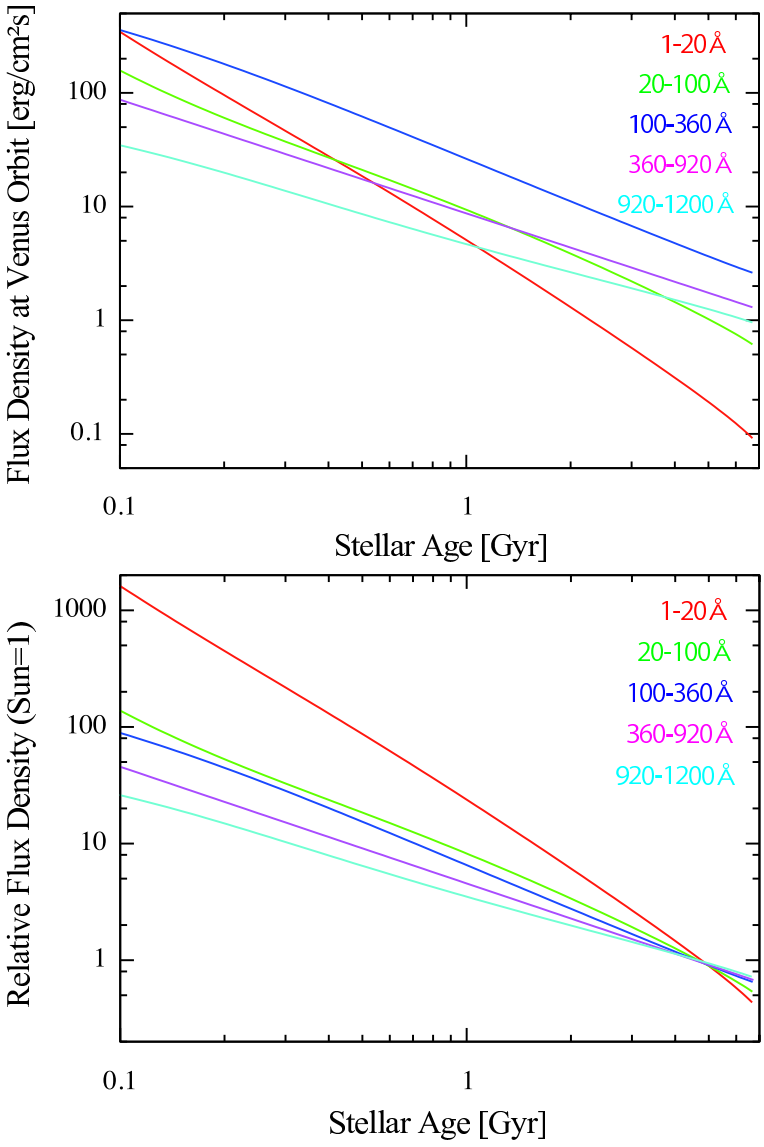


Figure 4.2: (top) Smoothed fits to the integrated irradiances in Table 4.1 for different wavelength intervals. The flux density is transformed into the values at Venus orbit. The parameters of the resulting power-law best-fitting relationships are given in Table 4.2. (bottom) Present solar-normalized fluxes vs. age for different stages of the evolution of solar-type stars for different wavelength intervals.

Table 4.2: Parameters of the Power-Law Fits to the Measured Integrated Fluxes

| $\lambda$ Interval (Å) | $\alpha$ | $\beta$ |
|---|---|---|
| 1-20 | 2.40 | -1.92 |
| 20-100 | 4.45 | -1.27 |
| 100-360 | 13.5 | -1.20 |
| 360-920 | 4.56 | -1.00 |
| 920-1180 | 2.53 | -0.85 |

# Chapter 5

# Validation of Numerical Model

## 5.1 Validation in an Isothermal Atmosphere

The solution technique is validated in an isothermal atmosphere, polytropic atmosphere, and adiabatic atmosphere. Here I validate my solution technique against analytical solutions for an isothermal atmosphere. Similar validation test can be found in Keppens & Goedbloed (1999) and Tian et al. (2005). In an isothermal atmosphere, Eq. (4.5)-(4.7) can be reduced to the density and the momentum equations. An analytical solution with a nonzero velocity distribution is available (Parker, 1964). Details of the analytical solution are described in Appendix C.1. Figure 5.1 shows that the resulting velocity of numerical solution is a good approximation to that of the analytical Parker solution with a few percent uncertainty (The numbers of grid cell are set to 1000).

In the numerical model, the density is imposed, and the mass flux is extrapolated at the lower boundary. The ratio of the gravitational potential energy and the molecular kinetic energy is important to identify the dynamic characteristics of the escape. The traditional Jeans escape parameter is defined by parameters at the exobase level. In an atmosphere in which hydrodynamic escape occurs, the location of the exobase is unknown prior to the simulations, so we define the hydrodynamic escape parameter (HEP) using the parameters at the lower boundary level: HEP $= GMm/r_0kT_0$, where $k$ is Boltzmann's constant, and $r_0$ and $T_0$ are the values of $r$ and $T$ in Eq. (4.5)-(4.7) at the lower boundary, respectively. When the kinetic energy of molecules is comparable to their gravitational potential energy, the HEP value is small and the escape flow is strong. When the gravitational energy is much larger than the kinetic energy, the HEP is large and the escape flow is weak.

Figure 5.2 shows that for different HEP values, the analytical solutions are approached increasingly well by the numerical solutions when the number of grid cells

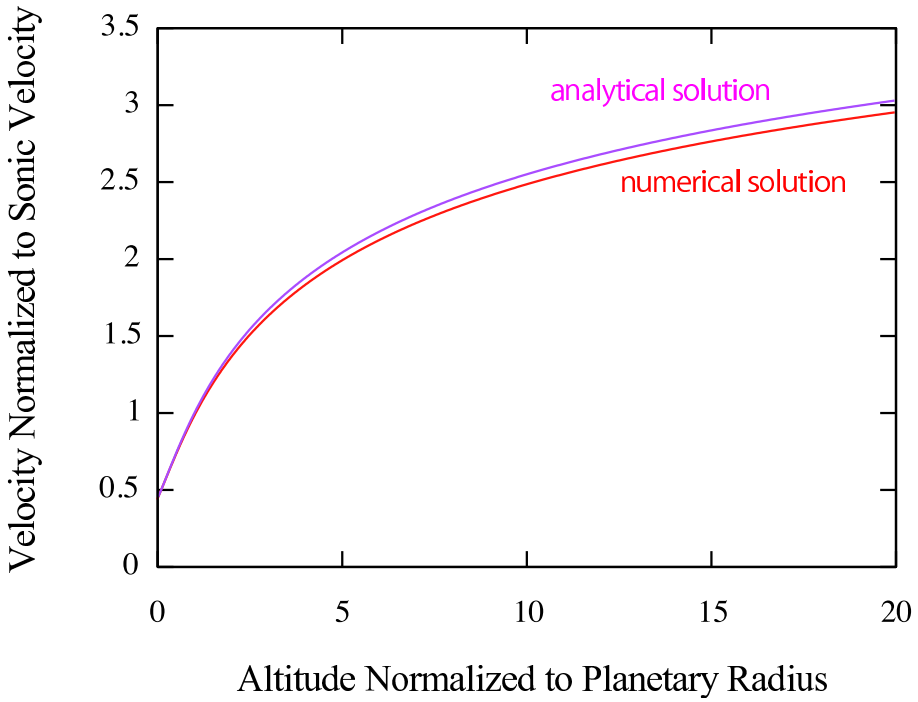


Figure 5.1: Comparison between the numerical solution and the analytical solution of velocity for the HEP = 5 case in an isothermal atmosphere.

is increased. In the case of hydrogen-dominated atmospheres, the simulation process is concluded if the escape rate in the steady state does not change by more than 10% when the number of grid cells is doubled. In this study, the number of grid cell is set to 3000, which presents enough resolution to consider the Venus' problem (Chapter 8 and 9).

Figure 5.3 shows that the normalized difference of all variables between time steps (Eq. (4.8)) converge a steady value in a few months. This means that it takes only a few months from the initial state to converge a steady value.

These simulations of an isothermal atmosphere produce a good approximation of the steady state hydrodynamic escape rate and large-scale atmospheric structure in a short timescale.

## 5.2 Validation in a Polytropic/Adiabatic Atmosphere

Next, I validate my solution technique against analytical solutions for polytropic atmosphere and adiabatic atmosphere. In a polytropic atmosphere, Eq. (4.7) can be

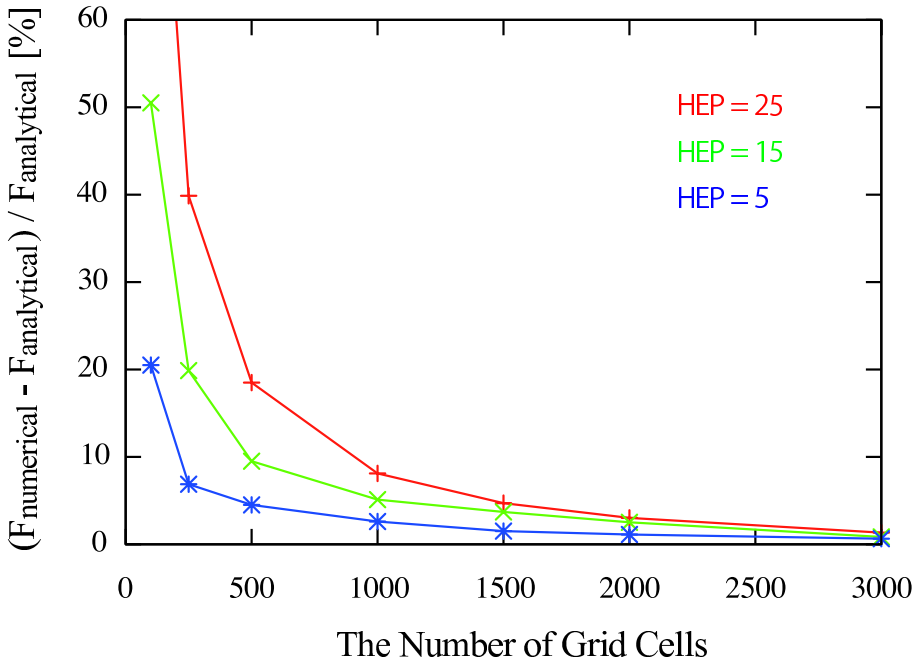


Figure 5.2: Comparison between the numerical solution and the analytical solution of flux. Analytical solutions of hydrodynamic escape from an isothermal atmosphere are approached when the number of grid cells is increased. The vertical axis is the relative deviation of the escape flux in the numerical solution compared with that in the analytical solutions for different HEP values.

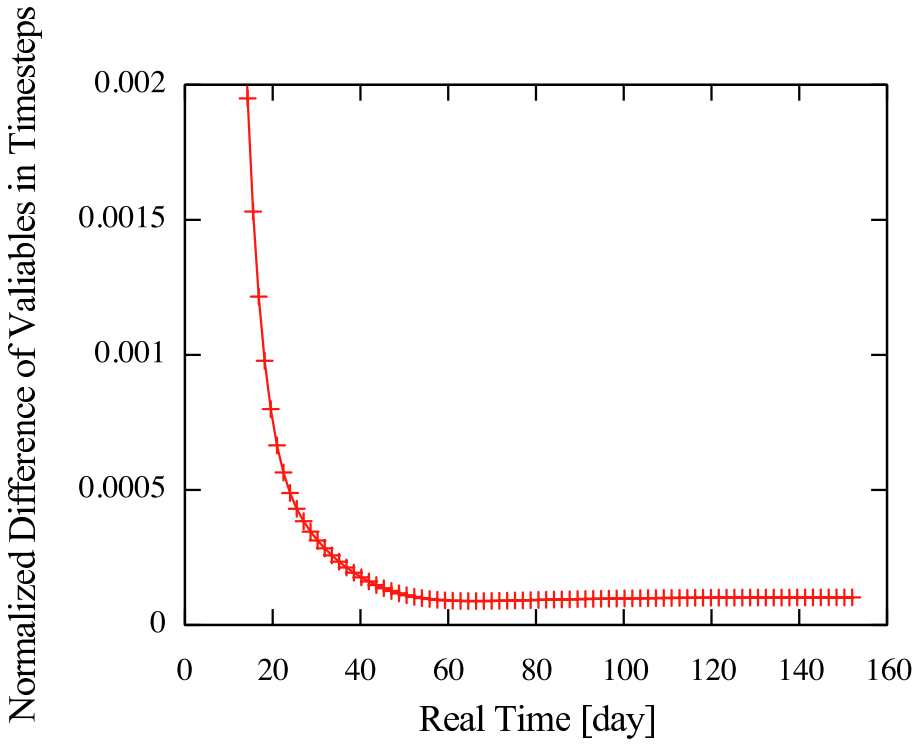


Figure 5.3: Normalized difference of all variables between time steps for the HEP = 5 case in an isothermal atmosphere.

replaced by the polytropic relation

$$T = T_0 \left(\frac{n}{n_0}\right)^{\alpha-1} \tag{5.1}$$

where $\alpha$ is the polytropic index. In the special case of adiabatic outflow of an ideal gas, $\alpha = c_p/c_v$. With the polytropic assumption, Euler equations can be solved quasi-analytically. Details of the quasi-analytical solution are described in Appendix C.2. Figure 5.4 shows that the resulting density, velocity, and temperature of numerical solution are good approximations to those of the quasi-analytical solution.

In an adiabatic atmosphere, the volume heating rate $q$ in Eq. (4.7) is zero. Figure 5.5 shows that the resulting density, velocity, and temperature of numerical solution for adiabatic atmosphere are very good much with those for polytropic atmosphere in the case of $\alpha = c_p/c_v$.

These validation results show that the numerical method is capable of accurately solving equation (4.1)-(4.3) for transonic flows.

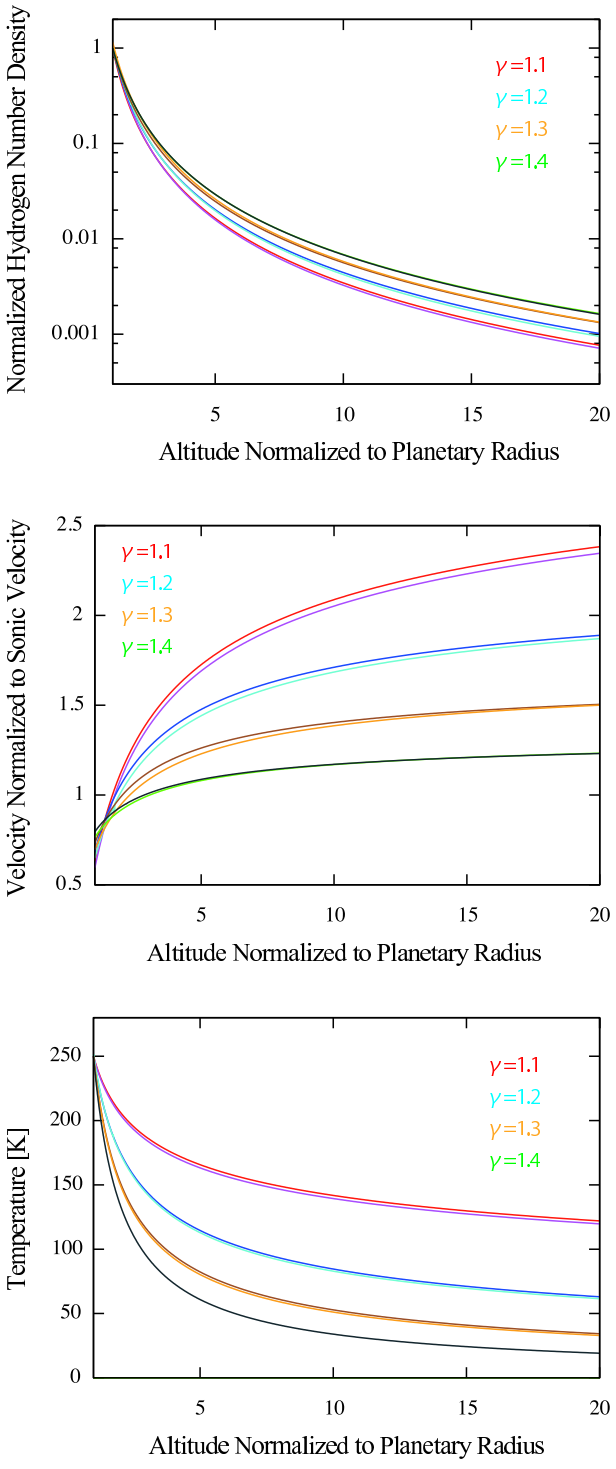


Figure 5.4: Comparison between the numerical solutions and the quasi-analytical solutions of polytropic atmosphere for different polytropic index. Normalized hydrogen number density, normalized velocity, and temperature are shown from above to bottom. Polytropic indices are 1.1 (red, purple), 1.2 (blue, cyan), 1.3 (yellow, brown), and 1.4 (green, black).

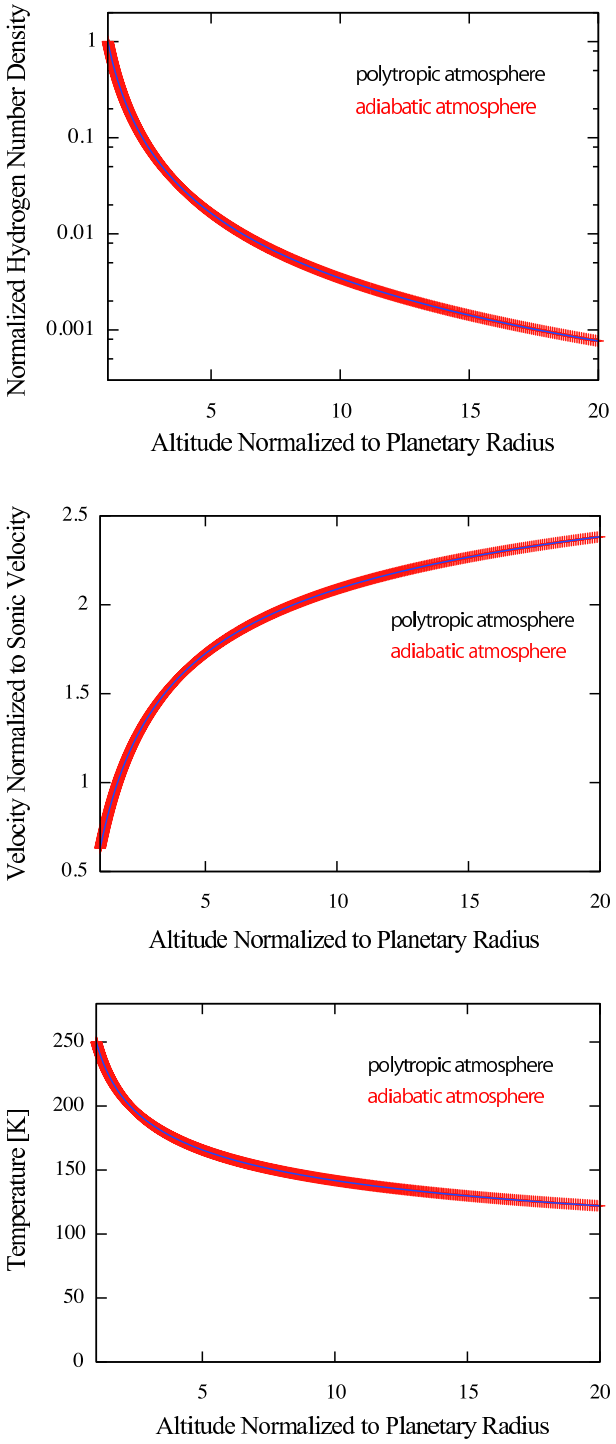


Figure 5.5: Comparison between the numerical solutions of polytropic atmosphere and adiabatic atmosphere. Normalized hydrogen number density, normalized velocity, and temperature are shown from above to bottom. Polytropic index is 1.1. Adiabatic solutions are shown by broad red lines for convenience of comparison of two lines.

# Chapter 6

# Multi-Component Numerical Model

Hydrodynamic escape of hydrogen from a planetary atmosphere can remove heavier gases, which can be dragged along with the escaping hydrogen (Hunten et al., 1987). The heated hydrogen escapes to space, and in the process its outward flow exerts upward drag forces on heavier atmospheric constituents. Figure 6.1 illustrates the mechanism of that for an atmosphere heated at high altitude by intense EUV radiation. Collisions of outward bound $H_2$ molecules with other atmospheric constituents exert net upward drag forces on them. Equilibrium between this upward drag and gravity leads to an increased average height for these species. However, if the $H_2$ escape flux is large enough, drag wins for Ne and it is entrained with the escaping $H_2$ and swept out of the atmosphere; progressively higher fluxes also remove Ar, Kr, and Xe. Under a constant $H_2$ escape flux, lighter species are more readily entrained and lost with the escaping hydrogen, leading to mass fractionation of the residual atmosphere. The importance of hydrodynamic escape, in the context of observed noble gas isotope distribution, is that it can implement loss and fractionation of species more massive than Ne which could not escape so much on their own by classical processes such as Jeans escape (Chamberlain & Hunten, 1987).

## 6.1 Extension of Hydrodynamic Escape Code

The one-dimensional time-dependent nonviscous hydrodynamic equations for each component in a multi-constituent atmosphere with thermal conduction in spherical geometry are deviated from Eq. (4.5)-(4.7):

$$\frac{\partial n}{\partial t} + u\frac{\partial n}{\partial r} = -n\frac{\partial u}{\partial r} - \frac{2nu}{r} \tag{6.1}$$

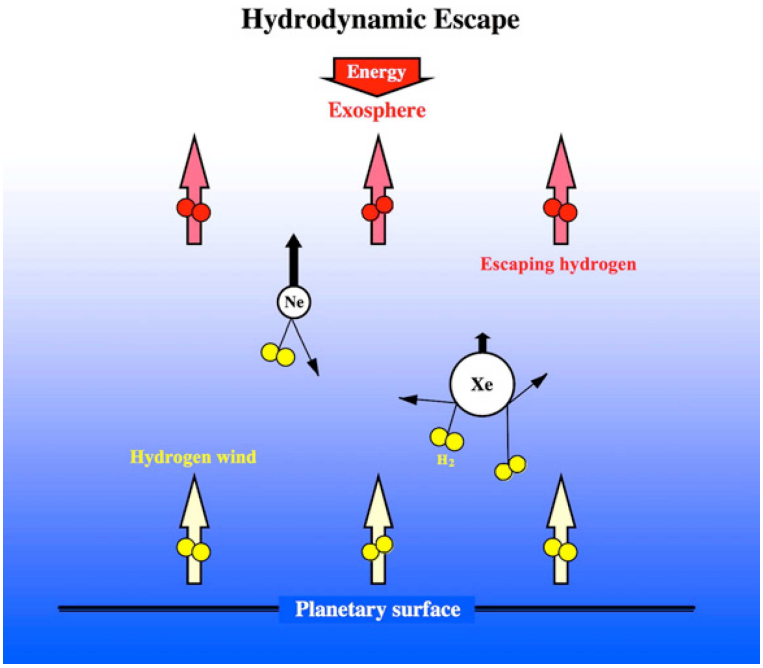


Figure 6.1: Hydrodynamic escape in a hydrogen-rich primordial planetary atmosphere, illustrated for input of external energy at high altitudes. Exospheric $H_2$ is heated to escape velocity by adsorption of strong solar EUV radiation. Escaping hydrogen is replenished by rising hydrogen wind. Collisions of outward bound $H_2$ molecules with other atmospheric constituents (illustrated here for Ne and Xe) exert net upward drag forces on them. This figure is after Fig. 4 in Pepin (2006).

$$\frac{\partial u}{\partial t} + u\frac{\partial u}{\partial r} = -\frac{1}{nm}\frac{\partial p}{\partial r} - \frac{GM}{r^2} + \sum_x \left[(u_x - u)n_x k_i - \frac{\alpha_T k}{m}\left(\frac{n_x}{n_x + n}\frac{\partial T}{\partial r}\right)\right] \quad (6.2)$$

$$\frac{\partial p}{\partial t} + u\frac{\partial p}{\partial r} = -\gamma p\frac{\partial u}{\partial r} - \frac{2\gamma p u}{r} + (\gamma - 1)q + \frac{\gamma - 1}{r^2}\frac{\partial}{\partial r}\left(\kappa r^2 \frac{\partial T}{\partial r}\right) \quad (6.3)$$

where, physical quantities labeled with subscript $x$ means the corresponding quantities for the other constituents besides itself. In the momentum equation, the effects of collisions with other species are included in the last two terms (Zahnle & Kasting, 1986). The first of these accounts for the transfer of momentum from one mean flow to the other; the parameter $k_i$ stands for the momentum transfer collision rate. The last term accounts for thermal diffusion; $\alpha_T$ is the thermal diffusion factor, and $k$ is Boltzmann's constant. In Table B.3, the relevant binary diffusion coefficients are collected. The binary diffusion coefficient $b_i$ is identified with the quantity $kT/mk_i$. Thermal diffusion concentrates the heavier constituent at lower temperatures. Thus it aids escape if temperature drops with altitude; it hinders escape for positive temperature gradients. The thermal diffusion factor $\alpha_T$ is given by some references (Mason et al., 1966; Chapman & Cowling, 1970). However, the inclusion of thermal diffusion is not expected to have a large impact on calculation actually. On the other hand, the fact that $b_i$ is itself temperature dependent can have a much larger effect.

## 6.2 Crossover Mass

Here, it is convenient to define the crossover mass $m_c$ between hydrogen and component $x$ as follows (Hunten et al., 1987):

$$m_c = m_{\mathrm{H_2}} + \frac{kTF_{\mathrm{H_2}}}{b_i g X_{\mathrm{H_2}}} \quad (6.4)$$

where, $m_{\mathrm{H_2}}$ is the mass of hydrogen, $k$ is the Boltzmann constant, $T$ is the temperature, $F_{\mathrm{H_2}}$ is the flux of hydrogen, $b_i$ is the binary diffusion coefficient between hydrogen and component $x$, $g$ is the acceleration due to gravity, and $X_{\mathrm{H_2}}$ is the mole fraction of hydrogen. For $m_x = m_c$ ($m_x$ is the mass of component $x$), the composition is still independent of height; the drag terms are just sufficient to equalize the density scale heights, but not to lift constituent $x$ out of the atmosphere (Hunten, 1973, 1985). If $m_x$ is greater than $m_c$, then the flux of component $x$ remains zero, but the density scale heights are no longer the same. For masses smaller than the crossover mass, constituent $x$ is swept out of the atmosphere with a flux proportional to the mole fraction and linearly varying with mass. This behavior is easily understood in terms of the competition between the downward weight of an atom or molecule and

the upward drag force, which has been taken to be independent of mass by the assumption of a universal value for $b_i$. At the crossover mass, the two forces are equal; lighter masses feel a net upward force, and heavier ones a downward force.

It is note that the crossover mass is the approximate solution. A more complete treatment of the problem would replace the solution of hydrodynamic equation. However, Zahnle & Kasting (1986) considered a more general case, and verify it is a good approximation for escape of a trace constituent provided that

$$\frac{m_c - m_x}{m_c - m_{\mathrm{H_2}}} > \frac{m_{\mathrm{H_2}}}{m_x} \tag{6.5}$$

which shows that the expressions of crossover mass are nearly correct when the difference in the masses of the two constituents is large. A similar argument is derived by Sasaki & Nakazawa (1988). For noble gases escaping in a hydrogen-dominated atmosphere, Eq. (6.4) is good for Ne, Ar, Kr, and Xe; it is less good for He because He is only weakly bound in terrestrial planet atmospheres and escape readily by hydrodynamic escape itself or by other processes. So I use the crossover mass for relatively heavy elements to roughly estimate the minimum required flux of hydrogen for Venusian atmosphere (chapter 8 and 9).

# Part II

# Application to the Early Venusian Atmosphere

# Chapter 7

# Introduction to the Problems

## 7.1 Introduction to Water Loss from Early Venus

Venus is free of oxygen but it is thought to have contained a primordial water ocean, giving rise to a dense steam atmosphere and a subsequent strong greenhouse effect. On the basis of the analysis of the Pioneer Venus large-probe neutral mass spectrometer data it was found that Venus' atmosphere is enriched in D over H relative to Earth by a factor of about 120±40 (de Bergh et al., 1991). They report a D/H ratio in the Venus clouds of $(1.6 \pm 0.2) \times 10^{-2}$, or about 100 times higher than the terrestrial value of $1.56 \times 10^{-4}$. If Venus and Earth had similar D/H ratios initially, this implies that Venus must have started out with at least 100 times as much water as is now present.

Geiss & Reeves (1981) have suggested that this isotopic fractionation is a result of low-temperature equilibrium reactions between gaseous and condensed phases in interstellar space prior to the formation of the solar nebula. Thus, the simplest solution is to assume that the initial D/H ratio on Venus was equal to the present value. However, theories of planetary formation indicate that any large spatial gradient of isotopic fractionation should have been smoothed out due to mixing during the accretion phase (Wetherill, 1981). And $H_2O$ could have been present also on early Venus in approximately terrestrial amounts. So, lacking a plausible chemical separation mechanism during the formation phase of the planetary atmospheres which would favor a water-rich early Earth and very dry Venus, one can hypothesize that early Venus may have had a comparable $H_2O$ inventory as the Earth.

So we should consider a hypothesis that the present lack of water is supposed to be due to photodissociation of $H_2O$ followed by thermal escape of H at early stage. Matsui & Abe (1986) and Abe & Matsui (1986) showed that due to thermal blanketing during the first $10^8$ years of a planet's life, temperatures as high as 1500 K might

be reached in the steam atmosphere heated by impacts. A part of $H_2O$ is dissolved in a hypothesized magma ocean. In the following cooling phase, $H_2O$ condenses and a water ocean is formed. The climate models of Kasting (1988) indicated that the runaway greenhouse effect occurs under these conditions nearly independently of the amount of $CO_2$ in the atmosphere. At high temperature, water vapor may be present in large amounts in the thermosphere and hydrodynamic escape of H, produced by photodissociation of $H_2O$, quite efficient. Ingersol (1969) has found that if the $H_2O$ mixing ratio at the mesopause exceeds a value of about 0.1, water vapor would have remained a major atmospheric species up to altitudes where it could be photodissociated and atomic hydrogen became the main species which could escape hydrodynamically. The atmosphere at this time was therefore rich in water vapor, yielding H and $H_2$ by photodissociation.

Part of the oxygen can be dragged off to space along with the escaping hydrogen, but if not, or if O escape is only partial, an $O_2$-rich atmosphere can accumulate during the early history of the planet. On the other hand, we know that there are negligible quantities of $O_2$ in the present Venus atmosphere. The lack of oxygen on Venus is puzzling. So, in the first instance, to pursue the idea if all oxygen can be escaped by $H_2$ drag in a quantitative fashion, one must examine in detail the processes by which hydrogen has escaped to space.

In chapter 8, I apply the developed numerical model to the escape of hypothetical early Venusian atmosphere to consider the water loss from early Venus.

## 7.2 Introduction to Fractionation of Noble Gases on Venus

How and from what sources the atmospheres of Earth, Mars and Venus formed, and how they evolved to their present states, are classic problems in the planetary sciences. Carbon dioxide is the principal species on Mars and Venus; on Earth, it's nitrogen. One might expect that these "sister" planets, not very different in mass or distance from the sun, would have acquired similar primordial atmospheres in their youth and followed similar evolutionary paths to the present. These primordial atmospheres were probably acquired in the same way from the same reservoir, not surprising for two planets with comparable masses and heliocentric distances. However, the difference between Venus and the other two sister planets is clearly demonstrated.

Table 7.1 lists the elemental abundances of noble gases, hydrogen, and carbon in solar, meteorites, comets, and atmospheres of the terrestrial planets and known

Table 7.1: Elemental Abundances in Solar, Meteorites, Comets and Terrestrial Planet Atmospheres and Known Crustal Reservoirs

| | $^{1}$H | $^{12}$C | $^{20}$Ne | $^{36}$Ar | $^{84}$Kr | $^{130}$Xe |
|---|---|---|---|---|---|---|
| Solar[a] | 7.58 (-01) | 3.90 (-03) | 1.56 (-03) | 8.97 (-05) | 5.84 (-08) | 8.07 (-10) |
| Meteorites | | | | | | |
| CI chondrites[b] | 6.68±0.83 (-03) | 3.7±0.70 (-02) | 2.89±0.77 (-10) | 1.25±0.10 (-09) | 3.57±0.15 (-11) | 7.0±1.9 (-12) |
| E chondrites[c] | | 4.2±1.6 (-03) | 2.0±2.0 (-11) | 3.3±2.8 (-10) | 3.0±2.7 (-12) | 4.1±2.9 (-13) |
| Comets[d] | 6.8±1.5 (-02) | 1.7±0.3 (-01) | $<$ 6.2 (-07) | 3.4 (-05) | 2.6 (-06) | 9.5 (-09) |
| Planets | | | | | | |
| Earth[e] | 3.10 (-05) | $1.0^{+0.7}_{-0.6}$ (-05) | 1.00±0.01 (-12) | 3.45±0.01 (-11) | 1.66±0.02 (-12) | 1.40±0.02 (-14) |
| Venus[f] | | 2.60±0.04 (-05) | 2.9±1.3 (-10) | 2.51±0.97 (-09) | $4.7^{+0.6}_{-0.4}$ (-12) | $8.9^{+2.5}_{-6.8}$ (-14) |
| Mars[g] | | 1.11±0.20 (-08) | 4.38±0.34 (-14) | 2.16±0.43 (-13) | 1.76±0.10 (-14) | 2.08±0.27 (-16) |

*Note.* Powers of ten multipliers in parentheses.

[a] Average of data from Cameron (1982) and Anders & Ebihara (1982).

[b] Kerridge (1985) for hydrogen and carbon; Mazor et al. (1970) for noble gases.

[c] Grady et al. (1986) for carbon; Crabb & Anders (1981) for noble gases.

[d] Delsemme (1988) and Dauphas & Marty (2002) for hydrogen and carbon in comets; Owen et al. (1992), Bar-Nun & Owen (1998), and Dauphas (2003) for measurements of noble gases trapped in amorphous water ice (55K).

[e] Rubey (1951) for hydrogen (from $H_2O$); Walker (1977) for carbon (uncertainties include the lower estimate of Rubey (1951) and the higher estimate of McElroy et al. (1977)).

[f] von Zahn et al. (1983) for carbon, neon, and argon; Donahue & Pollack (1983) for krypton; Donahue (1986) for xenon.

[g] Owen et al. (1977) Viking data for carbon; average of data from Wiens et al. (1986) and Swindle et al. (1986) for neon; Wiens et al. (1986) for argon; average of data from Becker & Pepin (1984) and Swindle et al. (1986) for krypton and xenon.

Table 7.2: Elemental Abundances Normalized by Averaged Solar Abundances

| | $^{1}$H | $^{12}$C | $^{20}$Ne | $^{36}$Ar | $^{84}$Kr | $^{130}$Xe |
|---|---|---|---|---|---|---|
| Solar | 1 | 1 | 1 | 1 | 1 | 1 |
| Meteorites | | | | | | |
| CI chondrites | 8.81±1.09 (-03) | 9.5±1.8 (0) | 1.85±0.49 (-07) | 1.39±0.11 (-05) | 6.11±0.26 (-04) | 8.7±2.4 (-03) |
| E chondrites | | 1.1±0.4 (0) | 1.3±1.3 (-08) | 3.7±3.1 (-06) | 5.1±4.6 (-05) | 5.1±3.6 (-04) |
| Comets | 9.0±2.0 (-02) | 4.4±0.8 (+01) | $<$ 4.0 (-04) | 3.8 (-01) | 4.5 (+01) | 1.2 (+01) |
| Planets | | | | | | |
| Earth | 4.09 (-05) | $2.6^{+1.8}_{-1.5}$ (-03) | 6.41±0.06 (-09) | 3.85±0.01 (-07) | 2.84±0.03 (-05) | 1.73±0.02 (-05) |
| Venus | | 6.67±0.10 (-03) | 1.9±0.8 (-07) | 2.80±1.08 (-05) | $8.0^{+1.0}_{-0.7}$ (-05) | $1.1^{+0.3}_{-0.8}$ (-04) |
| Mars | | 2.85±0.51 (-06) | 2.81±0.22 (-11) | 2.41±0.48 (-09) | 3.01±017 (-07) | 2.58±0.33 (-07) |

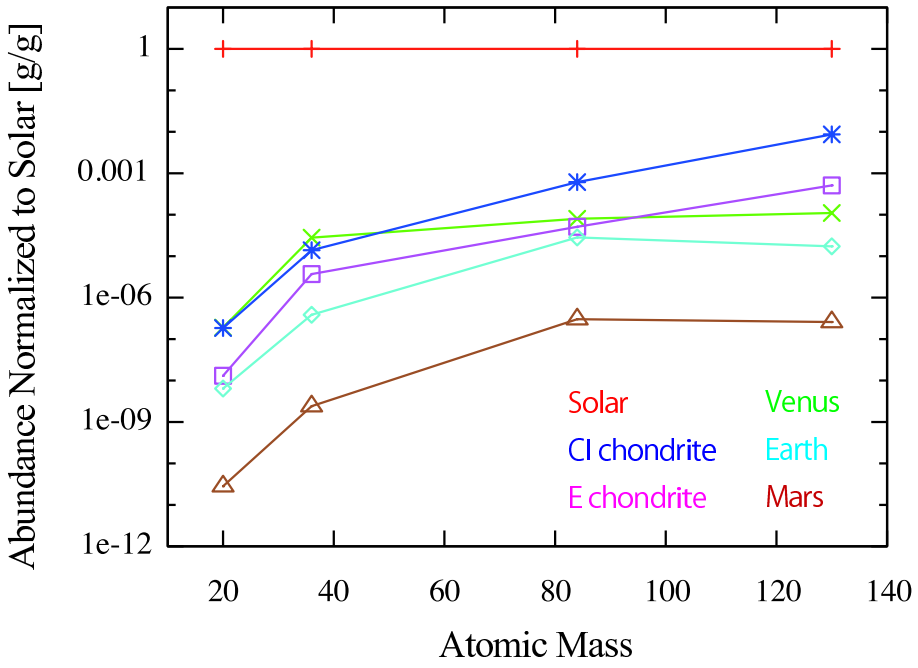


Figure 7.1: Relative abundances of noble gases in meteorites and the terrestrial planet atmospheres with respect to solar abundances. All the data used in this figure are listed in Table 7.2

crustal reservoirs (Pepin (1991) and references therein). The solar abundance represents the nebula one. The hydrogen and carbon contents on the atmospheres of the terrestrial planets are important as well as noble gases, because they are major components of the atmospheres of the terrestrial planets in the forms of CO, $CO_2$, $H_2O$, and so on. Table 7.2 lists the elemental abundances normalized by averaged solar abundance, and Figure 7.1 is plotted from the noble gases' values listed in Table 7.2. On Venus, not only is the heavy noble gas abundance pattern different from that on Earth and Mars, but also the abundances of both argon and neon are remarkably high (Fig. 7.1).

Free from the entanglements of chemical interactions, compositions of noble gasses are clues to the characteristics of their source reservoirs, and are ideal recorders of mass fractionations imprinted by physical processing such as escape from planetary gravitational fields. Information of noble gasses abundances for Venus comes from atmospheric measurements by mass spectrometers on the Venera and Pioneer Venus spacecraft (Wieler, 2002). Venus may have lost some Ne, since it is enriched about 10% in $^{22}Ne/^{20}Ne$ with respect to solar abundances. On the other hand, Venus appears to have lost no Ar, as indicated by near solar $^{36}Ar/^{84}Kr$ and $^{38}Ar/^{36}Ar$ ratios (Pepin, 1991). Nonradiogenic argon ($^{36}Ar$, $^{38}Ar$) is extremely abundant on Venus

compared to Earth. On a gram per gram basis, $^{36}$Ar is more abundant on Venus than in all but a few of the most gas-rich meteorites (Pepin, 1991).

In chapter 9, I apply the developed numerical model to the escape of hypothetical early Venusian atmosphere to consider the fractionation of noble gases on Venus.

Note that the assumed atmospheres in chapters 8 and 9 are different ones. The assumed atmosphere in chapter 8 consists of only dissociated $H_2O$, i.e., the abundance ratio of hydrogen and oxygen is about 1:1. The case that hydrogen, which would be originated from solar nebula and/or degassing atmosphere, is much more abundant than oxygen is not considered in this study. On the other hand, the assumed atmosphere in chapter 9 consists of hydrogen as a major component and noble gases as minor components. And CO is treated as a parameter (minor component to major component). Therefore, these two problems are treated independently in this study.

# Chapter 8

# Water Loss from Early Venus

## 8.1 Previous Studies

Watson et al. (1981) have investigated hydrodynamic escape from Venus under the assumption that the upper atmosphere consisted of pure molecular hydrogen. They found that XUV-driven energy-limited hydrodynamic conditions would have resulted in the upper limit of the hydrogen escape flux of about $10^{12}$ /cm$^2$s. Such an escape flux would evacuate the amount of a terrestrial water ocean in about 280My. However, Kasting & Pollack (1983) has pointed out that their calculation had several weak points. The escape flux calculated from their model depends sensitively upon the number density of hydrogen, which is treated essentially as a free parameter. Clearly, if one wishes to calculate the actual escape rate instead of simply an upper bound one must construct a model, which calculates thermospheric hydrogen densities self-consistently.

The hydrodynamic escape of hydrogen from Venus has been studied by Kasting & Pollack (1983) through a detailed one-dimensional photochemical-dynamic model of the high atmosphere. Their escape flux is approximately four times lower than the energy-limited flux calculated by Watson et al. (1981), because it is source limited at the base of the expansion. Kasting & Pollack (1983) showed that if water vapor was a major constituent of Venus' upper atmosphere, an amount of hydrogen comparable to that contained in Earth's oceans could have escaped over a time span of no more than a few hundred million years. They indicated, however, some of the oxygen left behind from the escape of hydrogen, and they would be consumed by oxidation of surface minerals. And then, by considering that H primitive escape is limited by available solar EUV energy, Chassefiére (1996) have confirmed the finding by Kasting & Pollack (1983), showing that planets like Venus or Mars are unlikely to have lost an important fraction of their oxygen, swept away together with hydrogen. However,

their models are not valid for a transonic flow; and the actual outflow would have been transonic. On the other hand, Zahnle & Kasting (1986) addressed the problem with a hydrodynamic escape model similar to that developed by Kasting & Pollack (1983) but eliminating that model's most obvious deficiencies, especially the assumption of subsonic flow. They concluded that substantial quantities of water may have been lost without the need to oxidize large amounts of the crust, which is contrast to Kasting & Pollack (1983).

As described above, many studies have been done to examine the problem "Water loss from early Venus" so far. However, their solutions to this problem are to abandon the goal of finding the exact critical solution and to simply approximate it as closely as possible by following subsonic paths. And their quantitative uncertainties cause their conclusions of this problem to be all different each other. This problem should be solved by use of the numerical method to derive the precise quantitative solution. In Part I, I succeeded in developing the numerical code of multi-component hydrodynamic escape for the first time. So, in this chapter, I apply the numerical code to consider the water loss problem, and determine whether the complete water loss from early Venus can be achieved or not.

## 8.2 Numerical Model

The model and the energy calculation method are applied to the atmosphere of a Venus-like planet in which the thermosphere is composed only of hydrogen and oxygen molecules. The lower boundary is fixed at approximately the altitude of the homopause (100km), and the lower boundary temperature is fixed at 330 K. The upper boundary is at an altitude of roughly 50000 km. The solar EUV radiation flux is set to four cases (0.05, 0.1, 0.5, 1.0 [Gyr]). I assume that hydrogen is the only energy reservoir of solar EUV radiation for hydrodynamic escape. The hydrogen and oxygen number densities at the lower boundary are treated as free parameters. The numerical conditions are summarized in Table 8.1.

In this study, constituent 1 is $H_2$ and constituent 2 is O. The question of whether constituent 2 could be $H_2O$ or $O_2$ may be raised in view of previous study (Kasting & Pollack, 1983). By considering their "case D" (Fig. 10 in their paper), the O mixing ratio at the base of the expansion (=200 km altitude) is small due to the rapid recombination of OH, produced by photodissociation of $H_2O$, with O, produced by photodissociation of $CO_2$, which yields $O_2$ and H. $H_2O$ is nevertheless more abundant

Table 8.1: Definition of Numerical Parameters

| Symbol | Meaning | Values |
|---|---|---|
| $R$ | Planetary radius | $1R_{\rm Venus} = 6052$ km |
| $M$ | Planetary mass | $1M_{\rm Venus} = 4.869{\times}10^{24}$ kg |
| $L$ | The number of numerical grid cells | 3000 grid |
| $r_0$ | Homopause altitude | $R_{\rm Venus}$+100 km = 6152 km |
| $r_L$ | Upper boundary altitude | $8R_{\rm Venus} = 48416$ km |
| $n_0$ | Homopause hydrogen number density | $3.0 \times 10^{14} \sim 2.0 \times 10^{16}$ /m$^3$ |
| $T_0$ | Homopause temperature | 330 K |
| $\alpha_T$ | Thermal diffusion factor | 0.3 |
| $\eta$ | Heating efficiency | 0.15 |
| $\tau$ | Age of the central star | 0.05, 0.1, 0.5, 1.0 Gyr |

than $O_2$ by a factor of 3 at 200 km. The ratio $n(H_2O)/n(H)$ is about 1/2 at 200 km, and there is therefore 1 O atom for 2 H atoms at the base of the expansion. $H_2O$, which is not much heavier than O, can be levitated by hydrodynamically escaping H but, for a flow velocity of about 3 cm/s, it may be roughly estimated that $H_2O$ molecules will be photodissociated in the first 100 km above the base of the expanding flow, O becoming the final form of escaping oxygen. Released OH radicals recombine quickly with O, over less than 10 km height, to give $O_2$. The fate of $O_2$ molecules in the high atmosphere is to be photodissociated in about 1 day, providing additional O atoms. Since solar EUV flux consumed in escape is deposited over a height of at least 1000 km, no major change is expected concerning O escape with respect to the case of dominant O at the base of the expansion ("case A" of Kasting & Pollack (1983); Fig. 9 in their paper). In "case A", O is dominant at 200 km and is still in a ratio of about 1/2 with respect to hydrogen. It may be therefore assumed that constituent 2 is oxygen. The conclusion is that escaping oxygen must be finally under the form of atomic oxygen.

## 8.3 Results

Because solar radiation and particle fluxes play a major role in all atmospheric processes, the evolution of the Venusian atmosphere can only be understood within the context of the evolving solar energy and particle fluxes. Figure 8.1 shows the change of hydrogen escape flux rate with varying solar age. I also calculate the required hydrogen escape flux rate to uplift oxygen, which is estimated roughly by use of crossover mass (Eq. 6.4). Under the lower limit of hydrogen flux, oxygen cannot

escape, so that the parameter of hydrogen homopause number density is selected to achieve enough hydrogen flux to be over the lower limit. The higher hydrogen escape flux rate is obtained in the case of younger solar age and the case of higher hydrogen homopause number density. The result is reasonable in view of physics. (This would provide assurance that our numerical code is correct.)

Assuming that the primitive Venus had $H_2$ as amount of terrestrial ocean, Fig. 8.1 indicates that timescales of water loss are $5.0 \times 10^6 - 5.0 \times 10^7$ (0.05Gy), $1.5 \times 10^7 - 1.5 \times 10^8$ (0.1Gy), $5.0 \times 10^7 - 5.0 \times 10^8$ (0.5Gy), and $1.5 \times 10^8 - 2.0 \times 10^9$ (1.0Gy). In considering the water loss from Venus, it is reasonable to select the solar age as several hundred million years because the runaway greenhouse effect occurs after a brief interval from the completion of Venus formation, and also because the hydrogen dissociated from $H_2O$ would continue to escape about a few hundred million years (Kasting & Pollack, 1983). In the following, I discuss the detail features of water loss mechanism adapting the solar age as 1.0 billion years, which may correspond to the last stage of water loss from Venus.

Figures 8.2, 8.3, and 8.4 show the steady state distributions of number density, gas flow velocity, and temperature for the different homopause hydrogen number densities in the case that the solar age is 1.0 Gyr.

The density distributions in the steady state of hydrodynamic escape from a hydrogen-oxygen-dominated atmosphere of a Venus-like planet are shown in Fig. 8.2. The calculated number density distributions deviate severely from those in hydrostatic equilibrium (Tian et al. (2005)). Therefore, the atmospheric structure cannot be described properly by the concept of the scale height (the altitude within which the density drops by a factor of $e$). Thus, the traditional definition of the exobase (the altitude at which the mean free path of particles is comparable to the scale height of the atmosphere) is not appropriate, and an equivalent definition of the exobase is the altitude at which the probability of collisions with the particles above the altitude is unity.

Near the upper boundary, the gas flow velocities approach and become super sonic (Fig. 8.3). Because of the decline of gravity with distance, near the upper boundary the escape velocity approaches to the gas flow velocity. Because the escape velocity will continue to decrease and the gas flow velocity remains super sonic beyond the upper boundary, it can be lost from the planet. In the case that $n_0 = 3.0 \times 10^{14}$ [molecules/m$^3$] (blue lines in Fig. 8.3), the column number density of hydrogen in the model is so small that the hydrogen escape flux rate is not enough to accelerate

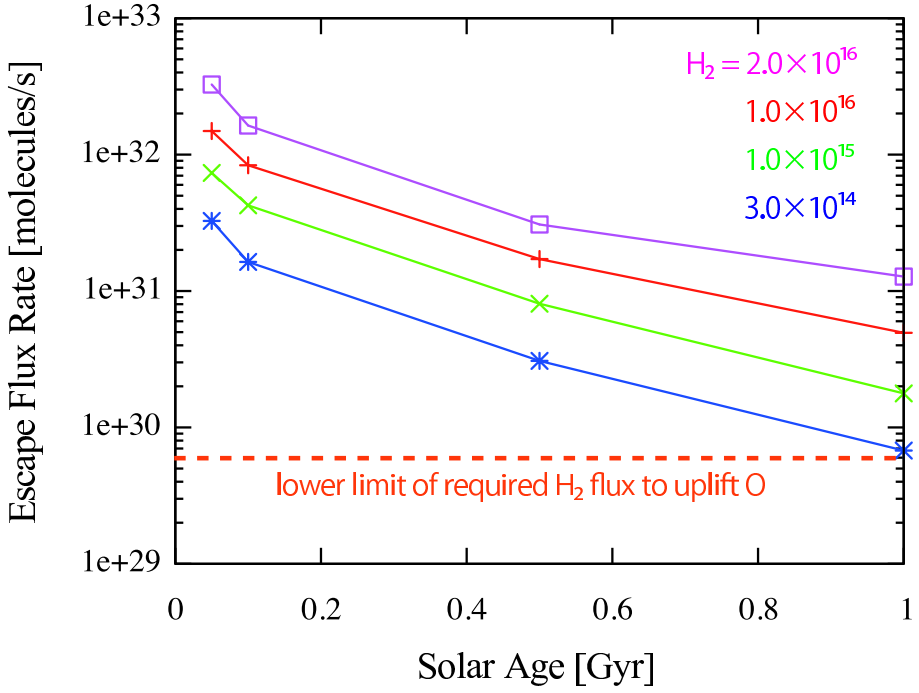


Figure 8.1: Hydrogen escape flux rate in the steady state of hydrodynamic escape of Venusian atmosphere. Abundance of $H_2$ and O is 1:1. Four solar age cases (0.05, 0.1, 0.5, 1.0 [Gyr]) are calculated. Hydrogen number densityies at the bottom of the atmosphere are $3.0\times10^{14}$ (blue), $1.0\times10^{15}$ (green), $1.0\times10^{16}$ (red), and $2.0\times10^{16}$ (purple) [molecules/$m^3$]. Orange dashed line shows the roughly estimated lower limit of required hydrogen escape flux rate to uplift oxygen in the Venusian gravitational field, which is calculated using crossover mass (see section 6.2).

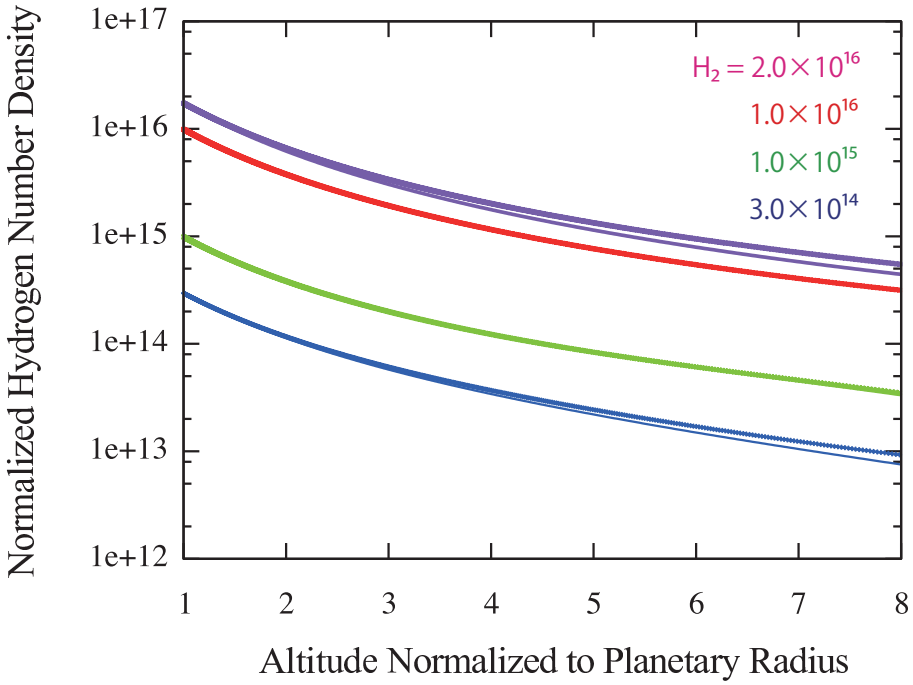


Figure 8.2: Number density distributions in the steady state of hydrodynamic escape of Venusian atmosphere. Solar age is 1.0 Gyr. Abundance of $H_2$ and O is 1:1. Hydrogen number densities at the bottom of the atmosphere are $3.0\times10^{14}$ (blue), $1.0\times10^{15}$ (green), $1.0\times10^{16}$ (red), and $2.0\times10^{16}$ (purple) [molecules/m$^3$]. The thinner lines correspond $H_2$ and the thicker ones correspond O.

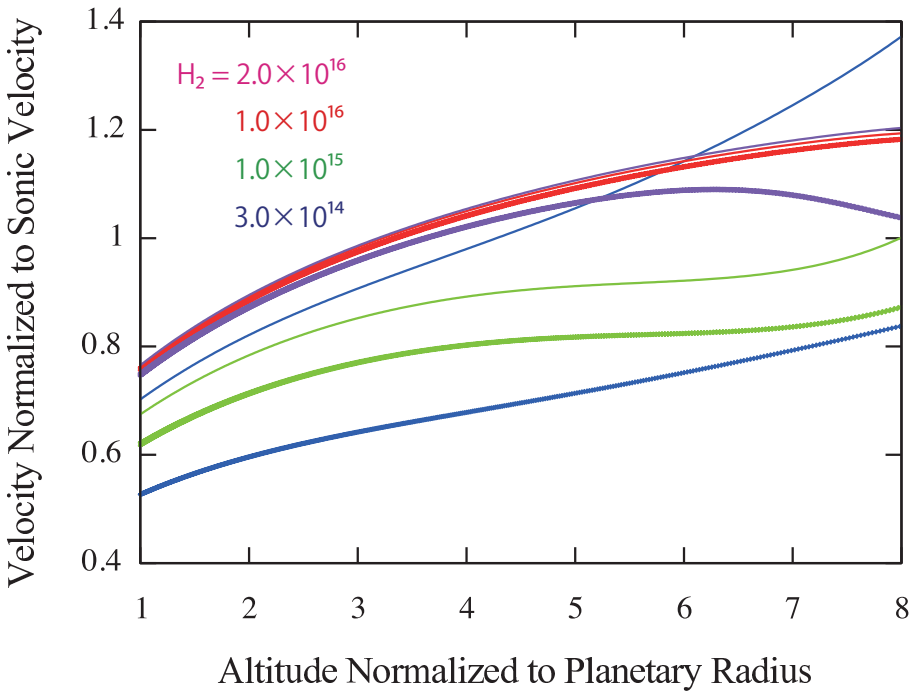


Figure 8.3: Gas flow velocity distribution in the steady state of hydrodynamic escape of Venusian atmosphere. Solar age is 1.0 Gyr. Abundance of $H_2$ and O is 1:1. Hydrogen number densities at the bottom of the atmosphere are $3.0\times10^{14}$ (blue), $1.0\times10^{15}$ (green), $1.0\times10^{16}$ (red), and $2.0\times10^{16}$ (purple) [molecules/m$^3$]. The thinner lines correspond $H_2$ and the thicker ones correspond O.

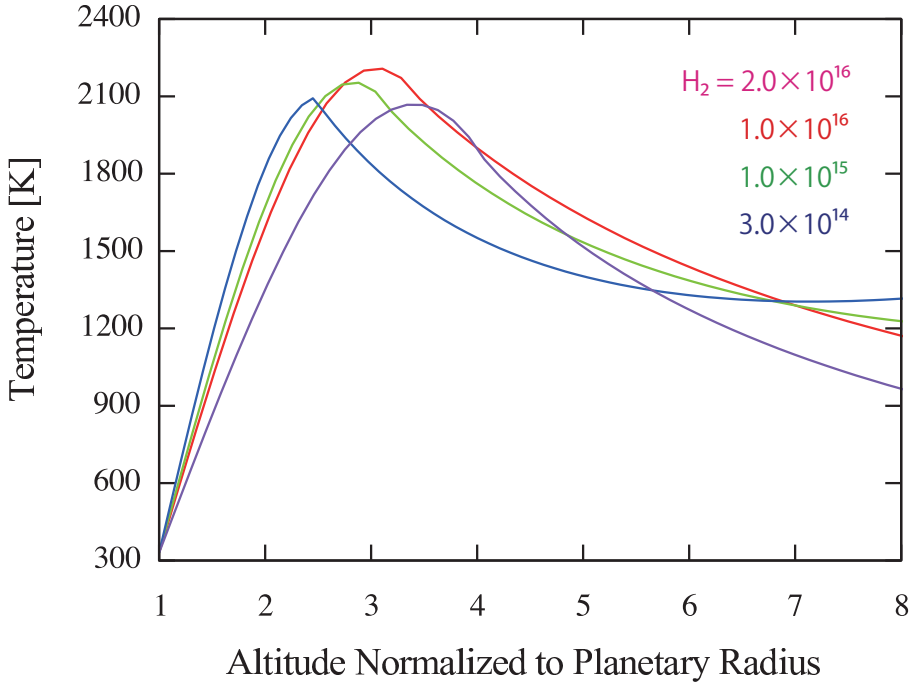


Figure 8.4: Temperature distribution in the steady state of hydrodynamic escape of Venusian atmosphere. Solar age is 1.0 Gyr. Abundances of $H_2$ and O is 1:1. Hydrogen number density at the bottom of the atmosphere is $3.0\times10^{14}$ (blue), $1.0\times10^{15}$ (green), $1.0\times10^{16}$ (red), and $2.0\times10^{16}$ (purple) [molecules/$m^3$].

the oxygen. Then next case ($n_0 = 1.0 \times 10^{15}$ [molecules/m$^3$], green lines in Fig. 8.3), the oxygen is accelerated sufficiently, which velocity is comparable to that of hydrogen, with increasing the hydrogen number density (i.e., with increasing the hydrogen escape flux rate). Meanwhile, the gas flow velocity of hydrogen decreases with increasing the drag effect by surrounding oxygen. Then next case ($n_0 = 1.0 \times 10^{16}$ [molecules/m$^3$], red lines in Fig. 8.3), because the acceleration of hydrogen by EUV heating is greater than the deceleration of hydrogen by surrounding oxygen's drag, the gas flow velocities of hydrogen and oxygen increase together. Finally, In the case that $n_0 = 2.0 \times 10^{16}$ [molecules/m$^3$] (purple lines in Fig. 8.3), with increasing oxygen atoms in the atmosphere, downward acceleration of oxygen due to gravity overcomes the upward lifting of oxygen by hydrogen hydrodynamic escape. Then, the power relationships between the acceleration and the deceleration are reversed so that the gas flow velocity of oxygen decreases dramatically. On the other hand, since the acceleration of hydrogen by EUV heating is increasing, the gas flow velocity of hydrogen continues to increase. These trends are also appeared in the density distributions (Fig. 8.2).

The temperature (Fig. 8.4) varies with escape flow because the escape flow carries out energy and produces adiabatic cooling. In addition to the hydrogen homopause number density, there are two effects related to the energy deposition and distribution that affect the escape rate. First, the total amount of EUV radiation absorbed is smaller in a low homopause density atmosphere than in a high homopause density atmosphere. Second, most of the energy absorption occurs at lower altitudes when the homopause hydrogen density is low, which causes a large temperature gradient near the lower boundary. With a large temperature gradient, energy is quickly lost through thermal conduction out of the lower boundary, which contributes to a weak escape flow. These nonlinear effects combined together intricately produce the resulted escape flux rate of atmosphere.

Altough the temperature is fixed to a constant at the lower boundary in the model, variation of the lower boundary temperature will have effects on the calculated hydrogen escape rate. Intuitively a higher temperature will result in a stronger escape flux. Moreover, the calculated value of the hydrodynamic escape flux depends upon the hydrogen number density in the lower thermosphere that, in turn, is controlled by a combination of chemical, diffusive, and advective processes. Heating and cooling rates, heat capacities, and thermal conductivities are also functions of atmospheric composition. These complicated effects and relationships should be built in the numerical code to study the early Venusian atmosphere more precisely.

Figures (8.2) to (8.4) show the atmospheric structures of hydrogen-oxygen mixing atmospheres. Then next, I discuss the results of atmospheric escape flux, which is directly concerned with the water loss from early Venus. The hydrogen and oxygen molecule escape flux rates corresponding to different abundances of $H_2$ and O are calculated for the Venusian atmosphere, with the lower boundary hydrogen densities set to be parameter (Fig. 8.5). And Fig. 8.6 shows only oxygen molecule escape flux rates corresponding to different abundances of $H_2$ and O in one figure. Lines-points in Fig. 8.5 show the range that oxygen can obtain the upward velocity accelerated by hydrogen's uplift effect as well as the escape flux rate of each molecule. In other words, the x-axis range where lines-points are not plotted means that oxygen has the downward velocity (i.e., the oxygen molecule cannot escape from the Venusian atmosphere) in this x-axis range. Out of this shown range, only hydrogen can escape from the Venusian atmosphere.

Figure 8.5 indicates the following three results. (1) Range of homopause hydrogen number density where oxygen can escape becomes narrower with increasing the relative abundance of oxygen to hydrogen in the Venusian atmosphere. (2) Absolute amount of escaping hydrogen and oxygen becomes smaller with increasing the relative abundance of oxygen to hydrogen in the Venusian atmosphere. This decline trend is shown obviously in Fig. 8.6. (3) Escape flux rate of oxygen is always smaller than that of hydrogen. Although there are narrow ranges where the escape flux rate of oxygen and hydrogen are approximately same amount (homopause number density is around $9.0 \times 10^{15}$ [molecules/m$^3$]), hydrogen is easy to escape in most hydrogen number density ranges including the ranges where oxygen cannot escape.

According to the results, water loss from early Venus can be achieved if the homopause number densities of $H_2$ and O are maintained around $9.0 \times 10^{15}$ [molecules/m$^3$] for a long time; in such a case, timescale of water loss as amount of terrestrial ocean is about $1.5 \times 10^8$ years. Except in that case (i.e., when the homopause number densities vary with time), the hydrogen molecules escape more than oxygen molecules from the water-rich Venusian atmosphere, and then the relative abundance of oxygen to hydrogen inevitably increases with time. Moreover, the larger the relative abundance of oxygen to hydrogen is, the harder the oxygen escapes from the Venusian atmosphere, so that the oxygen relative abundance would increase at an accelerating pace, which is often called "positive feedback."

Eventually, the results indicate that the complete water loss from early Venus by

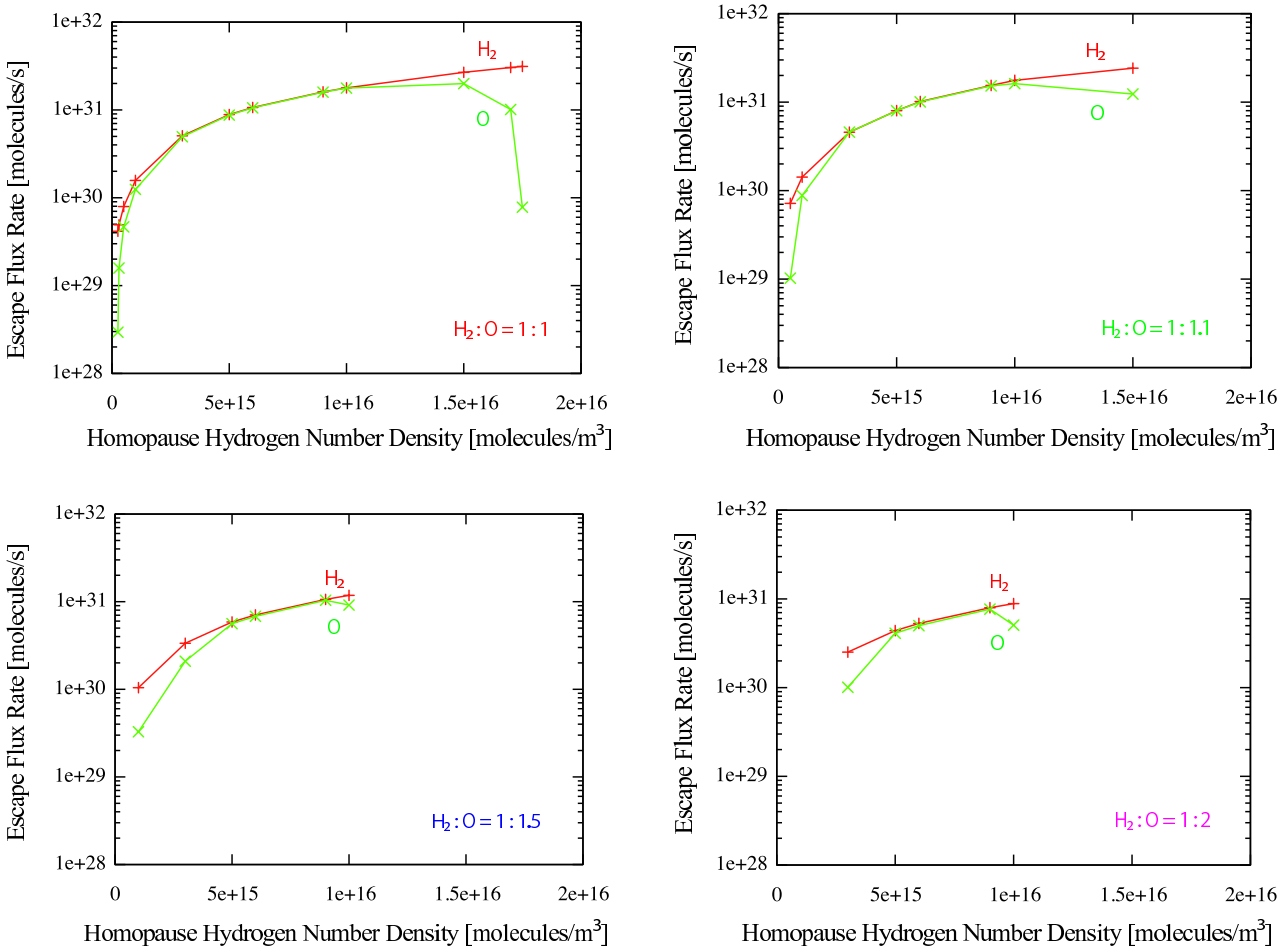


Figure 8.5: Hydrogen (red) and Oxygen (green) escape flux rate in the steady state of hydrodynamic escape of Venusian atmosphere. Solar age is 1.0 Gyr. The horizontal axis is hydrogen number density at the bottom of the atmosphere. Abundances of $H_2$ and O is 1:1 (upper left), 1:1.1 (upper right), 1:1.5 (lower left), and 1:2 (lower right).

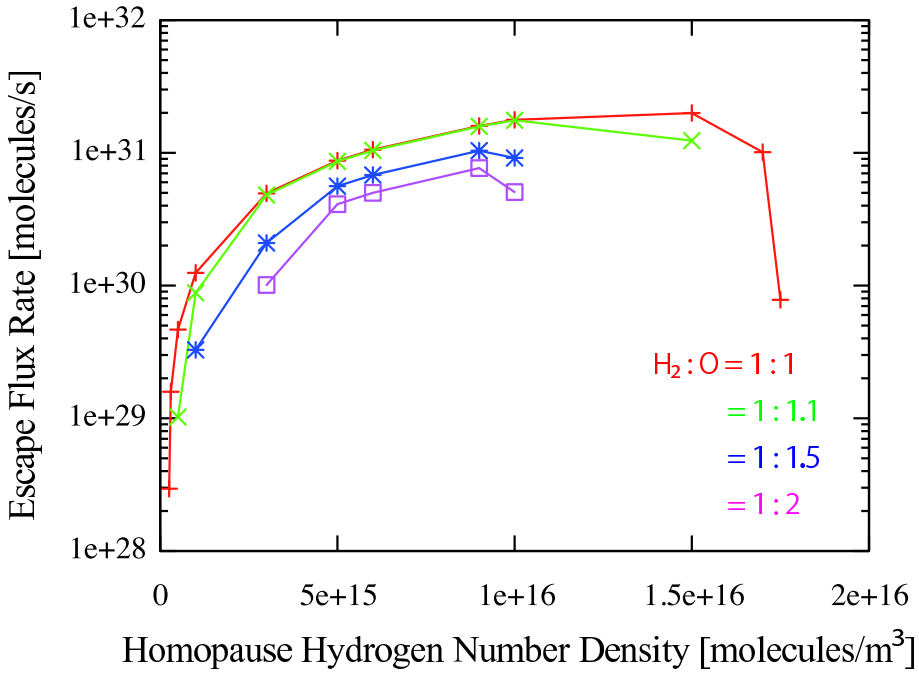


Figure 8.6: Oxygen escape flux rate in the steady state of hydrodynamic escape of Venusian atmosphere. Solar age is 1.0 Gyr. The horizontal axis is hydrogen number density at the bottom of the atmosphere. Abundances of $H_2$ and O is 1:1 (red), 1:1.1 (green), 1:1.5 (blue), and 1:2 (purple).

hydrodynamic escape of oxygen as well as hydrogen would be very difficult but not be impossible. Under special circumstances, hydrodynamic escape of $H_2$ and O by itself can solve the water loss problem for Venus. This is an important consequence of this study. However, in the most ranges of the parameter as the homopause number densities, the oxygen would be left behind while the hydrogen would escape from the Venus, so that the oxygen consequently concentrates in the Venusian atmosphere. Hence, we should next consider how the concentrated oxygen was consumed and/or escaped afterward.

Finally, I note that the assumed atmosphere in this chapter consists of only dissociated $H_2O$, i.e., the abundance ratio of hydrogen and oxygen is about 1:1. Under the case that hydrogen, which would be originated from solar nebula and/or degassing atmosphere, is much more abundant than oxygen, it would be easier to lose the complete water from early Venus by hydrodynamic escape. This case study should be an important future work.

## 8.4 Discussions

In this section, some possible mechanisms to consume/escape oxygen in the early Venusian atmosphere are reviewed according to some previous studies.

### 8.4.1 Oxygen Concentration

The topic of abiotic $O_2$ concentrations has been studied extensively in relation to the problem of the origin and early evolution of life on Earth. Although work on this problem dates back to the early 1960's, the problem was first formulated correctly by Walker (1977), who realized that the hydrogen released by volcanism and by water vapor photolysis must be balanced by escape of hydrogen to space. The amount of $O_2$ that could be produced abiotically can be estimated using a one-dimensional photochemical model (Kasting et al., 1984). An up-to-date discussion of this problem is given by Kasting (1993). There, the problem of balancing the atmospheric hydrogen budget is reviewed, and it is pointed out that rainout of reduced and oxidized gases should be taken into account. Lightning-induced decomposition of $CO_2$ is also a potentially important source of $O_2$ at low altitudes in such atmospheres. The calculated $O_2$ mixing ratio peaks at about 50 km at a value of just under 0.1% by volume. This high-altitude peak is produced by photolysis of $CO_2$ followed by recombination of O atoms with each other and with OH to form $O_2$. The $O_2$ concentration decreases rapidly towards the surface as a consequence of reaction with reduced volcanic gases,

catalyzed by radical species produced by $H_2O$ photolysis. At early stage of the planetary formation, the conclusion that atmospheric $O_2$ concentrations should be low is robust, because the primordial planets would have much reduced gases such as $H_2$ and CO. Higher solar UV fluxes in the past could have enhanced the $O_2$ concentration in the upper atmosphere, but they should have had little effect on ground-level $O_2$ concentrations (Canuto et al. 1982, 1983; Kasting et al. 1984; Kasting 1985).

On the other hand, Kasting (1996) point out that abiotically-produced $O_2$ concentrations could be much higher on planets for which the preceding criteria do not apply; for example, a Venus-like planet could build up a transient $O_2$-rich atmosphere as a consequence of rapid water loss and hydrogen escape. They implied that $O_2$ partial pressures of tens or hundreds of bars are theoretically possible in this case. (The partial pressure of a fully vaporized terrestrial ocean is 270 bars, 240 of which come from oxygen.) However, as shown in the previous section, the escape flux of hydrogen by hydrodynamic escape dramatically decreases under the high-concentration of oxygen in the primordial atmosphere. So, rapid water loss and hydrogen escape, which would bring about the transient high $O_2$ concentration in the primordial Venusian atmosphere, could not be achieved easily. In other words, it is inversely possible that the $H_2O$ is formed from the dissociated $H_2$ and O by backward reaction. In the case of that, complete loss of water on the Venus cannot be achieved. Unfortunately, we does not have valid criterion in deciding which atmospheric circumstances would bring the backward reaction yet. Therefore, the research of conditions of the $H_2O$ backward reaction must be critical to study the mechanism of water loss on the Venus.

If the backward reaction of $H_2O$ does not occur and the dissociated $H_2$ escape from the Venusian atmosphere completely, remaining oxygen could be consumed by oxidation of surface minerals or nonthermal escape of atmospheric oxygen. A problem is the question of how much the oxygen presumed to have been left behind after the hydrogen had escaped could be disposed.

### 8.4.2 Oxidation of Surface Minerals

Lewis and Prinn (1984) have pointed out that the loss of 110 bars of $O_2$ (a full terrestrial ocean contains close to 240 bar of oxygen) would entail the oxidation of about 80 km of Earth-like crust. Acting over 4.5 Gyr this would require an average rate of tectonic recycling approximately 15 times greater than is seen presently on Earth. And, if we suppose that the rate of resurfacing of crustal material by tectonic

activity during the first gigayear of Venus' existence was the same as on Earth, a typical quantity of about one-third amount of terrestrial ocean has been possibly absorbed by Fe oxidation, carbonate formation, and oxidation of the atmosphere (Chassefiére, 1996). However, since Venus today appears to be less tectonically active than Earth, the problem of disposing of this oxygen is potentially severe.

### 8.4.3 Nonthermal Escape

The upper parts of an atmosphere are partially ionized, by the agency of solar photons with wavelength generally below 100 nm. These ions are often suprathermal, and their interactions can produce suprathermal neutral atoms as well. These suprathermal processes are limited to modest quantities of gas, nevertheless, they can be important for minor constituents, such as N and O at present Mars and H at present Venus and Mars. (Hunten, 1993)

Another process involving ions pertains to Venus and Mars, which lack a significant intrinsic magnetic field (Luhmann and Kozyra, 1991). These planets posses a boundary, the ionopause, that separates the bound ionosphere from an outer region in which the solar wind is diverted and flows around and past the planet. This region still contains some neutral gas, and if such atoms are ionized by solar photons or electron impact, they are swept up in the flow. Some of these ions can re-impact the upper atmosphere with enough energy to remove additional atoms. Study of this field is still in its infancy, but there are suggestions that the process is significant for loss of O from Venus (McElroy et al., 1982).

Venus could have lost its magnetic field very early in its history. If a planetary atmosphere like that of Venus is not protected by a strong intrinsic magnetic field, the planetary neutral gas in the exosphere can be ionized due to charge exchange with the deflecting solar wind plasma flow, by electron impact and by the XUV radiation, and picked up by the solar wind plasma flow around the planet. The principal ionizing radiations responsible for the heating of the upper planetary atmospheres and the formation of planetary ionospheres from stellar or solar sources are ionizing X-rays and EUV radiation (XUV). It has been also suggested that the solar wind may have been much more massive in the distant past (Wood et al., 2002). Compelling observational evidence shows that zero-age-main-sequence solar-type stars rotate more than 10 times faster compared to the present Sun (Güdel et al., 1997). As a consequence, young solar-type GV stars, including the young Sun, have vigorous magnetic dynamos and correspondingly strong high-energy emissions. With enhanced high-

energy emissions and frequent flares young solar-type stars are also expected to have more powerful stellar winds. Without the protection of magnetic field, a strong solar wind of the young Sun could easily remove substantial amounts of oxygen that could have been left from a hydrodynamically escaping ocean.

Kulikov et al. (2006) studied the early Venusian thermosphere-exosphere region and the efficiency of the $O^+$ ion loss by the pick up process due to the evolving solar radiation and particle environment over the planet's history. They used minimum and maximum values of the solar wind mass flux inferred from stellar wind particle collisions with the interstellar medium which surrounds the solar proxies with different ages (Wood et al., 2002; 2005). If the incoming solar wind plasma penetrates a scale height deeper into the thermosphere, which is not protected by a strong intrinsic magnetic field, they obtain a total integrated oxygen loss over the planet's history of about 180-280 bar (= 70-110% Terrestrial Ocean) for the maximum solar wind values, about 40-60 bar (= 15-25% TO) for the average solar wind, and about 10-15 bar (= 4-6% TO) for the minimum solar wind.

We should keep in mind that their study took into account only the ion pick up process and no other nonthermal loss processes like atmospheric sputtering and atmospheric erosion by plasma instabilities. Additional loss processes like detached plasma clouds and sputtering will enhance the oxygen loss from an unprotected early Venus atmosphere to larger amounts, so that their calculations may represent only lower limits for nonthermal escape of oxygen. Therefore, It is expected that the Venusian oxygen, which might have remained in the atmosphere after the evaporation of an early water ocean could have also been lost to space by ion pick up for solar wind fluxes, if the flux exceed the average solar wind's value, and if the early Venusian atmosphere was not protected by an intrinsic Earth-like magnetic field.

### 8.4.4 Contribution of Water from Comet

Chyba (1990) has argued that the heavy bombardment by cometary material could have provided a full terrestrial ocean to early Earth, with a continuous supply of water during this period. If it is the case, water was brought at a relatively slow rate. Venus and the Earth are expected to have accreted about the same water amount through cometary impacts during the heavy bombardment phase (Chyba 1990), and my calculations show no significant O escape could occur on Venus over such a long period (over $10^8$ years). If Chyba (1990) is right, that is, if 0.2-0.7 TO was accreted

over 1 Gyr from impacting comets, the large amount of oxygen that could not be lost by hydrodynamic escape left behind on the early Venus. The contribution of water supply to early Venus from cometary heavy bombardment would make oxygen escape from Venusian atmosphere even harder.

### 8.4.5 D/H Fractionation

The hydrogen escape flux rate would have declined at lower $H_2O$ density, and the flux may have been smaller than found here if more O had accumulated in the Venus atmosphere. The last portion of the water would have been much more difficult to get rid of, because of the drastic decline in the H escape rate at low $H_2O$ density and possible oxygen accumulation after hydrodynamic escape of substantial amount of $H_2$ in the Venusian atmosphere. During the last stage of the hydrodynamic escape process the escape flux would have decreased rapidly and significant D/H fractionation should have occurred (Kasting & Pollack, 1983).

However, we should note that it is difficult to estimate the initial $H_2O$ reservoir on early Venus from the present D/H ratio, because all estimations depend on the non-steady or steady state Venus' water content and possible unknown D/H fractionation processes which could have had different rates over the planet's past compared to the present time. Although the amount of water on early Venus is implicitly assumed to be that of terrestrial ocean in this section, actually the amount of water is unknown. The question may be answered someday by performing chemical analyses to determine the oxidation state of Venusian crust in detail.

# Chapter 9

# Fractionation of Noble Gases on Venus

## 9.1 Previous Studies

Hydrodynamic escape driven by EUV heating has been envisioned for fractionating noble gases on terrestrial planets (Zahnle & Kasting, 1986; Sasaki & Nakazawa, 1988; Pepin, 1991; Pepin, 2006). The rapid escape of a light gas would have exerted an aerodynamic drag on heavier gases. The balance between the upward aerodynamic drag and the downward gravitational attraction resulted in a mass-dependent loss of noble gases. Mechanisms operating today on the terrestrial planets cannot remove species as massive as the heavy noble gases, and yet there is clear evidence that mass-dependent loss signatures are imprinted on atmospheric Ar, Kr, and Xe isotopes. So, the hydrodynamic escape process would have occurred on earlier epochs of planetary histories, when now-vanished energy sources such as strong EUV heating of the young Sun (Pepin, 2006) could have driven intense outflows of atmospheric gases. Actually, on the early stage of planetary formation, a massive hydrogen atmosphere could have been acquired by capture of nebular gases or could have resulted from the reduction or photodissociation of water (Kasting & Pollack, 1983), and the appropriate energy could have been deposited in the atmosphere as extreme ultraviolet radiation from the young evolving Sun (Ribas et al., 2005).

The noble gas depletion patterns in terrestrial planets' atmospheres are simply considered to be created from initially solar compositions via thermal escape of the atmospheres (Fig. 7.1). However, we should note that the atmosphere consisted of solar composition would be lacking in major components of present terrestrial planets' atmospheres such as H, C, and N. Anyway, the fractionation process by the hydrodynamic escape of primordial atmospheres would have a possibility of account-

ing for at least the noble gas patterns as the following observations: The Ar/Kr ratio on Venus is nearly solar while the Ar/Kr ratio on Earth and Mars is nearly meteorites, the absolute abundance of Ar on Venus is similar to or larger than that of the most argon-rich meteorites, the Ne/Ar elemental ratio is roughly the same on Earth, Mars, Venus and meteorites, and neon on planets is isotopically between solar wind and meteorites neon, and argon on Mars is isotopically heavier than either. So, it should be key to understand the atmospheric evolutional history of terrestrial planets that studying in detail the hydrodynamic escape process of a primordial planetary atmosphere, which is energize by EUV irradiation of the young Sun.

Recently, Pepin (2006) presented an outline of how atmospheric evolution may have proceeded on the terrestrial planets. Their objective was to account in detail for contemporary elemental and isotopic compositions. Although they indicated a possible evolution scenario of terrestrial planetary atmospheres, the fundamental question of weather nature actually shaped the atmospheres is still unanswered. Many mechanisms could have contributed to gain or loss of primordial planetary gases. Their model, however, has many uncertainties such as the origins, compositions, and lifetimes of primary reservoirs, the mechanisms responsible for transporting and fractionating volatile elements, and the environments in which such processes operated. Regretfully, we have no model-independent ways to assess the relative importance of possible primordial sources and evolutionary processes in shaping present atmospheres. So, we should not take complicated evolution scenario simply for the sake of accounting for the present atmospheric elementary patterns. We should consider the fundamental question of whether nature actually shaped the atmospheres in this way. Therefore, in contradiction to Pepin (2006), I take the simplest evolution scenario and consider which process would determine the atmospheric profile in this chapter.

In the first approximation, noble gas depletion patterns were assumed to be created from initially solar compositions by gravitational escape. Gravitational escape of atmospheric constituents is intrinsically mass-dependent, no matter the specific loss mechanism, and so both elements and isotopes in the residual atmospheres are fractionated with respect to initial compositions. High abundance of argon on Venus carry powerful evidence that their primordial parents had solar compositions, at least a certain amount, and that gravitational escape played a major role in their evolution. Analytical approximations to mass fractionation during hydrodynamic escape indicated that these fractionation could be achieved in some instances for the case of a heavy constituent being dragged along by a much lighter one (Zahnle & Kasting, 1986). In this study, the developed numerical model applied to the escape of

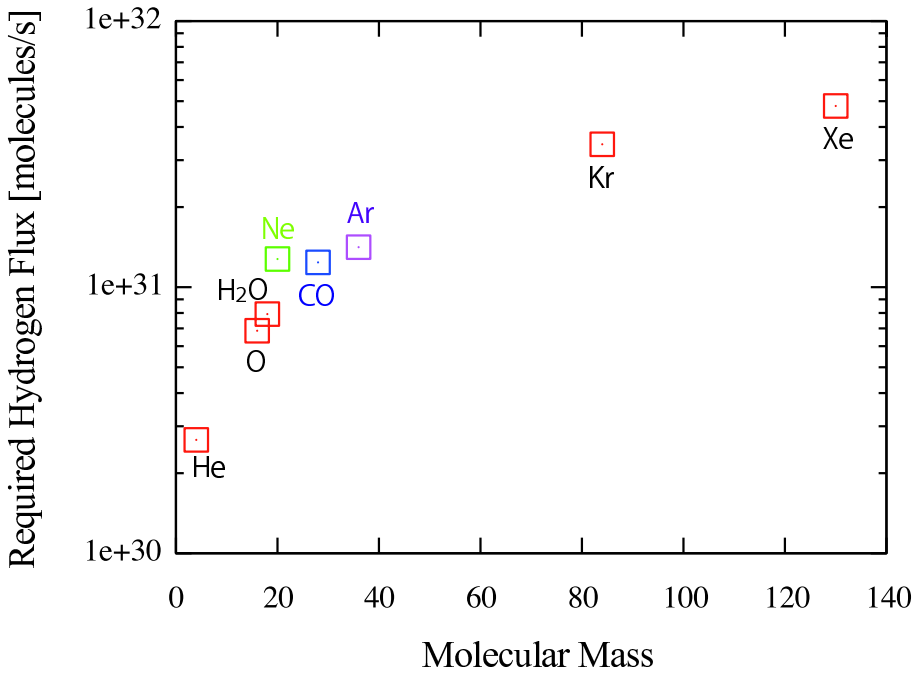


Figure 9.1: The hydrogen escape flux rate at which the various heavy elements would begin to escape. Note that required hydrogen flux to uplift Ne is like CO and slightly smaller than Ar.

noble gases in hydrogen escaping flow from the early Venus to examine whether the fractionation can be achieved or not.

### 9.1.1 Proposed Ne/Ar Fractionation Mechanism

Hydrodynamic escape of noble gases is a mass-dependent escape process, i.e., the lighter an element is, the more it escapes. So, is it possible to transform Ne/Ar ratio of Venusian atmosphere from solar nebula abundance (Ne/Ar $\sim$ 1) into present Venusian abundance (Ne/Ar $\sim$ 0.01) by mass-dependent hydrodynamic escape? In Fig. 9.1, I have indicated the points at which noble gases would have begun to escape calculated using crossover mass (Eq. (6.4)). Figure 9.1 shows that the difference of the required hydrogen escape flux of Ne and Ar is very slight. Hence, a fine-tuning of hydrogen escape flux is required to achieve a proper Ne/Ar fractionation. However, the long-term fine-tuning of hydrogen escape flux (i.e., the long-term fine-tuning of input solar EUV energy) would not be realistic. Thus, the fractionation of Ne and Ar, would not be explained simply by mass-dependent hydrodynamic escape.

Here, I consider a photochemical reaction to realize the fine-tuning of hydrogen escape flux, which make neon escape and argon unescape. I take notice of carbon

monoxide. Any wind capable of lifting Ne is also capable of lifting CO (Fig. 9.1). At the top of the atmosphere, infrared cooling by CO might then have radiated away EUV energy that would otherwise speed the flow. In other words, the wind may only have become strong enough to reach the threshold of removing CO, at which point any additional EUV energy input would be radiated away. On the other hand, Ar might not be removed by hydrogen hydrodynamic escape at the threshold speed, because the required hydrogen escape flux is slightly larger than Ne and CO. Thus, the infrared cooling by CO might control the atmospheric temperature (that is in proportion to the hydrogen escape flux) by self-sustained way to maintain the fine-tuning of hydrogen escape flux. It would therefore be expected that some loss of Ne occurred, however that no loss of the heavier Ar took place. The fractionation of the Venus' noble gases might be explained by this mechanism (Zahnle & Kasting, 1986).

Transient reducing atmospheres produced by mantle reactions with metallic iron have been studied by Kuramoto & Matsui (1996). The possible presence of free iron in the crust, during the earlier stages of accretion, suggests that the atmosphere could be reducing, with $H_2$ rather than $H_2O$, and CO (and/or $CH_4$) rather than $CO_2$. And also, it is likely that the early atmosphere of Venus is also reducing similarly to that of Earth since the atmospheres on both planets would be generated by degassing of planetesimals (Hashimoto et al., 2007). Carbon monoxide is, like $N_2$, an inevitable product of impact shock chemistry (e.g., Zahnle, 1990; Hashimoto et al., 2007). As one cannot build a planet or satellite without impacts, CO figures to have been a major constituent of the earliest atmospheres. Therefore, it is likeliest to have been present as a component of transient reducing atmospheres, which contain substantial amount of carbon monoxide.

## 9.2 Numerical Model

The model and the energy calculation method are applied to the atmosphere of a Venus-like planet in which the thermosphere is composed only of hydrogen, noble gases, and carbon monoxide molecules. The lower boundary is fixed at approximately the altitude of the homopause (100km), and the lower boundary temperature is fixed at 330 K. The upper boundary is at an altitude of roughly 50000 km. The $H_2$, Ne, Ar, and CO number densities at the lower boundary is treated as a free parameter. The parameters are chosen in reasonable ranges obtaining from the possible atmospheric sources shown in Fig. 9.2. The employed free parameters are summarized in Table 9.1. The effect of CO cooling in the atmosphere is taken into account using line-by-line

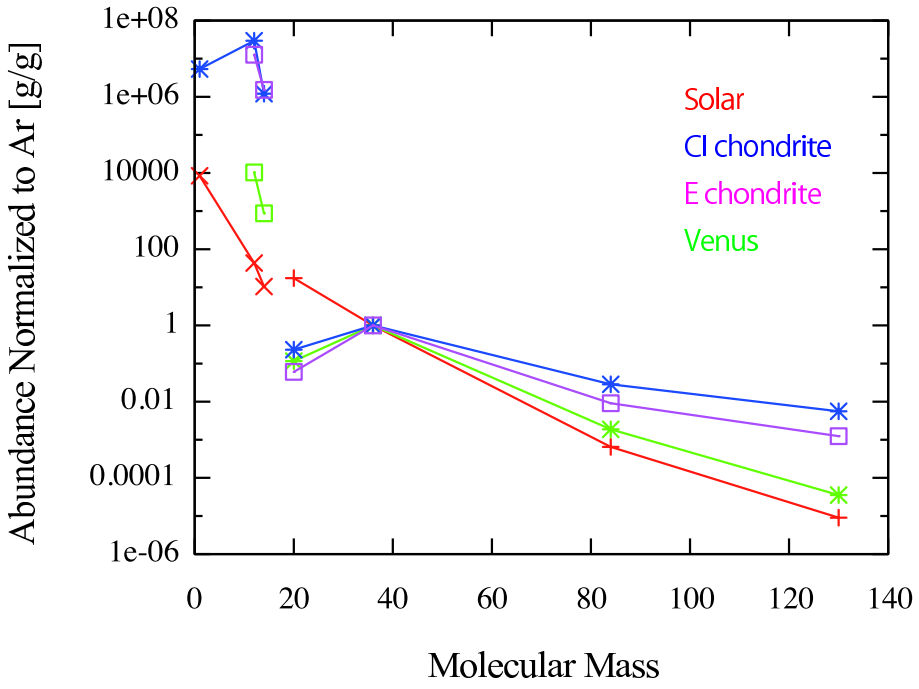


Figure 9.2: Relative abundances of noble gases in solar, meteorites, and the Venusian atmosphere normalized to each Ar abundance. All the data used in this figure are listed in Table 7.2

method as described below.

### 9.2.1 CO Rotational Cooling

Temperature change of the atmosphere by CO cooling is calculated by the following equation

$$\rho C_v \frac{dT}{dt} = -\Lambda_{\rm CO} \tag{9.1}$$

where $C_v$ is the specific heat of the atmosphere. Term in the right hand side represent the cooling term of CO. The radiative cooling rate $\Lambda_{\rm CO}$ due to a transition from level

Table 9.1: Employed Free Parameters

| Symbol | Meaning | Values |
|---|---|---|
| $n_{\rm H_2}$ | homopause hydrogen number density | $10^{13} \sim 10^{18}$ /m$^3$ |
| $n_{\rm Ne}$ | homopause neon number density | $10^{-7} \sim 10^{-3} \times n_{\rm H_2}$ |
| $n_{\rm Ar}$ | homopause argon number density | $= n_{\rm Ne}$ |
| $n_{\rm CO}$ | homopause carbon monoxide number density | $10^{-4} \sim 1.0 \times n_{\rm H_2}$ |
| $\tau$ | age of the central star | 0.01, 0.05, 0.1 Gyr |

$i$ to level $j$ of CO is given by

$$\Lambda_{\rm CO}(\nu_{ij}) = n_{\rm CO}(i) A_{ij} h\nu_{ij} \beta_{esc}(\tau_{ij}) \frac{S_{\rm CO}(\nu_{ij}) - P(\nu_{ij})}{S_{\rm CO}(\nu_{ij})} \tag{9.2}$$

where $n_{\rm CO}(i)$ is the population density in level $i$ of CO, $A_{ij}$ is the spontaneous transition probability, $h\nu_{ij}$ is the energy difference between level $i$ and level $j$, $\beta_{esc}(\tau_{ij})$ is the photon escape probability at the optical depth $\tau_{ij}$ of the line (Hollenbach & McKee, 1979; Tielens & Hollenbach, 1985a). The source function $S_{\rm CO}(\nu_{ij})$ is given by

$$S_{\rm CO}(\nu_{ij}) = \frac{2h\nu_{ij}^3}{c^2} \left( \frac{g_i n_j}{g_j n_i} - 1 \right)^{-1} \tag{9.3}$$

where $g_i$ and $g_j$ are the statistical weight of the levels and $c$ is the speed of light. $P(\nu_{ij})$ is the intensity of the background radiation. In calculating cooling rates due to the rotational lines of CO, the effects of the background radiation field are assumed to be ignored. So the cooling rates $\Lambda_{\rm CO}(\nu_{ij})$ is simplified from Eq. (9.2) to be the following equation

$$\Lambda_{\rm CO}(\nu_{ij}) = n_{\rm CO}(i) A_{ij} h\nu_{ij} \beta_{esc}(\tau_{ij}) \tag{9.4}$$

The optical depth averaged over the line is given by

$$\tau_{ij}(z) = \frac{A_{ij} c^3}{8\pi\nu_{ij}^3} \int_0^z n_i(z') \left[ \frac{n_j(z') g_i}{n_i(z') g_j} - 1 \right] \frac{dz'}{\delta\nu_d} \tag{9.5}$$

where $\delta\nu_d$ is the turbulent Doppler line width (= 2.7 km/s; Tielens & Hollenbach, 1985b), and the integration is carried out from the top of the atmosphere ($z = 0$) to depth $z$. Following de Jong & Boland (1980), the probability that a photon escapes through the nearest boundary is approximated by

$$\beta_{esc}(\tau) = \frac{1 - \exp(-2.34\tau)}{4.68\tau}, \quad \tau < 7 \tag{9.6}$$

$$= \left( 4\tau \left[ \ln \left( \frac{\tau}{\sqrt{\pi}} \right) \right]^{0.5} \right)^{-1}, \quad \tau \geq 7 \tag{9.7}$$

In these formulae it is implicitly assumed that half of the photons, those that are emitted to the planet's ground, do not escape. Because all opacity is assumed to be local in the escape probability formalism, these inwardly directed photons do not contribute to the cooling.

It is assumed that cooling rates due to the levels in non-LTE (Local Thermodynamic Equilibrium) are ignored. From the assumption, cooling efficiency of the

Table 9.2: Molecular line data for the CO model molecule

| J | $E$[cm$^{-1}$] | $\lambda$[mm] | $A_{ij}$ [s$^{-1}$] | $n_{\rm cr}$ [cm$^{-3}$] |
|---|---|---|---|---|
| 1 | 3.85 | 2.601 | 7.17 (-8) | $5.0\times T^{-0.66}$ (3) |
| 2 | 11.54 | 1.300 | 6.87 (-7) | $1.9\times T^{-0.45}$ (4) |
| 3 | 23.07 | 0.867 | 2.48 (-6) | $4.6\times T^{-0.35}$ (4) |
| 4 | 38.45 | 0.650 | 6.09 (-6) | $8.3\times T^{-0.28}$ (4) |
| 5 | 57.67 | 0.520 | 1.22 (-5) | $1.3\times T^{-0.22}$ (5) |
| 6 | 80.74 | 0.434 | 2.13 (-5) | $2.0\times T^{-0.18}$ (5) |
| 7 | 107.64 | 0.372 | 3.40 (-5) | $2.9\times T^{-0.16}$ (5) |
| 8 | 138.39 | 0.325 | 5.11 (-5) | $4.1\times T^{-0.14}$ (5) |
| 9 | 172.98 | 0.289 | 7.29 (-5) | $5.5\times T^{-0.12}$ (5) |
| 10 | 211.40 | 0.260 | 1.00 (-4) | $7.2\times T^{-0.11}$ (5) |
| 11 | 253.67 | 0.237 | 1.33 (-4) | $9.2\times T^{-0.10}$ (5) |
| 12 | 299.77 | 0.217 | 1.73 (-4) | $1.1\times T^{-0.09}$ (6) |
| 13 | 349.70 | 0.200 | 2.19 (-4) | $1.4\times T^{-0.08}$ (6) |
| 14 | 403.46 | 0.186 | 2.72 (-4) | $1.7\times T^{-0.075}$ (6) |
| 15 | 461.05 | 0.174 | 3.33 (-4) | $2.0\times T^{-0.07}$ (6) |
| 16 | 522.48 | 0.163 | 4.02 (-4) | $2.4\times T^{-0.065}$ (6) |
| 17 | 587.72 | 0.153 | 4.80 (-4) | $2.8\times T^{-0.06}$ (6) |
| 18 | 656.79 | 0.145 | 5.66 (-4) | $3.2\times T^{-0.055}$ (6) |
| 19 | 729.68 | 0.137 | 6.60 (-4) | $3.7\times T^{-0.05}$ (6) |
| 20 | 806.38 | 0.130 | 7.64 (-4) | $4.2\times T^{-0.045}$ (6) |
| 21 | 886.90 | 0.124 | 8.77 (-4) | $4.7\times T^{-0.04}$ (6) |
| 22 | 971.23 | 0.119 | 9.98 (-4) | $5.3\times T^{-0.035}$ (6) |
| 23 | 1059.37 | 0.113 | 1.13 (-3) | $5.9\times T^{-0.03}$ (6) |
| 24 | 1151.32 | 0.109 | 1.27 (-3) | $6.5\times T^{-0.025}$ (6) |
| 25 | 1247.06 | 0.104 | 1.42 (-3) | $6.8\times T^{-0.020}$ (6) |

*Note.* Powers of ten multipliers in parentheses. From left to right: upper level of the rotational lines $J \rightarrow J-1$, energy of the upper level, wavelength of the lines, Einstein transition probabilities for spontaneous emission, and fits to the critical densities. The data are given according to Kamp & van Zadelhoff (2001).

transition from level $i$ is taken into account at the $r$ if $n(r) > n_{cr}$, where $n_{cr}$ is the critical density. Concerning the levels above $J = 26$, the critical densities exceed $10^{17}$ molecules/m$^3$. So, I use the number density of CO that is always less than $10^{17}$ molecules/m$^3$ in the calculations. It consists of 26 levels up to $J = 25$ and has 351 CO-$H_2$ collisional rate coefficients (Schinke et al., 1985). The pumping of CO levels by infrared radiation is included. The molecular line data is summarized in Table 9.2. The data in Table 9.2 is applicable to wide temperature range (McKee et al., 1982).

Therefore, a formula for the CO cooling is

$$\Lambda_{\rm CO} = \sum_{J=1}^{25} h\nu_{JJ'} n_J({\rm CO}) A_{JJ'} \beta_{esc}(\tau_{JJ'}) \tag{9.8}$$

where $J' = J - 1$. The level population $n_J$(CO) is calculated in the assumption of LTE

$$n_J({\rm CO}) = \frac{n({\rm CO}) g_J \exp\left(-\frac{E_J}{k_B T}\right)}{Z} \tag{9.9}$$

where $n$(CO) is total number density of CO, $g_J = 2J + 1$ is the statistical weight, $Z$ is the partition function.

## 9.3 Results

Although I use a broad parameter range (Table 9.1), the calculated results can be classified into three categories in a simple way: Typical results are shown in Table 9.3. (1) Both neon and argon escape in almost same escape flux rate by uplifting of hydrogen hydrodynamic escape ($\triangle$ in Table 9.3). (2) Neon obtain more escape flux rate than argon by well-balanced force condition between an acceleration by uplifting of hydrogen hydrodynamic escape and deceleration by cooling of carbon monoxide's emission (escape flux ratios ($F_{\rm Ar}/F_{\rm Ne}$) are roughly shown in Table 9.3). (3) Neither neon nor argon escape, because the cooling of carbon monoxide's emission excessively weakens uplifting force of hydrogen hydrodynamic escape or because the downward drag force of carbon monoxide overcomes uplifting force of hydrogen ($\bigtriangledown$ in Table 9.3).

Typically, the result changes from category (1) to (3) along with increasing the homopause carbon monoxide number density. In other words, along with increasing the cooling effect of carbon monoxide's emission, the temperature of Venusian atmosphere drops and the hydrogen escape flux rate decreases, so that the noble gases cannot get enough upward force from surrounding hydrogen.

Table 9.3 also indicates that neon/argon fractionation before the 50 Myr could not occur because the solar EUV irradiation from the central star would be too high to fractionate neon and argon. In this case, even in the most extreme case (i.e., $n_{\mathrm{Ne,Ar}}$ is $10^{-4} \times n_{\mathrm{H_2}}$ and $n_{\mathrm{CO}}$ is $1.0 \times n_{\mathrm{H_2}}$), CO cooling does not decrease the atmospheric temperature (and consequently the hydrogen escape flux rate) enough to fractionate of neon and argon. On the other hand, at solar age of 100 Myr, the neon/argon fractionation occurs only in the limited cases such as $n_{\mathrm{Ne,Ar}}$ is $10^{-4} \times n_{\mathrm{H_2}}$ and $n_{\mathrm{CO}}$ is $1.0 \times n_{\mathrm{H_2}}$. However, it is note that, if the homopause number densities of $H_2$ and CO are more than $1.0 \times 10^{17}$, downward drag force of CO to $H_2$ becomes too large so that noble gases cannot escape by hydrogen hydrodynamic escape regardless of their number densities at homopause.

Figure 9.3 shows calculated temperature of Venusian atmosphere under the various homopause CO number densities. The homopause hydrogen number density set to $1.0\times10^{15}$ [molecules/m$^3$]. With increasing the homopause CO number density, the atmospheric temperature is decreasing especially in the case of CO = $1.0\times10^{15}$ [molecules/m$^3$]. The result means that the CO cooling is actually effective in decreasing the atmospheric temperature.

Figure 9.4 shows calculated escape flux rates under the various homopause CO number densities for the typical case that Ne/Ar fractionation occurs. The homopause hydrogen number density are $1.0\times10^{15}$, and both Ne and Ar is $1.0\times10^{10}$ [molecules/m$^3$]. Hydrogen escape flux rate is decreasing with increasing homopause CO number density, and along with that, the escape flux rate of neon and argon are also decreasing (Fig. 9.4). Then when carbon monoxide is the same amount as hydrogen at the homopause, the Ne/Ar fractionation ($F_{\mathrm{Ar}}/F_{\mathrm{Ne}} = 0.1$) occurs. In this case, the fractionation of neon and argon due to the CO cooling actually occurs as expected in section 9.1.1 or Zahnle & Kasting (1986).

So, can we get the observed Ne/Ar ratio of present Venusian atmosphere via hydrodynamic escape of proto atmosphere with gravitationally attracted solar nebula components? Unfortunately, the answer would be "No." Here, let us consider the following three extreme cases for compositions of primordial Venusian atmosphere.

(1) The case that the Venusian primordial atmosphere consists entirely of solar nebula compositions: According to Genda & Abe (2003, 2005), without an ocean at the surface of a planet, the atmospheric mass after the stage of giant impacts is

Table 9.3: Calculated Escape Flux Ratio ($F_{\mathrm{Ar}}/F_{\mathrm{Ne}}$)

| $\tau$ | $n_{\mathrm{H_2}}$ | $n_{\mathrm{Ne,Ar}}$ | $n_{\mathrm{CO}}$ | $F_{\mathrm{Ar}}/F_{\mathrm{Ne}}$ |
|---|---|---|---|---|
| 0.01 | 1.0e14 | 1.0e10 | 1.0e14 | $\triangle$ |
| 0.01 | 1.0e15 | 1.0e11 | 1.0e15 | $\triangle$ |
| 0.01 | 1.0e16 | 1.0e12 | 1.0e16 | $\triangle$ |
| 0.05 | 1.0e14 | 1.0e10 | 1.0e14 | $\triangle$ |
| 0.05 | 1.0e15 | 1.0e11 | 1.0e15 | $\triangle$ |
| 0.05 | 1.0e16 | 1.0e12 | 1.0e16 | $\triangle$ |
| 0.1 | 1.0e14 | 1.0e9 | 1.0e14 | $\triangle$ |
| 0.1 | 1.0e14 | 1.0e10 | 1.0e10 | $\triangle$ |
| 0.1 | 1.0e14 | 1.0e10 | 1.0e12 | $\triangle$ |
| 0.1 | 1.0e14 | 1.0e10 | 1.0e14 | $\sim 0.1$ |
| 0.1 | 1.0e15 | 1.0e9 | 1.0e11 | $\triangle$ |
| 0.1 | 1.0e15 | 1.0e10 | 1.0e11 | $\triangle$ |
| 0.1 | 1.0e15 | 1.0e10 | 1.0e13 | $\triangle$ |
| 0.1 | 1.0e15 | 1.0e10 | 1.0e15 | $\sim 0.1$ |
| 0.1 | 1.0e15 | 1.0e10 | 1.0e15 | $\triangle$ |
| 0.1 | 1.0e15 | 1.0e11 | 1.0e11 | $\triangle$ |
| 0.1 | 1.0e15 | 1.0e11 | 1.0e13 | $\triangle$ |
| 0.1 | 1.0e15 | 1.0e11 | 1.0e15 | $\triangledown$ |
| 0.1 | 1.0e16 | 1.0e11 | 1.0e12 | $\triangle$ |
| 0.1 | 1.0e16 | 1.0e11 | 1.0e14 | $\triangle$ |
| 0.1 | 1.0e16 | 1.0e11 | 1.0e16 | $\sim 0.9$ |
| 0.1 | 1.0e16 | 1.0e12 | 1.0e12 | $\triangle$ |
| 0.1 | 1.0e16 | 1.0e12 | 1.0e14 | $\triangle$ |
| 0.1 | 1.0e16 | 1.0e12 | 1.0e16 | $\triangledown$ |
| 0.1 | 1.0e17 | 1.0e13 | 1.0e17 | $\triangledown$ |

*Note.* A small portion of the results are shown here.

$\triangle$: Both neon and argon escape in almost same flux along with hydrogen.

$\triangledown$: Neither neon nor argon escape along with hydrogen.

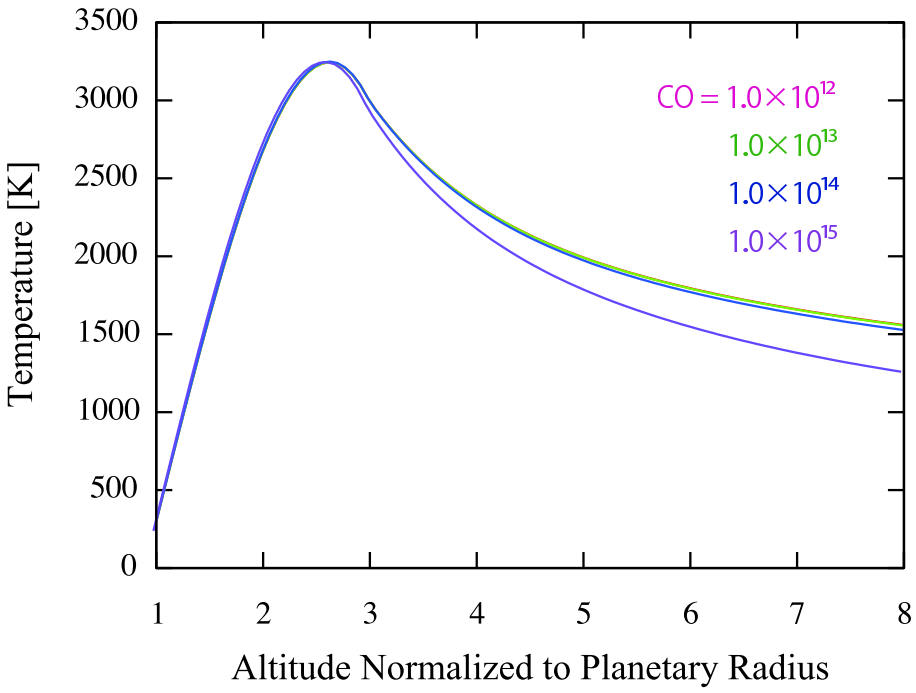


Figure 9.3: Temperature distribution in the steady state of hydrodynamic escape of Venusian atmosphere. Solar age is 0.1 Gyr. Abundance of $H_2$ and CO is parameter. Hydrogen number density at the bottom of the atmosphere is $1.0\times10^{15}$ [molecules/m$^3$]. CO number densities at the bottom of the atmosphere are $1.0\times10^{12}$ (red), $1.0\times10^{13}$ (green), $1.0\times10^{14}$ (blue), and $1.0\times10^{15}$ (purple) [molecules/m$^3$].

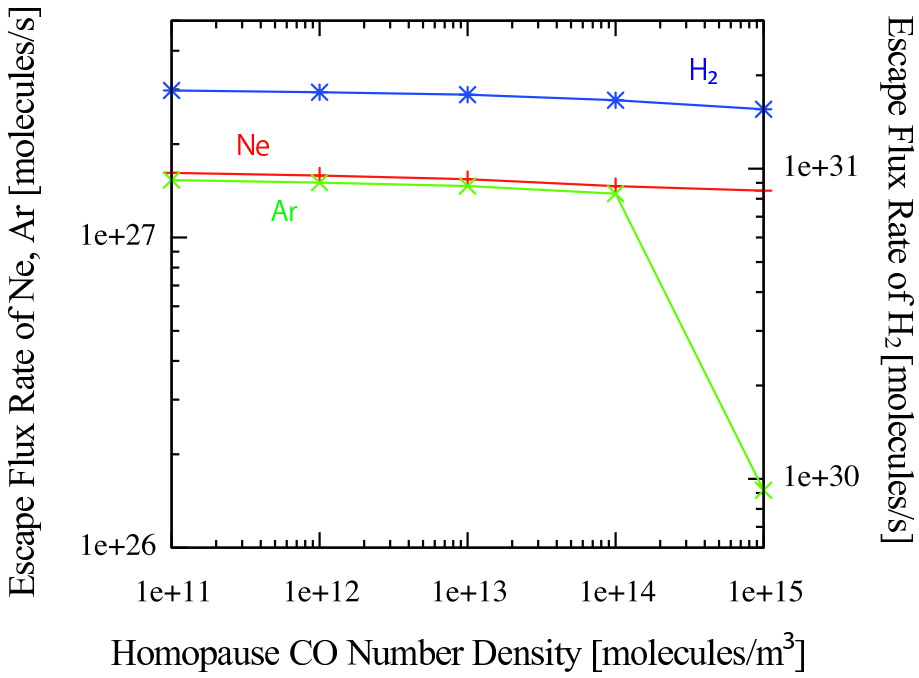


Figure 9.4: Hydrogen, Neon, and Argon escape flux rates in the steady state of hydrodynamic escape of Venusian atmosphere. Solar age is 0.1 Gyr. The $H_2$ number densities at the bottom of the atmosphere are $1.0\times10^{15}$, Ne is $1.0\times10^{10}$, and Ar is $1.0\times10^{10}$ [molecules/m$^3$]. The horizontal axis is CO number density at the bottom of the atmosphere. The escape flux rates of Ne (red) and Ar (green) refer to the left vertical axis, and that of $H_2$ (blue) refers to the right.

approximately a few times the atmospheric mass of a protoplanet. Hence, because the early Venus is considered not to have an ocean at the surface, the amount of a protoplanet's atmosphere approximately gives the one of the Venusian atmosphere after the giant impacts stage. The mass of the nebula gas which a protoplanet gravitationally attracts in the nebula gas is $8.4 \times 10^{21}$ kg, which is the total atmospheric mass within the Hill radius (Hayashi, 1979). This mass would be upper limit of primordial atmosphere on the protoplanet because the decrease of the density at Hill radius results in the decrease of total atmospheric mass (Mizuno et al., 1982). The atmosphere of $8.4 \times 10^{21}$ kg with the solar abundance contains krypton of $4.9 \times 10^{14}$ kg (Table 7.1). On the other hand, the present Venusian atmosphere contains krypton of $2.3 \times 10^{14}$ kg. Therefore, the pre giant impact atmosphere is enough to contain the present Venusian krypton content; The same is true for argon and xenon in Venusian atmosphere. Because the krypton would be too heavy to escape and retain the initial amount to the present, the mass of the pre giant impact atmosphere can be estimated inversely to be order of $10^{20}$ kg to satisfy the present Venusian krypton contents (Genda & Abe, 2005).

The atmosphere of order of $10^{20}$ kg with the solar abundance contains argon of order of $10^{16}$ kg, which is approximately the same amount of the present Venusian argon of $1.2 \times 10^{16}$ kg. In the meanwhile, the amount of neon of the Venusian post giant impact atmosphere is $1.6 \times 10^{17}$ kg, which is about two order more than the present Venusian neon contents of $1.4 \times 10^{15}$ kg. This overabundant neon must escape by hydrogen hydrodynamic escape, which does not take off Venusian argon so much. However, CO abundance in the solar nebula would be much smaller than hydrogen abundance (about two order smaller). Hence, CO cooling is ineffective in fractionating the Ne/Ar escape flux rate (Table 9.3 and Fig. 9.4). Therefore, we cannot get the observed Ne/Ar ratio of present Venusian atmosphere via hydrodynamic escape of solar abundance atmosphere.

(2) The case that the Venusian primordial atmosphere consists entirely of degassing compositions: Unlike with the case (1), CO abundance in meteorites at the maximum would be same as hydrogen abundance (Table 7.1). So, there is a possibility that effective Ne/Ar fractionation due to the CO cooling would occur in this case (Table 9.3 and Fig. 9.4). However, this degassing dominant atmosphere has a fatal flaw in the first place, i.e., even the most volatile-rich meteorites have less abundant argon than present Venusian atmosphere. In other words, the atmosphere consisted entirely of degassing compositions from meteorites is absolutely lacking in the amount

of argon as compared to present Venusian atmosphere. Therefore, we cannot get the observed Ne/Ar ratio of present Venusian atmosphere via hydrodynamic escape of degassing atmosphere.

(3) The case that the Venusian primordial atmosphere consists of mixture of solar nebula and degassing compositions: The mixing ratio of solar nebula and degassing compositions is unknown. So, let us consider the most optimistic case, i.e., noble gases are supplied from solar nebula (that is, enough to contain the present Venusian argon content) and carbon monoxide is supplied from most volatile meteorites' degassing (that is, the same amount as hydrogen). In this case, it seems possible to achieve present Venusian Ne/Ar ratio by hydrodynamic escape of neon and argon under the effective CO cooling circumstance in the primordial Venusian atmosphere.

However, in practice, the maximum fractionation ratio as $F_{\rm Ar}/F_{\rm Ne} = 0.1$ (Fig. 9.4) does not account for the present Ne/Ar ratio of the Venusian atmosphere. The atmosphere of $10^{20}$ kg with the solar abundance contains neon of $1.6 \times 10^{17}$ kg (Table 7.1), and meanwhile the present Venusian atmosphere contains neon of $1.4 \times 10^{15}$ kg. So, neon should be reduced to over two order lower amount via escape process. Then, if the argon escape rate is tenth part of the neon escape rate, argon in the primordial Venusian atmosphere almost vanish because the atmosphere of $10^{20}$ kg with the solar abundance contains argon of only $9.0 \times 10^{15}$ kg, which is over one order less than neon in the atmosphere. Therefore, even in the most optimistic case, we cannot get the observed Ne/Ar ratio of present Venusian atmosphere via hydrodynamic escape of mixture atmosphere of solar nebula and degassing compositions.

## 9.4 Discussions

As shown in the previous section, even in the most optimistic case, appropriate Ne/Ar fractionation cannot be achieved by hydrogen hydrodynamic escape of primordial Venusian atmosphere even if the temperature control by CO cooling is considered in the numerical model. In this chapter, other possibilities of achieving noble gas patterns of present Venusian atmosphere are discussed.

### 9.4.1 $H_2O$ Rotational Cooling

At high $H_2O$ levels, cooling in the water vapor rotation band becomes important as well as CO rotational cooling. However, it is very difficult to calculate the $H_2O$ cooling rate precisely because $H_2O$ has broad continuous rotational absorption lines

so that line-by-line method cannot be applied. So, approximate expressions are used here to roughly estimate the effect of $H_2O$ cooling compared with CO cooling. $H_2O$ molecules are excited to higher rotational states by collisions with other molecules, mostly H atoms produced from $H_2O$ photolysis. Infrared cooling of a mixture of H and $H_2O$ has been studied in connection with interstellar shocks (Hollenbach and McKee, 1979) and I have simply adopted their parameterization as Kasting & Pollack (1983). The cooling is approximated by:

$$\Lambda_{H_2O} = n(H)n(H_2O)L_{H_2O} \tag{9.10}$$

where $n(H)$ and $n(H_2O)$ are the number densities of atomic H and $H_2O$ vapor and $L_{H_2O}$ is a rotational line cooling coefficient given by:

$$L_{H_2O} = \frac{2(kT)^2 A_0}{nE_0}\left[\frac{2 + y_m + 0.6y_m^2}{1 + C_\tau + \frac{n_{cr}}{n} + 1.5(\frac{n_{cr}}{n})^{1/2}}\right] \tag{9.11}$$

The parameters in Eq. (9.11) are:

$$y_m = \ln\left[1 + \frac{C_\tau}{1 + 10\frac{n_{cr}}{n}}\right] \tag{9.12}$$

$$C_\tau = \tau_T\left(2\pi \ln\left[2.13 + \left(\frac{\tau_T}{e}\right)^2\right]\right)^{1/2} \tag{9.13}$$

$$\tau_T = \frac{4N(H_2O)A_0}{\eta_{JT}(1.18\times 10^7)(\Delta V)_5(E_0/k)^2} \tag{9.14}$$

$$n_{cr} = \frac{4kTA_0}{E_0\sigma_H V_T} \tag{9.15}$$

$$V_T = \left(\frac{8kT}{\pi m_0}\right)^{1/2} \tag{9.16}$$

where $n = n(H)$; $m_0$ is mass of H atom; $A_0 = 2.3\times 10^2$ sec$^{-1}$; $e = 2.718$; $E_0/k = 17$ K; $\sigma_H = 3\times 10^{16}$ cm$^2$; $\eta_{JT} = 7.7(T/1000)^{1/2}$; $(\Delta V)_5 = 1$ is Doppler width of $H_2O$ lines in units of $10^5$ cm/s; and $N(H_2O)$ is column density of $H_2O$ out to inf. The derivation of Eq. (9.11) and a discussion of the individual terms is given in Hollenbach and McKee (1979). They estimate that this formulation is accurate to within a factor of 2 at all optical depths.

Figure 9.5 shows the cooling efficiency ratio between CO and $H_2O$ ($\Lambda_{H_2O}/\Lambda_{CO}$) in the case that both CO and $H_2O$ have the same homopause number density (= $1.0\times 10^{15}$ molecules/m$^3$) as hydrogen. Though the cooling efficiency ratio differs for each altitude, $H_2O$ cooling is always much more effective than CO cooling (Fig. 9.5).

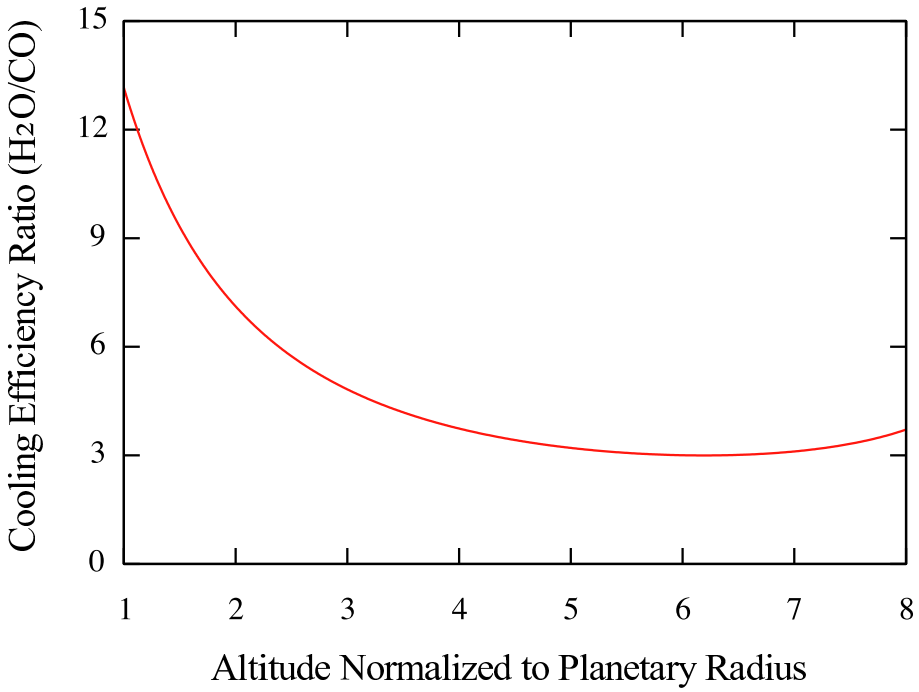


Figure 9.5: Cooling efficiency ratio between CO and $H_2O$ ($\Lambda_{H_2O}/\Lambda_{CO}$). The homopause number density of both CO and $H_2O$ is $1.0\times10^{15}$ and that of $H_2$ is $1.0\times10^{16}$ [molecules/$m^3$].

Therefore, with substantial amount of $H_2O$ component in the primordial Venusian atmosphere, it could be possible to drop the atmospheric temperature enough to fractionate neon and argon effectively (i.e., the difference of escape flux rate between neon and argon could be larger than $10:1$). However, because $H_2O$ is much easier to uplift than neon and argon (Fig. 9.1), the self-sustaining temperature control cannot occur in Ne-$H_2O$-Ar atmosphere unlike in Ne-CO-Ar atmosphere. So, how $H_2O$ cooling affects the fractionation of neon and argon is not a simple question. It will be an important future work to discuss the effect of $H_2O$ cooling to the primordial Venusian atmosphere quantitatively. Additionally, wether a "cold trap" could be formed in the lower part of the atmosphere should be considered. The cold trap is defined as the altitude at which the saturation $H_2O$ mixing ratio reaches its minimum value. If $H_2O$ can go through the cold trap properly, the $H_2$ cooling would be effective to decrease the temperature of upper part of the atmosphere.

### 9.4.2 Additional Origins of Noble Gases

Although hydrodynamic escape of primordial Venusian atmosphere would play a role in atmospheric evolution, particularly affecting the fractionation of neon, Venusian

argon might be escaped too much by this mechanism. A way to overcome this problem would be addition of other atmospheric sources to the Venusian atmosphere after a completion of hydrodynamic escape of primordial Venusian atmosphere. Possible additional origins of noble gases for Venusian atmosphere have been proposed such as solar wind implanted materials (Whetherill, 1981; Sasaki, 1991; Ballentine, 2005) or extremely low-temperature condensates in comets which quantitatively trap argon (neon freezes only if hydrogen freezes, Owen et al., 1999).

Implantation of solar wind is considered to be a noble gas source for lunar soils (Eberhardt et al., 1970), gas-rich meteorites (Suess et al., 1964; Goswani et al., 1984; Caffee et al., 1988) and Venus (Wetherill, 1981; McElroy & Prather, 1981). Anisotropy of high-energy particle tracks in meteorite grains suggests that noble gases in gas-rich meteorites were implanted at the surfaces of parent bodies (Goswani et al., 1984). However, there is also evidence that implies earlier irradiation by high-energy particles before accretion (Heymann and Palma, 1986; Caffee et al., 1987). The dust and small fragments are envisioned as constantly being formed by collisions and re-accreted into planetesimals. Most of these materials are eventually incorporated into planets. Because much of the planetary material becomes exposed to the solar wind, noble gases accrete early and more or less homogeneously. Enrichment of Venus in implanted gas would be a consequence of the irradiated material being initially confined to the innermost edge of the radially opaque circumsolar planetesimal disk. Wetherill (1981) speculated that the high noble gas abundances on Venus, comparable to those in gas-rich meteorites, could be the result of accretion of planetesimals or their fragments that have trapped significant amounts of ancient solar wind. And Sasaki (1989, 1991) implied that an appreciable amount of solar wind species is trapped and the high abundances of solar-type noble gases in gas-rich meteorites and Venus can be explained. However, although the solar-wind implantation can account for nearly solar Ar/Kr in Venusian atmosphere, it fails to account for low Ne/Ar.

On the other hand, comets would deliver an already fractionated mixture of gas. Fractionation in icy planetesimals occurs for temperatures above 30 K because the differing sizes and polarizabilities of the atoms lead to competition for the available sites in the ice (Notesco et al., 2003). However, neon is not trapped in amorphous ice except at temperatures below 20 K (Laufer et al., 1987; Bar-Nun et al., 1988). A relatively late impact by a large comet (or group of comets) formed at a temperature near or above 30 K would can account for the fractionation of noble gases on Venus by

bringing in a nearly solar mixture of the noble gases except neon after the completion of hydrodynamic escape of primordial atmosphere (Wetherill, 1990).

Unfortunately, we have never acquired reliable observed values of nobles gases in any comets nor solar-implanted materials. So, how these additional origins of atmosphere quantitatively affect the Venusian noble gas patterns has been unknown yet. Future observations of noble gases' abundance in comets and researches of primordial materials such as solar-implanted materials are important future work to explanation of noble gas patterns of Venusian atmosphere.

# Chapter 10

# Conclusions

In this paper, a robust numerical model is developed to study multi-component hydrodynamic escape from planetary atmospheres. The numerical code is solved using CIP method, which is well suited to solve the transonic flow. A two-dimensional numerical model is also developed to calculate the deposition of solar EUV radiation in an extended atmosphere.

The numerical model is applied to the early Venusian atmosphere to consider "water loss from early Venus" and "fractionation of noble gases on Venus" problems quantitatively. The former application (water loss from early Venus) indicates that Venus was able to lost entire water, that is assumed to be terrestrial ocean amount, under the special circumstances such that the homopause number densities of $H_2$ and O are maintained around $9.0 \times 10^{15}$ [molecules/m$^3$] for about $1.5 \times 10^8$ years. However, except in that special case, Venus could not have lost much oxygen, which dissociated from water on early Venus. This means that a substantial amount of oxygen left on Venus after hydrodynamic escape of hydrogen. This result implies that other ways of taking the oxygen away from Venusian atmosphere should be discussed more precisely in the future. On the other hand, the latter application (fractionation of noble gases on Venus) indicates that present Venusian Ne/Ar abundance ratio cannot be achieved by hydrodynamic escape even if an atmospheric temperature controlled by CO cooling is taken into consideration. However, other cooling mechanism such as $H_2O$ cooling and other noble gases' sources such as solar implanted materials and/or comets might make it possible to achieve the proper Ne/Ar fractionation. This result implies that more detailed studies of atmospheric cooling processes and other noble gases' sources are required to understand the fractionation of Venusian atmospheric noble gases. Moreover, time-evolutional numerical code is required for the future study to solve the Venusian atmospheric evolution more precisely. Because both the solar EUV flux

and the hydrogen supply are expected to decline with time, the lighter elements are more depleted and relatively more fractionated than the heavier elements by real hydrodynamic escape.

# Appendix A

# CIP Method

## A.1 Basic Concepts

Although nature operates in a continuous world, a discretization process is unavoidable for implementing numerical simulations. The CIP method tries to construct a solution inside the grid cell that is close enough to the real solution of the given equation, with some constraints (Takewaki & Yabe, 1987; Yabe & Aoki, 1991; Yabe et al., 2001). Yabe et al. proposed an approximation of the profile as shown below. If we differentiate Eq. (A.1) with spatial variable $x$ , we get Eq. (A.2)

$$\frac{\partial f}{\partial t} + u\frac{\partial f}{\partial x} = 0 \tag{A.1}$$

$$\frac{\partial g}{\partial t} + u\frac{\partial g}{\partial x} = -\frac{\partial u}{\partial x}g \tag{A.2}$$

Equation (A.2) gives a simple translational motion of a wave with velocity $u$, and $g$ stands for the spatial derivative of $f$, i.e., $\partial f/\partial x$. In the simplest case where the velocity $u$ is constant, Eq. (A.2) coincides with Eq. (A.1) and represents the propagation of a spatial derivative with velocity $u$. Using these equations, we can trace the time evolution of $f$ and $g$. If $g$ is predicted after propagation, the profile after one step is limited to a specific profile. It is easy to imagine that by this constraint, the solution becomes much closer to the initial profile that is the real solution. Most importantly, the solution thus created gives a profile consistent with Eq. (A.1) even inside the grid cell. If two values of $f$ and $g$ are given at two grid points, the profile between these points can be interpolated by the cubic polynomial

$$F(x) = ax^3 + bx^2 + cx + d \tag{A.3}$$

Thus, the profile at the $n+1$ step can be obtained by shifting the profile by $u\Delta t$ so that

$$f^{n+1} \;=\; F(x - u\Delta t) \tag{A.4}$$

$$g^{n+1} = \frac{dF(x-u\Delta t)}{dx} \tag{A.5}$$

Then, $f$ and $g$ values at $i$th grid cell are given by

$$f_i^{n+1} = a_i\xi^3 + b_i\xi^2 + g_i^n\xi + f_i^n \tag{A.6}$$

$$g_i^{n+1} = 3a_i\xi^2 + 2b_i\xi + g_i^n \tag{A.7}$$

$$a_i = \frac{g_i + g_{iup}}{D^2} + \frac{2(f_i - f_{iup})}{D^3} \tag{A.8}$$

$$b_i = \frac{3(f_{iup} - f_i)}{D^2} - \frac{2g_i + g_{iup}}{D} \tag{A.9}$$

where we define $\xi = -u\Delta t$. Here, $D = -\Delta x$, $iup = i-1$ for $u \geq 0$ and $D = \Delta x$, $iup = i+1$ for $u < 0$. The CIP advection scheme can be sorted out as a kind of semi-Lagrangian method in the sense that the CIP advection scheme employs a Lagrangian invariant solution. Semi-Lagrangian methods that trace back along the characteristics in time depend on an interpolation of the initial profile to determine the value at the upstream departure point (which may not coincide with the computational grid point). To solve nonlinear problems, it is expedient to separate the solution procedure into several fractional steps.

Let us consider a hyperbolic equation,

$$\frac{\partial f}{\partial t} + \frac{\partial fu}{\partial x} = g \tag{A.10}$$

where the source term $g$ can be a function of $f$. The equation can be split into two phases; the nonadvection phase

$$\frac{\partial f}{\partial t} = G \tag{A.11}$$

and the advection phase

$$\frac{\partial f}{\partial t} + u\frac{\partial f}{\partial x} = 0 \tag{A.12}$$

Here I have moved the compression term $f\frac{\partial u}{\partial x}$ on the left-hand side of Eq. (A.10) to the right-hand side and have introduced,

$$G = g - f\frac{\partial u}{\partial x} \tag{A.13}$$

The CIP solvers that were given in Eq. (A.6)-(A.9) are applied only to the advection phase after the nonadvection phase is solved with a finite-difference approach. For the spatial derivative of Eq. (A.10), we have

$$\frac{\partial f'}{\partial t} + u\frac{\partial f'}{\partial x} = G' - f'\frac{\partial u}{\partial x} \tag{A.14}$$

This equation is also split into two phases:

$$\frac{\partial f'}{\partial t} = G' - f'\frac{\partial u}{\partial x} \tag{A.15}$$

$$\frac{\partial f'}{\partial t} + u\frac{\partial f'}{\partial x} = 0 \tag{A.16}$$

Actual method to solve the Euler equations (Eq. (4.5)-(4.7)) separately for the non-advection and the advection phases is described in the following subsections.

## A.2 Nonadvection phase

The equation for $f$, $\partial f/\partial t = G$, is simply solved using finite differencing,

$$f_i^* = f_i^n + G_i \Delta t, \tag{A.17}$$

where $^*$ on $f$ means the time after one time step in the nonadvection phase. Even if $G$ includes the diffusion term and must be solved implicitly, the implicit solver can be applied to this phase. We need not convert Eq. (A.14) for $f'$ into a finite-difference form. As has been discussed previously (Takewaki & Yabe, 1987), a simple treatment is possible. The time evolution of $f'$ associated with $G'$ can be estimated from Eq. (A.17). Thus, we approximate the time evolution of $f'$ with the finite difference of the time evolution of $f$ to be

$$\frac{f_i'^* - f_i'^n}{\Delta t} = \frac{f_{i+1}^* - f_{i-1}^* - f_{i+1}^n + f_{i-1}^n}{2\Delta x \Delta t} \tag{A.18}$$

Another term $f'\partial u/\partial x$ in Eq. (A.15) can simply be solved with finite differencing; thus we have

$$\frac{f_i'^* - f_i'^n}{\Delta t} = \frac{f_{i+1}^* - f_{i-1}^* - f_{i+1}^n + f_{i-1}^n}{2\Delta x \Delta t} - f_i'^n \frac{u_{i+1} - u_{i-1}}{2\Delta x} \tag{A.19}$$

Here we adapted an approach that uses staggered meshes to solve these equations. First, we describe a solution in a staggered mesh system; that is, $\rho$ and $p$ are defined at the grid point $x_i$ and $u$ is defined at $x_{i+1/2}$. The finite-difference forms in the nonadvection phase of Eq. (4.5)-(4.7) can be written as

$$\frac{n_i^* - n_i^n}{\Delta t} = -n_i^n \frac{u_{i+1/2}^n - u_{i-1}^n}{\Delta x} - \frac{2n_i^n u_{i+1/2}^n}{x_i} \tag{A.20}$$

$$\frac{u_{i+1/2}^* - u_{i+1/2}^n}{\Delta t} = -\frac{2}{\rho_{i+1}^n + \rho_i^n}\frac{p_{i+1}^n - p_i^n + \nu_{i+1}^n - \nu_i^n}{\Delta x} - \frac{GM}{x_i^2} \tag{A.21}$$

$$\frac{p_i^* - p_i^n}{\Delta t} = -\gamma p_i^n \frac{u_{i+1/2}^n - u_{i-1}^n}{\Delta x} - \frac{2\gamma p_i^n u_{i+1/2}^n}{x_i} + (\gamma - 1) q_i \tag{A.22}$$

$$+\frac{\gamma - 1}{x_i^2} \left[ \left( \kappa x_i^2 \frac{T_{i+1} - T_i}{\Delta x} \right)_{i+1} - \left( \kappa x_i^2 \frac{T_i - T_{i-1}}{\Delta x} \right)_i \right] / \Delta x \tag{A.23}$$

We adopted the numerical viscosity $\nu$, which has the same dimension as pressure, used by Nishiguchi and Yabe (1983). Large number ranges and steep gradients pose a difficult challenge to numerical approximation techniques, and it can generally be expected that in regions of large gradients numerical accuracy may decrease. So, in the non-advection phase of conservation of momentum equation, an explicit diffusion term is required. This diffusion acts to damp sharp gradients on the grid, providing numerical stability. The numerical viscosity $\nu$ is given by the equation

$$\nu_i = -c_\nu \gamma \rho_i (u_{i+1/2}^n - u_{i-1/2}^n) \left[ \sqrt{\frac{p_i^n}{\rho_i^n}} - \frac{\gamma + 1}{2} (u_{i+1/2}^n - u_{i-1/2}^n) \right] \tag{A.24}$$

if $u_{i+1/2}^n - u_{i-1/2}^n < 0$. If $u_{i+1/2}^n - u_{i-1/2}^n \geq 0$, $\nu_i = 0$. Here $c_\nu$ is the numerical viscosity coefficient, and we adapt $c_\nu = 0.75$ in this study.

Because of the large density curvature near the lower boundary (especially for the large-HEP case), the diffusion term is not negligible there. In the steady state, the time derivative term in the continuity equation goes to zero. If the explicit diffusion term is small, a nearly constant momentum can be obtained. However, near the lower boundary for large HEP the momentum must adjust itself to meet the large density curvature in the diffusion term, and thus it deviates from the analytical solution. As a result, in the numerical results the momentum and the flow velocity are not calculated as accurately in the region of the domain close to the lower boundary as in the rest of the domain. However, it is interesting to note that the deviation in momentum close to the lower boundary at low resolution does not influence the calculated value of the mass flux at the outflow boundary significantly (Tian et al., 2005). This is because the diffusion term becomes very small in most of the atmosphere since the gradients are low.

## A.3 Advection phase

After $f$ and $f'$ are advanced in the nonadvection phase, the CIP solver is applied to the advection phase. The interpolated profile is determined from Eq. (A.6)-(A.9) using $f^*$ and $f'^*$ on the right-hand side.

These two phases complete one time step of the calculation; then after replacing $f^{n+1}$ and $f'^{n+1}$ by $f^n$ and $f'^n$, we return to the nonadvection phase again. These procedures are iterated until achieving the steady state solution.

# Appendix B

# Supporting Materials for Numerical Model

## B.1 Data for Solar EUV Spectrum

For aeronomic studies, reference solar irradiance spectra representative of conditions during solar cycle 22 (1986-1996) are presented here. These reference spectra are primarily established from actual observations; however, results from selected solar irradiance proxy models are used in creating and validating the reference solar spectra in the XUV and EUV range. These reference spectra are given in 1 nm intervals on 0.5 nm centers. A reference spectrum for solar cycle 22 minimum conditions is listed in Table B.1.

## B.2 Data for Cross-Sections of Photoabsorption for Molecular Hydrogen

In Table B.2 the data are presented on cross-sections for photoabsorption. The accuracy of the recommended absolute values of cross-sections determined by averaging of the available experimental data is better than $\pm 20\%$.

## B.3 Two-Dimensional Energy Deposition

As shown in Fig. B.1, a solar radiation beam is absorbed (Beer's Law) in a layer with depth $\Delta s$. The energy deposition in a given layer along each path is then multiplied with the area of the ring, $2\pi D \Delta D$ (Fig. B.1), to obtain the total energy deposited into the shell segment. Here $D$ is the distance from the planet center to the solar radiation beam. Note that for one shell with radius $r$, shell segments may have different $D$

Table B.1: Reference Spectrum for Solar EUV

| $\lambda$ (nm) | @$\lambda$+0nm | @$\lambda$+1nm | @$\lambda$+2nm | @$\lambda$+3nm | @$\lambda$+4nm |
|---|---|---|---|---|---|
| 0.5 | 3.700 | 6.000 | 7.000 | 7.455 | 7.834 |
| 5.5 | 8.282 | 8.288 | 8.409 | 8.247 | 8.395 |
| 10.5 | 8.000 | 7.902 | 7.739 | 7.755 | 8.218 |
| 15.5 | 8.206 | 8.542 | 9.192 | 8.827 | 8.782 |
| 20.5 | 8.422 | 8.285 | 8.645 | 8.392 | 8.778 |
| 25.5 | 8.986 | 8.381 | 8.723 | 8.590 | 8.393 |
| 30.5 | 9.873 | 9.045 | 8.799 | 8.807 | 8.849 |
| 35.5 | 8.750 | 8.892 | 8.381 | 8.025 | 7.980 |
| 40.5 | 8.215 | 8.003 | 7.976 | 8.268 | 7.957 |
| 45.5 | 7.923 | 8.471 | 8.099 | 8.337 | 8.628 |
| 50.5 | 8.532 | 8.061 | 8.093 | 8.192 | 8.048 |
| 55.5 | 8.700 | 8.172 | 8.156 | 8.903 | 8.286 |
| 60.5 | 8.734 | 8.403 | 9.024 | 8.410 | 7.823 |
| 65.5 | 7.691 | 7.682 | 7.688 | 8.224 | 8.077 |
| 70.5 | 8.541 | 8.174 | 8.012 | 8.133 | 8.229 |
| 75.5 | 8.443 | 8.865 | 8.735 | 8.964 | 8.663 |
| 80.5 | 8.641 | 8.702 | 8.876 | 9.150 | 8.981 |
| 85.5 | 9.032 | 9.063 | 9.144 | 9.207 | 9.296 |
| 90.5 | 9.375 | 9.269 | 8.821 | 8.777 | 8.632 |
| 95.5 | 8.438 | 8.460 | 9.699 | 8.775 | 8.968 |
| 100.5 | 8.582 | 8.649 | 9.568 | 9.589 | 8.802 |

*Note.* A reference spectrum for solar cycle 22 minimum condition is listed in 1 nm intervals on 0.5 nm centers and at a solar distance of 1 AU (Woods and Rottman, 2002). The values of the log (base-10) of the irradiance are the irradiances in units of [photons/cm$^2$s].

Table B.2: Photoabsorption Cross-Sections for Molecular Hydrogen

| $\lambda$ (nm) | $\sigma$ ($10^{-18}$ cm$^2$) |
|---|---|
| 0.1-0.3 | 1.5e-6 |
| 0.3-0.44 | 1.8e-6 |
| 0.44-0.8 | 4.1e-6 |
| 0.8-1.8 | 4.1e-5 |
| 1.8-2.3 | 1.2e-4 |
| 2.3-3.1 | 3.1e-4 |
| 3.1-4.4 | 1.0e-3 |
| 4.4-5.0 | 2.0e-3 |
| 5.0-6.15 | 3.4e-3 |
| 6.15-10 | 1.2e-2 |
| 10-15 | 4.8e-2 |
| 15-20 | 0.14 |
| 20-25 | 0.40 |
| 25-30 | 0.76 |
| 30-35 | 1.34 |
| 35-40 | 2.1 |
| 40-45 | 2.9 |
| 45-50 | 3.8 |
| 50-55 | 5.0 |
| 55-60 | 6.3 |
| 60-65 | 7.8 |
| 65-70 | 8.9 |
| 70-75 | 11.1 |
| 75-80 | 12.8 |
| 80-85 | 14.3 |
| 85-90 | 16.0 |
| 90-95 | 26.3 |
| 95-100 | 32.9 |
| 100-105 | 25.2 |

*Note.* The intervals of wavelength are given according to Avakyan et al. (1998).

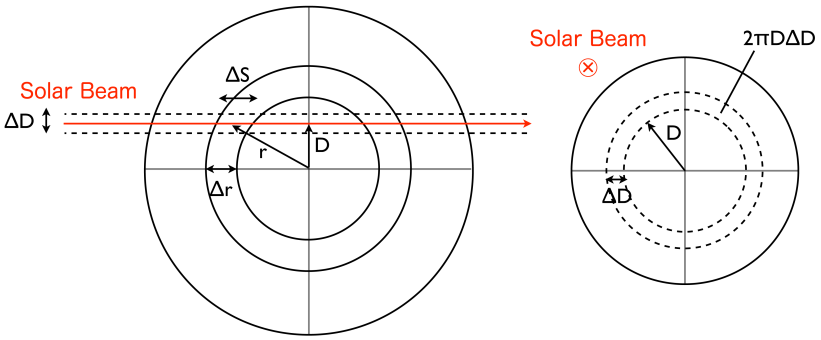


Figure B.1: Schematic of the two-dimensional energy deposition calculation method. (left) Solar beam is in the plane of the figure. (right) Solar beam is perpendicular to the surface of the paper. This figure is modified after Fig. 6 in Tian et al. (2005)

values (from $D = 0$ to $D = r$). When all shell segments belonging to the same shell are included, the total energy deposited into the shell is obtained. The total energy $E_{\rm total}$ divided by the total volume of the shell $V_{\rm shell}$ gives the volume heating rate $q$ in the shell:

$$q(r) = \frac{E_{\rm total}}{V_{\rm shell}} \tag{B.1}$$

$$E_{\rm total} = \int_0^r \Delta S(r) \cdot E(r) \cdot \sigma \cdot n(r) \cdot 2\pi D \Delta D \tag{B.2}$$

$$V_{\rm shell} = \frac{4}{3}\pi r^3 - \frac{4}{3}\pi (r - \Delta r)^3 \tag{B.3}$$

where, $E(r)$ is the solar EUV energy entering the shell (see section B.1); $\sigma$ is the cross-section of photoabsorption for molecular hydrogen (see section B.2); $n(r)$ is the number density of molecular hydrogen in the shell. $\Delta S(r)$ is described by

$$\Delta S(r) = \sqrt{\left(r + \frac{\Delta r}{2}\right)^2 - D^2} - \sqrt{\left(r - \frac{\Delta r}{2}\right)^2 - D^2} \tag{B.4}$$

$$= \sqrt{r^2 - D^2} - \sqrt{(r - \Delta r)^2 - D^2} \tag{B.5}$$

And $E(r)$ is given by

$$E(r) = E(r+1) \cdot (1 - n(r+1) \cdot \sigma \cdot \Delta S(r+1)) \tag{B.6}$$

## B.4 Data for Binary Diffusion Coefficient

In Table B.3, the relevant binary diffusion coefficients are collected. Also shown are relative values of $\Phi_i$, normalized so that $\Phi_i = 1$ for $^{36}$Ar in $H_2$ at $T = 300$ K.

Table B.3: Binary Diffusion Coefficient

| Species | $\Phi_i$ | $b_i$ in $H_2$ [$10^{17}$/cm·s] |
|---|---|---|
| $^{4}He$ | 4.83 | $5.23\times T^{0.75}$ |
| $^{16}O$ | 2.10 | $3.0\times T^{0.75}$ |
| $^{18}H_2O$ | 2.7 | $5.23\times T^{0.75}$ |
| $^{20}Ne$ | 1.29 | $4.37\times T^{0.731}$ |
| $^{28}CO$ | 1.36 | $2.65\times T^{0.75}$ |
| $^{36}Ar$ | 1.00 | $2.81\times T^{0.75}$ |
| $^{84}Kr$ | 0.494 | $2.3\times T^{0.76}$ |
| $^{130}Xe$ | 0.358 | $2.7\times T^{0.712}$ |

*Note.* The data are given according to Zahnle & Kastig (1986) and references therein.

This parameter $\Phi_i$ is a dimensionless ratio of the relative importance of upward drag to gravity on the minor constituent (Zahnle & Kasting, 1986). These provide an indication of the relative ease with which different constituents may escape (Zahnle & Kasting, 1986). It is worth noting that from the perspective of fractionation during hydrodynamic escape, Ne and CO are effectively equivalent. It is also apparent that O and $H_2O$ are lost much more easily than any noble gas save He.

# Appendix C

# Analytical Solutions

## C.1 Parker Solution

For the isothermal atmosphere, the exact solution (Parker, 1964) is

$$\frac{v^2}{c_0^2} - \ln\frac{v^2}{c_0^2} = \frac{v_0^2}{c_0^2} - \ln\frac{v_0^2}{c_0^2} + 4\ln\xi - \frac{2w^2}{c_0^2}\left(1 - \frac{1}{\xi}\right) \tag{C.1}$$

where, $v$ is the velocity, $v_0$ is the velocity at the bottom of atmosphere, $c_0$ is the sonic velocity at the bottom of atmosphere, $\xi = r/a$ is the dimensionless variable, $a$ is the radius of planet, and $w^2 = GM/a$ is the gravitational potential at the bottom of atmosphere. The critical point is

$$\xi_c = \frac{w^2}{2c_0^2}\ , \qquad v(\xi_c) = c_0 \tag{C.2}$$

so that $v_0$ is given by

$$\frac{v_0^2}{c_0^2} - \ln\frac{v_0^2}{c_0^2} = -3 - 4\ln\frac{w^2}{2c_0^2} + \frac{2w^2}{c_0^2} \tag{C.3}$$

and $v(\xi)$ is given by

$$\frac{v^2}{c_0^2} - \ln\frac{v^2}{c_0^2} = -3 - 4\ln\frac{2c_0^2\xi}{w^2} + \frac{2w^2}{c_0^2\xi} \tag{C.4}$$

According to Eq. (C.4), we can get the exact solution of velocity normalized sonic velocity $v/c_0$ for the isothermal atmosphere.

## C.2 Quasi-Analytical Solution for Polytropic Atmosphere

For the polytropic atmosphere, the following relations are assumed.

$$\left(\frac{p}{p_0}\right)^{\frac{\gamma-1}{\gamma}} = \left(\frac{\rho}{\rho_0}\right)^{\gamma-1} = \frac{T}{T_0} \tag{C.5}$$

Equation (C.5) is reduced to

$$\frac{1}{p}\frac{dp}{dr} = \gamma\frac{1}{\rho}\frac{d\rho}{dr} \tag{C.6}$$

The terms $dp/dr$ and $d\rho/dr$ are eliminated from Eq. (4.1), (4.2), and Eq. (C.5), we can get

$$\frac{r}{u}\left(u^2 - \gamma\frac{kT}{m}\right)\frac{du}{dr} = 2\gamma\frac{kT}{m} - \frac{GM}{r} \tag{C.7}$$

Then, $dp/dr$ and $d\rho/dr$ are determined using $du/dr$

$$\frac{dp}{dr} = -\rho\left(u\frac{du}{dr} + \frac{GM}{r^2}\right) \tag{C.8}$$

$$\frac{d\rho}{dr} = -\rho\left(\frac{1}{u}\frac{du}{dr} + \frac{2}{r}\right) \tag{C.9}$$

If the critical point (= sonic point) does in fact exist, the following relations are required at this point

$$u_c^2 - \gamma\frac{kT_c}{m} = 0 \quad \Leftrightarrow \quad u_c = \sqrt{\gamma\frac{kT_c}{m}} \tag{C.10}$$

$$2\gamma\frac{kT_c}{m} - \frac{GM}{r_c} = 0 \quad \Leftrightarrow \quad r_c = \frac{1}{\gamma}\frac{GMm}{2kT_c} \tag{C.11}$$

where, subscript $c$ means the value at the critical point. Then, the slope $(du/dr)_r$ at this critical point may be evaluated from Eq. (C.7) by use of L'Hôpital's rule:

$$\left(\frac{du}{dr}\right)_c = \frac{(df/dr)_c}{(dg/dr)_c} \tag{C.12}$$

Here, $f$ and $g$ are

$$f = u\left(2\gamma\frac{kT}{m} - \frac{GM}{r}\right) \tag{C.13}$$

$$g = r\left(u^2 - \gamma\frac{kT}{m}\right) \tag{C.14}$$

Equation (C.13) and (C.14) are differentiated respectively,

$$\frac{df}{dr} = \frac{du}{dr}\left(2\gamma\frac{kT}{m} - \frac{GM}{r}\right) + u\left(2\gamma\frac{k}{m}\frac{dT}{dr} + \frac{GM}{r^2}\right) \tag{C.15}$$

$$\begin{aligned} \Leftrightarrow \left(\frac{df}{dr}\right)_c &= u_c\left[2\gamma\frac{k}{m}\left(\frac{dT}{dr}\right)_c + \frac{GM}{r_c^2}\right] \\ &= -2(\gamma-1)u_c^2\left(\frac{du}{dr}\right)_c - 2(2\gamma-3)\frac{u_c^3}{r_c} \end{aligned} \tag{C.16}$$

$$\frac{dg}{dr} = \left(u^2 - \gamma\frac{kT}{m}\right) + r\left(2u\frac{du}{dr} - \gamma\frac{k}{m}\frac{dT}{dr}\right) \tag{C.17}$$

$$\begin{aligned} \Leftrightarrow \left(\frac{dg}{dr}\right)_c &= r_c\left[2u_c\left(\frac{du}{dr}\right)_c - \gamma\frac{k}{m}\left(\frac{dT}{dr}\right)_c\right] \\ &= (\gamma+1)r_c u_c\left(\frac{du}{dr}\right)_c + 2(\gamma-1)u_c^2 \end{aligned} \tag{C.18}$$

Eq. (C.12), (C.16), and (C.18) are reduced to the following quadratic equation

$$(\gamma+1)\xi^2 + 4(\gamma-1)\xi + 2(2\gamma-3) = 0 \tag{C.19}$$

where, $\xi = \frac{r_c}{u_c}\left(\frac{du}{dr}\right)_c$, and Eq. (C.19) can be solved using the quadratic formula. The correct critical point slope is obtained by choosing the smaller root of the resulting quadratic equation in $(du/dr)_c$. The larger root corresponds to the unphysical transonic solution where $u$ is subsonic at large distances. For the polytropic winds considered here all the partial derivatives in Eq. (C.12) may be evaluated analytically, so that the slope $(du/dr)_r$ is determined exactly. The solution to Eq. (C.7) is then obtained by numerically integrating $u$ inward and outward from the critical point, using the usual Runge-Kutta method. In the same way, $p$ and $\rho$ are obtained by numerically integrating Eq. (C.8) and (C.9).

# Acknowledgments

I would like to express my sincere appreciation to my supervisor Dr. Y. Abe. His advice, encouragement, and comment guided this study properly. And many discussions with him improve not only this thesis but also my philosophy of planetary science.

I am deeply grateful to Dr. H. Genda for his helpful advises and comments throughout this work. His constructive comment on numerical study is essential to developing the numerical code.

I would like to express my gratitude to Dr. E. Tajika, Prof. K. Kuramoto, Prof. S. Sasaki, and Dr. N. Iwagami for their meaningful reviews and comments, which greatly improve this thesis.

I would like to thank Prof. M. Ozima, Prof. H. Nagahara, Dr. S. Sugita, Dr. S. Tachibana, and other members in Earth and Planetary System Science Colloquium and Seminar for their fruitful suggestions and comments.

I would like to thank Dr. R. Machida, K. Hamano, K. Morizono, A. Sakamoto, K. Watanabe, K. Tetsuzaki, D. Tsuihiji, K. Abuku, and J. Miki for fruitful discussions and comments. I would also like to thank S. Watanabe, T. Ishii, A. Suzuki, H. Ichikawa, H. Sato, K. Ishibashi, K. Kitazato, Y. Saito for friendly competitions and encouragements each other.

This thesis was financially supported by JSPS Research Fellowship.

Finally, I am grateful to my parents and grandparents for their enduring encouragements and supports.

# Bibliography


[1] Y. Abe and T. Matsui, Evolution of an Impact-Generated $H_2O$-$CO_2$ Atmosphere and Formation of a Hot Proto-Ocean on Earth, *J. Atmos. Sci.* **45**, 3081-3101, 1988.

[2] Y. Abe, E. Ohtani, T. Okuchi, K. Righter and M. Drake, Water in the early Earth in: *Origin of the Earth and Moon* (Univ. Arizona Press, Ed. by R.M. Canup and K. Righter, Tucson) 413-433, 2000.

[3] E. Anders and M. Ebihara, Solar-system abundances of the elements, *Geochim. Cosmochim. Acta* **46**, 2363-2380, 1982.

[4] S.V. Avakyan, R.N. Il'In, V.M. Lavrov and G.N. Ogurtsov, Cross Sections for Photoionization and Primary Photoelectron and Auger Electron Spectra in: *Collision Processes and Excitation of UV Emission from Planetary Atmospheric Gases* (Gordon & Breach) 1-36, 1998.

[5] C.J. Ballentine, B. Marty, B.S. Lollar and M. Cassidy, Neon isotopes constrain convection and volatile origin in the Earth's mantle, *Nature* **433**, 33-38, 2005.

[6] P.M. Banks and G. Kockarts, *Aeronomy* (Academic Press, New York), 1973.

[7] A. Bar-Nun, I. Kleinfeld and E. Kochavi, Trapping of gas mixtures by amorphous water ice, *Phys. Rev. B* **38**, 7749-7754, 1988.

[8] A. Bar-Nun and T. Owen, Trapping of gases in water ice and consequences to comets and the atmospheres of the inner planets in: *Solar System Ices* (Kluwer, Ed. by B. Schmitt, C. De Bergh and M. Festou, Dordrecht) 353-366, 1998.

[9] R.H. Becker and R.O. Pepin, The case for a martian origin of the shergottites: Nitrogen and noble gases in EETA 79001, *Earth Planet. Sci. Lett.* **69**, 225-242, 1984.

[10] M.W. Caffee, C.M. Hohenberg and T.D. Swindle, Evidence in meteorites for an active early sun, *ApJ* **313**, L31-L35, 1987.

[11] M.W. Caffee, J.N. Goswani, C.M. Hohenberg, K. Marti and R.C. Reedy, Irradiation records in meteorites in: *Meteorites and the Early Solar System* (Univ. Arizona Press, Ed. by J.F. Kerridge and M.S. Matthews, Tucson) 205-245, 1988.

[12] A.G.W. Cameron, Elemental and nuclidic abundances in the solar system in: *Essays in Nuclear Astrophysics* (Cambridge Univ. Press, Ed. by C.A. Barnes, D.D. Clayton and D.N. Schramm, Cambridge) 23-43, 1982.

[13] V.M. Canuto, J. Levine, T. Augustsson and C. Imhoff, UV radiation from the young Sun and oxygen levels in the pre-biological paleoatmosphere, *Nature* **296**, 816-820, 1982.

[14] V.M. Canuto, J. Levine, T. Augustsson, C. Imhoff and M.S. Giampapa, The young Sun and the atmosphere and photochemistry of the early Earth, *Nature* **305**, 281-286, 1983.

[15] J.W. Chamberlain and D.M. Hunten, *Theory of Planetary Atmospheres* (Academic Press, New York), 1987.

[16] S. Chapman and T.G. Cowling, *The Mathematical Theory of Nonuniform Gases* (Cambridge Univ. Press, Cambridge), 1970.

[17] E. Chassefiére, Hydrodynamic escape of hydrogen from a hot water-rich atmosphere: The case of Venus, *JGR* **1996**, 26039-26056, 1996.

[18] C.F. Chyba, Impact Delivery and Erosion of Planetary Oceans in the Early Inner Solar System, *Nature* **343**, 129-133, 1990.

[19] J. Crabb and E. Anders, Noble gases in E-chondrites, *Geochim. Cosmochim. Acta* **45**, 2443-2464, 1981.

[20] N. Dauphas and B. Marty, Inference on the nature and the mass of Earth's late veneer from noble metals and gases, *JGR* **107**, 5129, 2002.

[21] N. Dauphas, The Dual Origin of the Terrestrial Atmosphere, *Icarus* **165**, 326-339, 2003.

[22] C. de Bergh, B. Bézard, T. Owen, D. Crisp, J.-P. Maillard and B.L. Lutz, Deuterium on Venus: Observations from Earth, *Science* **251**, 547-549, 1991.

[23] T. de Jong, A. Dalgarno and W. Boland, Hydrostatic models of molecular clouds, *A&A* **91**, 68-84, 1980.

[24] H. De Sterck, A. Csík, D.V. Abeele, S. Poedts and H. Deconinck, Stationary Two-Dimensional Magnetohydrodynamic Flows with Shocks: Characteristic Analysis and Grid Convergence Study, *J. Comput. Phys.* **166**, 28-62, 2001.

[25] A.H. Delsemme, The chemistry of comets, *Phil. Trans. R. Soc. London* **325**, 509-523, 1988.

[26] T.M. Donahue and J.B. Pollack, Origin and evolution of the atmosphere of Venus in: *Venus* (Univ. Arizona Press, Ed. by D. Hunten, L. Colin, T. Donahue and V. Moroz, Tucson) 1003-1036, 1983.

[27] T.M. Donahue, Fractionation of Noble Gases by Thermal Escape from Accreting Planetesimals, *Icarus* **66**, 195-210, 1986.

[28] J.D. Dorren and E.F. Guinan, The Sun in time: detecting and modeling magnetic inhomogeneities on solar-type stars in: *IAU Colloquium No. 143: The Sun as a Variable Star, Solar and Stellar Irradiance Variations* (Cambridge Univ. Press, Ed. by J.M. Pap, C. Frölich, H.S. Hudson and S.K. Solanki, Cambridge) 206-216, 1994.

[29] B. Durney, Transition From a Supersonic to a Subsonic Solar Wind in: *Solar Wind* (NASA, Ed. by C.P. Sonett, P.J. Coleman and J.M. Wilcox, Washington) 232-235, 1972.

[30] P. Eberhardt, J. Geiss, H. Graf, N. Grögler, U. Krähenbühl, H. Schwaller, J. Schwarzmüller and A. Stettler, Trapped solar wind noble gases, exposure age and K/Ar-age in Apollo 11 lunar fine material, *Prc. Apollo 11 Lunar Sci. Conf.*, 1037-1070, 1970.

[31] J.L. Fox and A. Dalgarno, Ionization, Luminosity and Heating of the Upper Atmosphere. of Mars, *JGR* **84**, 7315-7333, 1979.

[32] J. Geiss and H. Reeves, Deuterium in the solar system, *Astron. Astrophys.* **93**, 189-199, 1981.

[33] H. Genda and Y. Abe, Survival of a Proto-Atmosphere Through the Stage of Giant Impacts: the Mechanical Aspects, *Icarus* **164**, 149-162, 2003.

[34] H. Genda and Y. Abe, Enhanced Atmospheric Loss on Protoplanets at the Giant Impact Phase in the Presence of Oceans, *Nature* **433**, 842-844, 2005.

[35] L.A. Girardi, A. Bressan, G. Bertelli and C. Chiosi, Evolutionary Tracks and Isochrones for Low- and Intermediate-Mass Stars: From 0.15 to 7 M , and from Z= 0.0004 to 0.03, *Astron. Astrophys. Suppl.* **141**, 371-383, 2000.

[36] J.N. Goswani, D. Lal and L.L. Wilkening, Gas-rich meteorites: probes for particle environment and dynamical processes in the inner solar system, *Space Sci. Rev.* **37**, 111-159, 1984.

[37] M.M. Grady, I.P. Wright, L.P. Carr and C.T. Pillinger, Compositional differences in enstatite chondrites based on carbon and nitrogen stable isotope measurements, *Geochim. Cosmochim. Acta* **50**, 2799-2813, 1986.

[38] M. Güdel, E.F. Guinan and S.L. Skinner, The X-Ray Sun in Time: A Study of the Long-Term Evolution of Coronae of Soar-Type Stars, *ApJ* **483**, 947-960, 1997.

[39] H.J.M. Hanley, R.D. McCarty and H. Interman, The viscosity and thermal conductivity of dilute gaseous hydrogen from 15 to 500 K, *J. Res. Nat. Bur. Stand. Sect. A* **74**, 331-350, 1970.

[40] G.L. Hashimoto, Y. Abe and S. Sugita, The Chemical Composition of the Early Terrestrial Atmosphere: Formation of a Reducing Atmosphere from CI-Like Material, *JGR* **112**, E05010, 2007.

[41] C. Hayashi, K. Nakazawa and H. Mizuno, Earth's Melting Due to the Blanketing Effect of the Primordial Dense Atmosphere, *Earth Planet. Sci. Lett.* **43**, 22-28, 1979.

[42] D. Heymann and R.L. Palma, Discovery of solar wind neon in the Allende meteorite, *JGR* **91**, 460-466, 1986.

[43] D. Hollenbach and C.F. McKee, Molecule Formation and Infrared Emission in Fast Interstellar Shocks. I. Physical Processes, *ApJ* **41**, 555-592, 1979.

[44] D.M. Hunten, The Escape of Light Gases from Planetary Atmospheres, *Journal of the Atmospheric Sciences* **30**, 1481-1494, 1973.

[45] D.M. Hunten, Blowoff of an atmosphere and possible application to Io, *GRL* **12**, 271-273, 1985.

[46] D.M. Hunten, R.O. Pepin and J.C.G. Walker, Mass Fractionation in Hydrodynamic Escape, *Icarus* **69**, 532-549, 1987.

[47] D.M. Hunten, Kuiper Prize Lecture: Escape of Atmospheres, Ancient and Modern, *Icarus* **85**, 1-20, 1990.

[48] D.M. Hunten, Atmospheric Evolution of the Terrestrial Planets, *Science* **259**, 915-920, 1993.

[49] S. Ida and D.N.C. Lin, Toward a Deterministic Model of Planetary Formation I. A Desert in the Mass and Semimajor Axis Distributions of Extrasolar Planets, *ApJ* **604**, 388-413, 2004.

[50] A.P. Ingersoll, The runaway greenhouse: A history of water on Venus, *J. Atmos. Sci.* **26**, 1191-1198, 1969.

[51] I. Kamp and G.-J. van Zadelhoff, On the Gas Temperature in Circumstellar Disks Around A Stars, *A&A* **373**, 641-656, 2001.

[52] J.F. Kasting and J.B. Pollack, Loss of Water from Venus I. Hydrodynamic Escape of Hydrogen, *Icarus* **53**, 479-508, 1983)

[53] J.F. Kasting, J.B. Pollack and D. Crisp, Effects of High $CO_2$ Levels on Surface Temperature and Atmospheric Oxidation State of the Early Earth, *J. Atmos. Chem.* **1**, 403-428, 1984.

[54] J.F. Kasting, Photochemical consequences of enhanced $CO_2$ levels in Earth's early atmosphere in: *The Carbon Cycle and Atmospheric $CO_2$ Natural Variations Archean to Present* (American Geophysical Union, Ed. by E.T. Sundquist and W.S. Broecker, Washington D. C.) 612-622, 1985.

[55] J.F. Kasting, Runaway and Moist Greenhouse Atmospheres and the Evolution of Earth and Venus, *Icarus* **74**, 472-494, 1988.

[56] J.F. Kasting, Early evolution of the atmosphere and ocean in: *The Chemistry of Life's Origins* (Kluwer Academic Publishers, Ed. by J.M. Greenberg, C.X. Mendoza-Gomez and V. Pirronello, Dordrecht) 149-176, 1993.

[57] J.F. Kasting, Planetary Atmosphere Evolution: Do Other Habitable Planets Exist and Can We Detect Them?, *Astrophysics and Space Science* **241**, 3-24, 1996.

[58] R. Keppens and J.P. Goedbloed, Numerical Simulations of Stellar Winds: Polytropic Models, *A&A* **343**, 251-260, 1999.

[59] J.F. Kerridge, Carbon, hydrogen and nitrogen in carbonaceous chondrites: Abundances and isotopic compositions in bulk samples, *Geochim. Cosmochim. Acta* **49**, 1707-1714, 1985.

[60] E. Kokubo and S. Ida, Formation of Protoplanets from Planetesimals in the Solar Nebula, *Icarus* **143**, 15-27, 2000.

[61] Y.N. Kulikov, H. Lammer, H.I.M. Lichtenegger, N. Terada, I. Ribas, C. Kolb, D. Langmayr, R. Lunding, E.F. Guinan, S. Barabash and H.K. Biernat, Atmospheric and Water Loss from Early Venus, *Planet. and Space Sci.* **54**, 1425-1444, 2006.

[62] K. Kuramoto and T. Matsui, Partitioning of H and C between the mantle and core during the core formation in the Earth: Its implications for the atmospheric evolution and redox state of early mantle, *JGR* **101**, 14909-14932, 1996.

[63] D. Laufer, E. Kochavi and A. Bar-Nun, Structure and dynamics of amorphous water ice, *Phys. Rev. B* **36**, 9219-9227, 1987.

[64] J.S. Lewis and R.G. Prinn, *Planets and Their Atmospheres* (Academic Press, São Paulo), 1984.

[65] J.G. Luhmann and J.U. Kozyra, Dayside Pickup Oxygen Ion Precipitation at Venus and Mars: Spatial Distributions, Energy Deposition and Consequences, *JGR* **96**, 5457-5467, 1991.

[66] E.A. Mason, R.J. Munn and F.J. Smith, Thermal diffusion in gases, *Adv. At. Mol. Phys.* **2**, 33-91, 1966.

[67] T. Matsui and Y. Abe, Evolution of an Impact-Induced Atmosphere and Magma Ocean on the Accreting Earth, *Nature* **319**, 303-305, 1986.

[68] E. Mazor, D. Heymann and E. Anders, Noble gases in the terrestrial planets, *Nature* **293**, 535-539, 1970.

[69] M.B. McElroy, T.Y. Kong and Y.L. Yung, Photochemistry and evolution of Mars' atmosphere: A Viking perspective, *JGR* **82**, 4379-4388, 1977.

[70] M.B. McElroy and M.J. Prather, Noble gases in the terrestrial planets, *Nature* **293**, 535-539, 1981.

[71] M.B. McElroy, M.J. Prather and J.M. Rodriguez, Loss of Oxygen from Venus, *GRL* **9**, 649-651, 1982.

[72] C.F. McKee, J.W.V. Storey, D.M. Watson and S. Green, Far-Infrared Rotational Emission by Carbon Monoxide, *ApJ* **259**, 647-656, 1982.

[73] H. Mizuno, K. Nakazawa and C. Hayashi, Gas Capture and Rare Gas Retention by Accreting Planets in the Solar Nebula, *Planet. Space Sci.* **30**, 765-771, 1982.

[74] A. Nishiguchi and T. Yabe, Second-Order Fluid Particle Scheme, *J. Comput. Phys.* **52**, 390-413, 1983.

[75] G. Notesco, A. Bar-Nun and T. Owen, Gas Trapping in Water ice at Very Low Deposition Rates and Implications for Comets, *Icarus* **162**, 183-189, 2003.

[76] T. Owen, K. Biemann, D.R. Rushneck, J.E. Biller, D.W. Howarth and A.L. Lafleur, The composition of the atmosphere at the surface of Mars, *JGR* **82**, 4635-4639, 1977.

[77] T. Owen, A. Bar-Nun and I. Kleinfeld, Possible cometary origin of heavy noble gases in the atmospheres of Venus, Earth and Mars, *Nature* **358**, 43-46, 1992.

[78] T. Owen, P. Mahaffy, H.B. Niemann, S. Atreya, T. Donahue, A. Bar-Nun and I. de Pater, A Low-Temperature Origin for the Planetesimals that Formed Jupiter, *Nature* **402**, 269-270, 1999.

[79] E.N. Parker, Dynamical Properties of Stellar Coronas and Stellar Winds I. Integration of the Momentum Equation, *ApJ* **139**, 72-92, 1964.

[80] R.O. Pepin, On the Origin and Early Evolution of Terrestrial Planet Atmospheres and Meteoritic Volatiles, *Icarus* **92**, 2-79, 1991.

[81] R.O. Pepin, Atmospheres on the Terrestrial Planets: Clues to Origin and Evolution, *Earth Planet. Sci. Lett.* **252**, 1-14, 2006.

[82] I. Ribas, E.F. Guinan, M. Güdel and M. Audard, Evolution of the Solar Activity over Time and Effects on Planetary Atmospheres I. High-Energy Irradiances (1-1700 A), *ApJ* **622**, 680-694, 2005.

[83] P.G. Richards, J.A. Fennelly and D.G. Torr, EUVAC: A solar EUV flux model for aeronomic calculations, *JGR* **99**, 8981-8992, 1994.

[84] W.W. Rubey, Geologic history of sea water, *Bull. Geo. Soc. Amer.* **62**, 1111-1147, 1951.

[85] S. Sasaki and K. Nakazawa, Origin of Isotopic Fractionation of Terrestrial Xe: Hydrodynamic Fractionation during Escape of the Primordial $H_2$-He Atmosphere, *Earth Planet. Sci. Lett.* **89**, 323-334, 1988.

[86] S. Sasaki, Penetration of the solar wind after dissipation of the solar nebula: Origin of Venusian Ar by off-disk implantation of the solar wind, *Prc. NIPR Symp. Antarct. Meteorites* **24**, 155-172, 1989.

[87] S. Sasaki, Off-Disk Penetration of Ancient Solar Wind, *Icarus* **91**, 29-38, 1991.

[88] R. Schinke, V. Engel, U. Buck, H. Meyer and G.H.F. Diercksen, Rate Constants for Rotational Transitions of CO Scattered by Para-Hydrogen, *ApJ* **299**, 939-946, 1985.

[89] M. Sekiya, K. Nakazawa and C. Hayashi, Dissipation of the Rare Gases Contained in the Primordial Earth's Atmosphere, *Earth Planet. Sci. Lett.* **50**, 197-201, 1980.

[90] T. Simon, G. Herbig and A.M. Boesgaard, The Evolution of Chromospheric Activity and the Spin-Down of Solar-Type Stars, *ApJ* **293**, 551-570, 1985.

[91] V.V. Sobolev, *Light Scattering in Planetary Atmospheres* (Pergamon, Oxford), 1975.

[92] S.E. Strom, S. Edwards and M.F. Skruskie, Evolutionary time scales for circumstellar disks associated with intermediate- and solar-type stars in: *Protostars and Planets III* (Univ. Arizona Press, Ed. by E.H. Levy and J.I. Lunine, Tucson) 837-866, 1993.

[93] H.E. Suess, H. Wänke and F. Wlotzka, On the origin of gas-rich meteorites, *Geochim. Cosmochim. Acta* **28**, 595-607, 1964.

[94] T.D. Swindle, M.W. Caffee and C.M. Hohenberg, Xenon and other noble gases in shergottites, *Geochim. Cosmochim. Acta* **50**, 1001-1015, 1986.

[95] H. Takewaki and T. Yabe, The Cubic-Interpolated Pseudo Particle (CIP) Method: Application to Nonlinear and Multi-dimensional Hyperbolic Equations, *J. Comput. Phys.* **70**, 355-372, 1987.

[96] F. Tian, O.B. Toon and A.A. Pavlov, Transonic Hydrodynamic Escape of Hydrogen from Extrasolar Planetary Atmosphere, *ApJ* **621**, 1049-1060, 2005.

[97] A.G.G.M. Tielens and D. Hollenbach, Photodissociation Regions. I. Basic Model, *ApJ* **291**, 722-746, 1985a.

[98] A.G.G.M. Tielens and D. Hollenbach, Photodissociation Regions. II. A Model for the Orion Photodissociation Region, *ApJ* **291**, 747-754, 1985b.

[99] E.F. Toro, *Riemann Solvers and Numerical Methods for Fluid Dynamics: A Practical Introduction* (Springer, Berlin), 1999.

[100] A. Vidal-Madjar, A. Lecavelier des Etangs, J.-M. Désert, G.E. Ballester, R. Ferlet, G. Hébrard and M. Mayor, An Extended Upper Atmosphere around the Extrasolar Planet HD209458b, *Nature* **422**, 143-146, 2003.

[101] U. von Zahn, S. Kumar, H. Niemann and R. Prinn, Compositions of the Venus atmosphere in: *Venus* (Univ. Arizona Press, Ed. by D. Hunten, L. Colin, T. Donahue and V. Moroz, Tucson) 299-430, 1983.

[102] J.C.G. Walker, *Evolution of the Atmosphere* (Macmillan, New York), 1977.

[103] A.J. Watson, T.M. Donahue and J.C.G. Walker, The Dynamics of a Rapidly Escaping Atmosphere: Applications to the Evolution of Earth and Venus, *Icarus* **48**, 150-166, 1981.

[104] G.W. Wetherill, Solar Wind Origin of $^{36}$Ar on Venus, *Icarus* **46**, 70-80, 1981.

[105] G.W. Wetherill, Comparison of analytical and physical modeling of planetesimal accumulation, *Icarus* **88**, 336-354, 1990.

[106] R.C. Wiens, R.H. Becker and R.O. Pepin, The case for a martian origin of the shergottites, II. Trapped and indigenous gas components in EETA 79001 glass, *Earth Planet. Sci. Lett.* **77**, 149-158, 1986.

[107] R. Wieler, Noble gases in the solar system in: *Noble Gases in Geochemistry and Cosmochemistry, Rev. Mineral. Geochem., vol. 47* (, Ed. by D. Porcelli, C.J. Ballentine and R. Wieler) 21-70, 2002.

[108] B.E. Wood, H.-R. Müller, G.P. Zank and J.L. Linsky, Measured Mass-Loss Rates of Solar-Like Stars as a Function of Age and Activity, *ApJ* **547**, 412-425, 2002.

[109] B.E. Wood, H.-R. Müller, G.P. Zank, J.L. Linsky and S. Redfield, New Mass-Loss Measurements from Astrospheric Ly$\alpha$ Absorption, *ApJ* **628**, L143-L146, 2005.

[110] T.N. Woods and G.J. Rottman, Solar Ultraviolet Variability Over Time Periods of Aeronomic Interest in: *Atmospheres in the Solar System: Comparative Aeronomy* (AGU, Ed. by M. Mendillo, A. Nagy and J.H. Waite) 221-233, 2002.

[111] T. Yabe and T. Aoki, A universal solver for hyperbolic equations by cubic-polynomial interpolation I. One-dimensional solver, *Comput. Phys. Communications* **66**, 219-232, 1991.

[112] T. Yabe, F. Xiao and T. Utsumi, The Constrained Interpolation Profile Method for Multiphase Analysis, *J. Comput. Phys.* **169**, 556-593, 2001.

[113] K.J. Zahnle and J.F. Kasting, Mass Fractionation during Transonic Escape and Implications for Loss of Water from Mars and Venus, *Icarus* **68**, 462-480, 1986.

[114] K.J. Zahnle, Atmospheric chemistry by large impacts in: *Global Catastrophes in Earth History* (Geol. Soc. of Am., Ed. by V.L. Sharpton and P.D. Ward, Boulder, Colo.) 271-288, 1990.

[115] K. Zahnle, Origins of Atmospheres, *ORIGINS ASP Conference Series* **148**, 364-391, 1998.